EFFICIENCY OF PERFORATED BREAKWATER AND ASSOCIATED ENERGY DISSIPATION

A Thesis

by

H. A. KUSALIKA SURANJANI ARIYARATHNE

Submitted to the Office of Graduate Studies of
Texas A&M University
in partial fulfillment of the requirements for the degree of

MASTER OF SCIENCE

December 2007

Major Subject: Civil Engineering

EFFICIENCY OF PERFORATED BREAKWATER

AND ASSOCIATED ENERGY DISSIPATION

A Thesis

by

H. A. KUSALIKA SURANJANI ARIYARATHNE

Submitted to the Office of Graduate Studies of
Texas A&M University
in partial fulfillment of the requirements for the degree of

MASTER OF SCIENCE

Approved by:

Chair of Committee,	Kuang-An Chang
Committee Members,	Billy Edge
	Achim Stoessel
Head of Department,	David Rosowsky

December 2007

Major Subject: Civil Engineering

ABSTRACT

Efficiency of Perforated Breakwater and Associated Energy Dissipation.

(December 2007)

H. A. Kusalika Suranjani Ariyarathne, B.S.; M.S., University of Peradeniya

Chair of Advisory Committee: Dr. Kuang-An Chang

The flow field behavior in the vicinity of a perforated breakwater and the efficiency of the breakwater under regular waves were studied.

To examine the efficiency of the structure thirteen types of regular wave conditions with wave periods T = 1, 1.2, 1.6, 2, 2.5 sec and wave heights H_i = 2, 4, 6, 8, 10 cm in an intermediate water depth of 50 cm were tested. The incoming, reflected and transmitted wave heights were measured using resistance type wave gauges positioned at the required locations. The efficiency of the structure was calculated considering the energy balance for the system. The efficiency of the structure for different wave conditions and with different parameters are shown and compared.

Seven types of regular waves with wave periods T = 1, 1.6, 2, 2.5 sec and wave heights H_i = 4, 6, 8, 10 cm in an intermediate water depth of 50 cm were tested for the flow behavior study. In order to study the flow field variation with phase, ten phases were considered per one wave. The Particle Image Velocimetry (PIV) technique was employed to measure the two dimensional instantaneous velocity field distribution and MPIV (Matlab toolbox for PIV) and DaVis (a commercial software) were used to

calculate the velocity vectors. By repeating the experiments and taking an average, the mean velocity field, mean vorticity field, mean turbulent intensity and mean turbulent kinetic energy field were calculated for each phase and for each wave condition. The phase average fields for each wave condition for each of the above mentioned parameters were calculated taking the average of ten phases. The phase averaged velocity, vorticity and turbulent kinetic energy fields are presented and compared. The energy dissipation based on both elevation data and the velocity data are presented and compared.

It was found that for more than 75% of the tested wave conditions, the energy dissipation was above 69%. Thus the structure is very effective in energy dissipation. Further it was found that for all the tested wave conditions most of the turbulent kinetic energy form near the free surface and near the front wall, where as behind the back wall of the structure the turbulent kinetic energy was very small.

To Ruchira Tharanga Amarasinghe (RT)

ACKNOWLEDGEMENTS

I would like to express my deep gratitude to my advisor, Professor Kuang-An Chang, of the Ocean Engineering program in the Civil Engineering Department for introducing me to this subject area, continuous support, guidance, advice, encouragement, patience and understanding at all times.

I would like to thank Professor Billy Edge of the Ocean Engineering program in the Civil Engineering Department and Professor Achim Stoessel in the Department of Oceanography for serving as my committee members.

Thanks also go to Dr. Jong In Lee and Dr. Yonguk Ryu for initiating this research and continuous support.

I wish to thank the Fulbright Commission for providing financial support for my master's degree.

I wish to thank my colleagues, Ho Joon Lim and Dong-Guan Seol, and Lab technician, John Reed, for their support while working in the lab.

I also want to extend my gratitude to my parents and thanks to my sisters for love and support from overseas.

Finally, thanks to my husband Ruchira Amarasinghe for his love, patience, understanding, kind support, encouragement and for making this work interesting and a success.

NOMENCLATURE

PIV	Particle Image Velocimetry
FOV	Field Of View

TABLE OF CONTENTS

CHAPTER Page

Page

LIST OF FIGURES

FIGURE Page

FIGURE Page

FIGURE Page

LIST OF TABLES

CHAPTER I

INTRODUCTION

1.1. Background of perforated breakwaters

Breakwaters have been widely constructed to prevent coastal erosion, to provide a calm basin by reducing wave induced disturbances for ships and to protect harbour facilities from rough seas. Rubble mound breakwaters are the oldest type and have been widely used for sheltering harbors. However, with time, innovative vertical structures like vertical caisson perforated breakwaters became popular among coastal engineers providing a better alternative to the classical types.

Rubble mound breakwaters block littoral drift and cause severe erosion or accretion in neighbouring beaches. In addition, they do not allow water to pass through, preventing water circulation and causing the water quality within the harbour to deteriorate, thus causing environmental hazards. They also obstruct the passage of fish and bottom dwelling microorganisms. Building rubble mound breakwaters will be expensive where the required materials are not readily available. Even though vertical caisson breakwaters have positive aspects compared to rubble mound breakwaters, they reflect much of the incoming wave energy back to the sea, thus causing severe erosion in front of the structure, as a result making structure stability problems with time. They also

---

This thesis follows the style of Coastal Engineering.

do not allow water circulation.

In order to resolve the above mentioned problems, perforated breakwaters were first introduced by Jarlan (1961). He introduced a breakwater with a front perforated wall, a wave energy dissipating chamber and a solid back wall. Significant damping of incoming waves can be achieved by the generation of eddies and turbulence near the perforations in the front wall (Jarlan, 1961) and a substantial reduction of wave impact loads (Takahashi & Shimosako, 1994; Takahashi et al., 1994) and wave overtopping (Isaacson et al., 1998a, b) can be achieved. It also allows water circulation and rubbish clearance creating a clean environment inside the harbour, providing passage for fishes and microorganisms. It became very popular in engineering practice due to its high effectiveness in energy dissipation and has been investigated intensively and used increasingly worldwide. It improves hydraulic performance, total cost, quality control, environmental aspects, construction time and maintenance.

After the introduction of perforated breakwaters in 1961, several improvements have been proposed and tested to investigate its hydraulic performance and hydrodynamic characteristics. Using single or multiple vertical screens, single or multiple chambers, vertically stacked voided concrete blocks and filling the wave chamber of the Jarlan type with large diameter rock and replacing the front perforated wall by vertical porous wave absorber are some of the introduced modifications. All of the modifications attempt to take advantage of the process of wave dissipation inside a vertical perforated structure. The functional efficiency of these vertically sided

perforated breakwaters have been analyzed analytically, numerically and experimentally mainly by evaluating the reflection and transmission coefficients.

1.2. Literature review

Several analytical and numerical models have been developed, but very few experimental studies have been done. Most of the studies were done for breakwaters having a front perforated wall, a core and a solid back wall with regular waves. Few attempts were made to study breakwaters having many perforated walls, or having perforated walls for both front and back.

Most of the studies were made to study wave reflection due to various wave parameters and various geometry of the structure. Terrett et al. (1968) did model test studies to find wave reflection and wave forces on a perforated breakwater. They proposed a criterion for designing perforated breakwater structures based on their experimental results. Kondo & Toma (1972) did experimental studies to find the effect of characteristics of incident waves and of the thickness of structure on wave reflection and transmission. They concluded that the relative thickness (= B/L, where B = the width of the structure and L = wave length) of the structure has appreciable effects on reflected and transmitted wave energies. Their study has shown that the reflection coefficient reaches a maximum for B/L of 0.2 – 0.25, then decreases as the B/L increases, and remains approximately uniform for B/L larger than about 0.6. They have also shown that the transmission coefficient decreases exponentially as B/L increases. They found that

there exists a pattern of standing waves having a antinodes at the front face and a node at the rear face. Massel & Mei (1977) presented an analytical model to find the reflection and transmission due to random waves impinging on a dissipative breakwater. Kondo (1979) derived an analytical model to estimate reflection and transmission coefficients for permeable and impermeable upright breakwaters having two perforated slotted walls. The model has been verified with experimental data with good agreement. They showed that for both types of breakwaters, the minimum reflection occurs for $B/L \approx 0.25$, where B is the width of the structure and L is the wavelength. They concluded that impervious breakwaters having two perforated walls could bring much lower reflection coefficient compared to Jarlan's type. Hagiwara (1984) did an analytical study to find reflection and transmission coefficients using an integral equation derived for the horizontal velocity component in a pervious wall. Factors related to wave dissipation were investigated for a breakwater with pervious vertical walls at both seaward and landward sides. With experimental data he showed that the integral method could explain the energy dissipation. Bennet et al. (1992) developed a theory for calculating the reflection properties of wave screen breakwaters. Based on this theory, the reflection coefficient was calculated for both an isolated screen and a screen with a solid back wall. The theory has been verified with experiments. Kakuno et al. (1992) did a theoretical and experimental study on scattering of small amplitude water waves by an array of vertical cylinders with a solid vertical back wall. The energy loss due to flow separation near the cylinders was modeled by introducing a blockage coefficient. The theory was compared with experimental data with good agreement. Mallayachari & Sundar (1994) proposed a

numerical model to investigate reflection characteristics of a permeable vertical seawall. The variation of reflection coefficient with the porosity of the wall, its friction factor and the relative wall width were studied and compared with available analytical results. The model has been used to study the reflection characteristics of sloping permeable walls. The behaviour of vertical and sloping permeable walls in reflecting wave energy has been discussed. The results for reflection coefficient for a seawall placed on a sloping bed was obtained and compared with the results for a wall on a flat bed. It was shown that the model agrees well with the available data. They concluded that the reflection is less for walls on sloping beds than those on flat beds for lower friction factor values. They also concluded that vertical walls on milder slopes reflect less energy for longer waves and the change in the slope does not have any effect on reflection for short waves. Isaacson et al. (1998a) developed a theoretical analysis and associated numerical model to assess the performance of a breakwater consisting of a perforated front wall, an impermeable back wall and a rock filled core. In the numerical model they utilized a boundary condition at the perforated wall, which accounts for energy dissipation. The model has been validated with data from previous numerical studies. The wave reflection coefficient, wave run up and wave force were discussed. Subsequently, Isaacson et al. (2000) discussed the effects of porosity, breakwater geometry and relative water depth on reflection. Zhu & Chwang (2001) proposed an analytical model to investigate the interaction between waves and a slotted seawall. The model has been verified with experimental data and they concluded that reflection characteristics mainly depend on porosity and incident wave height. They found that the reflection coefficient

reaches its minimum value when the chamber width is about a quarter of the incident wavelength. Requejo et al. (2002) proposed a mathematical model to solve the potential flow around and inside a porous breakwater. The reflection, transmission, dissipation, horizontal and vertical forces and overturning moment were solved. The model has been verified with experimental data. The influence of structure width, porosity, wave height, period and water depth were examined.

All the above studies were done considering regular, normally incident waves. Few studies were made for oblique incident waves. Suh & Park (1995) developed an analytical model for predicting wave reflection due to obliquely incident waves on a perforated wall caisson breakwater having a solid back wall mounted on a rubble mound foundation. The model has been verified and compared with available data. They further showed that the minimum reflection occurs at $B\cos\theta/L \approx 0.25$, where B is the width of the chamber, θ is the incident angle and L is the wavelength. Li et al. (2003) proposed an analytical model to examine the reflection of oblique incident waves by breakwaters that consist of a double-layered perforated wall and an impermeable back wall. They have included the evanescent waves for the model. The effect of porosity, relative width and relative water depth were discussed and compared to experimental data.

Yip & Chwang (2000) introduced a horizontal plate as a modification to the structure. They developed an analytical model to study the performance of a perforated wall breakwater with an internal horizontal plate under regular waves with linear wave theory. The wave reflection with different porosity, physical dimensions and wave conditions were analyzed. They concluded that the porous effect parameter is an

important parameter to determine the performance of a breakwater. They also concluded that by adjusting the submergence of the horizontal plate the reflection could be reduced. In addition they concluded that by introducing the horizontal plate, the perforated breakwater could be designed with a higher degree of confidence and reliability.

Some researchers developed formulas to calculate various parameters. Urashima et al. (1986) proposed formulas to compute reflection, transmission and force based on measured total force/total head loss on a single slotted wall. The calculated values have been verified with experiments. They concluded that the optimum value of the void ratio lies around 0.2-0.4. They also concluded that for a constant wall thickness, the reflection could be reduced by increasing the slit width. Isaacson et al. (1998b) developed a numerical model to study wave interaction with a thin vertical slotted barrier extending from the water surface to some distance above the seabed. They developed expressions for transmission and reflection coefficients, wave run up, maximum horizontal force and overturning moment. Experiments have been done to verify the model. The effects of porosity, relative wavelength, wave steepness, and irregular waves were discussed. Aoul & Lambert (2003) proposed a formula to find the pressure distribution and forces acting on the different faces of a perforated caisson breakwater and verified the model with experimental data.

Few attempts have been made to study breakwaters having more than two wave absorbers. Twu & Lin (1991) developed an analytical model to study the reflection coefficient for a wave absorber containing a number of porous plates with various porous effect parameters. They showed that wave reflection was affected significantly

by the spacing between the adjacent porous plates as well as the alignment of these plates. They proposed that for intermediate depth water waves, it is appropriate to maintain spacing between the adjacent porous plates, and between the last plate and the end wall, at a value of 0.88 times the water depth. They also suggested that the absorber will be more efficient if the porosity magnitudes of plates are arranged in a progressively decreasing order from the front to the back of the wave absorber. The model has been verified with experimental data with good agreement. Losada et al. (1993) developed an analytical model to study the energy dissipation on multilayered porous media under obliquely impinging waves. The variation of reflection coefficient with kA (where k is the wave number and A is the width of a unit cell consisting of two layers) was discussed. They concluded that by increasing the number of absorber units the reflection could be reduced. They also showed that the increase in the angle of wave incidence decreases the dependence of reflection coefficient on kA, and for large angles of incidence the reflection is almost constant and negligible. Twu & Wang (1994) developed a numerical model to study the flow behaviour at a set of multilayer porous media in front of a solid wall. They concluded that the larger number of layers the media has the better function it would provide and less space it would occupy.

All the above studies were done for regular waves; few studies have been done for irregular waves. Suh et al. (2001) developed an analytical model that predicts the reflection of irregular waves normally incident upon a perforated wall caisson breakwater. To examine the predictability of the model, experiments were conducted. They concluded that the reflection of irregular waves from a perforated wall caisson

breakwater depends on the wave frequency. Subsequently, Suh et al. (2002) proposed several analytical models to calculate the reflection coefficient of irregular waves from a perforated wall caisson breakwater. The first method was to approximate the irregular waves as single regular waves whose height and period were root mean squared wave height and significant wave period. The second was to use the regular wave repeatedly for each frequency component of irregular wave. The third method was same as the second, but the wave height corresponding to energy of each component wave was used. Comparing with experimental data they have shown the second method to be the most adequate. Suh et al. (2006) proposed a numerical model that calculates reflection of irregular waves from a partially perforated caisson breakwater. They modified the previously developed model for calculating reflection coefficient for regular waves and a fully perforated wall, to calculate the reflection coefficient for partially perforated and irregular waves. The model has been verified with experimental data.

1.3. Objective and scope of the present study

Even though many analytical and numerical models are developed to understand the phenomenon, laboratory experiments are necessary due to the fact that the flow near the perforations is very chaotic and no numerical or analytical model has been developed so far to model the actual complex environment in detail. In spite of such extensive applications, practical interest and demand, rigorous study of the flow field behaviour in the vicinity of the perforated breakwaters does not seem to have received the deserved

attention. Although this process has been analyzed for decades, all the analysis so far is limited to free surface elevation data studies. Hence there is a lack of quantitative measurements of velocity data in the vicinity of the structure due to wave and structure interaction. This is the crucial problem to progress in studying of wave and structure interaction and in gaining a physical insight to the problem. In most of the numerical and analytical models, the linear wave theory is assumed, and in all the experimental studies free surface measurements are made using wave gauges. Considering energy conservation, the wave energy provided by the incoming wave has been equated to the addition of outgoing reflected wave energy, transmitted wave energy and the dissipated wave energy within the chamber. So far, no velocity measurements have been made in the vicinity of the structure due to wave structure interaction.

In engineering practice, owing to the stability requirements of the structure, the front wall of caisson breakwater is often partially perforated. A conventional perforated breakwater consists of a front perforated wall, a wave chamber and a back wall. The weight of the caisson is less than that of a vertical solid caisson with the same width and most of its weight is concentrated on the backside. Hence, difficulties are faced when designing the structure, due to the possibility of sliding and overturning failure. If the bearing capacity of the seabed is not large, the weight on the backside can have an adverse effect. In order to solve the above mentioned problems, partially perforated breakwaters, which provide additional weight in the front side, are often used.

The objective of the present study is to find the efficiency of a partially perforated, vertical breakwater using both wave elevation data and velocity data and to

study the flow field in the vicinity of the structure employing the Particle Image Velocimetry (PIV) method. PIV technique is a whole field measurement tool, which provides quantitative measurements of thousands of velocity vectors with high accuracy and without disturbing the flow. Details of the PIV method are presented in chapter II. To find the efficiency of the structure thirteen different wave conditions were considered. The incoming, reflected and transmitted wave heights were measured using resistance type wave gauges and the efficiency of the structure can be calculated based on the linear wave theory and considering the energy balance for the system. In order to distinguish the effect of wave parameters in the wave structure interaction, seven different wave parameters were used. To study the variations of flow field with phase, a wave is divided to ten phases. Image processing and post processing was done using MPIV toolbox (Mori & Chang, 2003) and DaVis 5.4.4, from LaVision (a commercial software). By repeating the experiments and taking average, the mean velocity field, mean vorticity field, mean turbulent intensity and mean turbulent kinetic energy field were calculated for each phase and for each wave condition. The phase average fields for each wave condition for each of the above mentioned parameters were calculated taking the average of ten phases. The phase averaged velocity, vorticity and turbulent kinetic energy fields are presented and compared. The energy dissipation based on both elevation data and the velocity data are presented and compared.

In this thesis, the experimental set up is explained in chapter II. In chapter III, the measured incoming, reflected and transmitted wave heights and calculated energy dissipation for different wave conditions are shown, compared and discussed. Chapter

IV presents and compares the phase average velocity fields in the vicinity of the structure for different wave conditions. In chapter V phase average vorticity for different wave conditions are presented and compared. Chapter VI presents and discusses phase average turbulent kinetic energy, depth average turbulent kinetic energy, horizontally average turbulent kinetic energy and spatially average turbulent kinetic energy for different wave conditions. The energy dissipation based on elevation data and velocity data are also compared. The summary and conclusion is presented in chapter VII.

CHAPTER II

EXPERIMENTAL SET UP

The experiments were conducted in a wave tank (see figure 2.1), which is 37 m long, 0.91 m wide and 1.22 m deep and is located in the Civil Engineering Department at Texas A&M University. The tank is made of steel with glass sides for optical access. A beach with a slope of 1:5.5 is installed at the end of the tank starting at 29.7 m from the wave generator. A layer of horsehair is placed on the beach to absorb the incoming wave energy and to reduce the wave reflection.

In the experiments the water depth was kept at 50 cm. The model of the perforated breakwater was kept 20.15 m away from the wave maker. The model is 0.46 m long, 0.91 m wide and 0.65 m high (see figure 2.2). In order to cover the required area in the vicinity of the structure eight Field Of View (FOV) (25 cm x 25 cm) were used (see figure 2.3). To examine the flow field variation with phases, ten phases were used per wave (see figure 2.4). To examine the effect of perforations on the flow two light sheets were selected, one through the perforations (Light sheet 1) and one through the solid wall (Light sheet 2) (see figure 2.2). In order to distinguish the effect of wave parameters in the wave structure interaction, seven types of regular waves with wave periods T = 1, 1.6, 2 and 2.5 sec and wave heights H_i = 4, 6, 8 and 10 cm (see table 2-1) were used. Each test was repeated three times. The incoming, reflected and transmitted wave heights were measured using resistance type wave gauges.

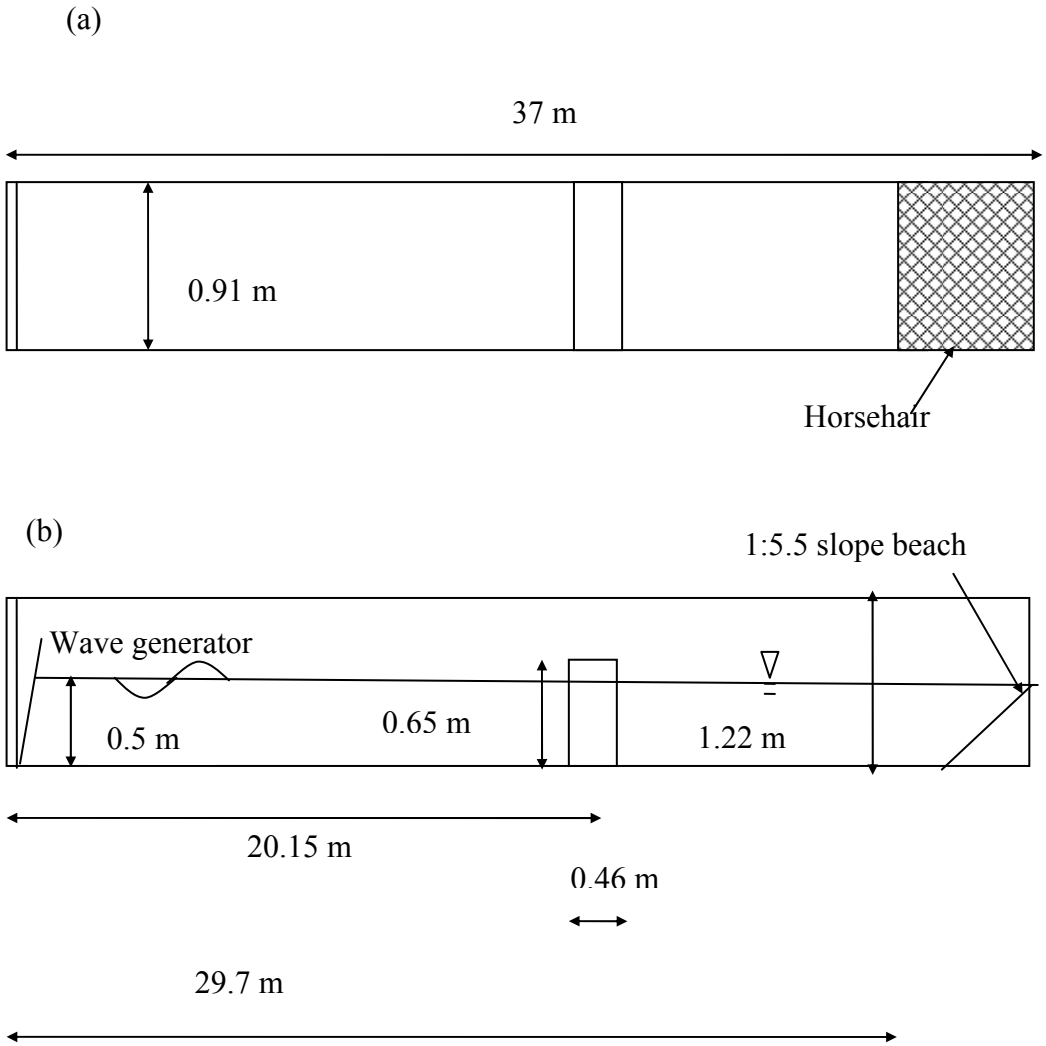

Fig. 2.1. Wave tank schematic. (a) Top view. (b) Side view.

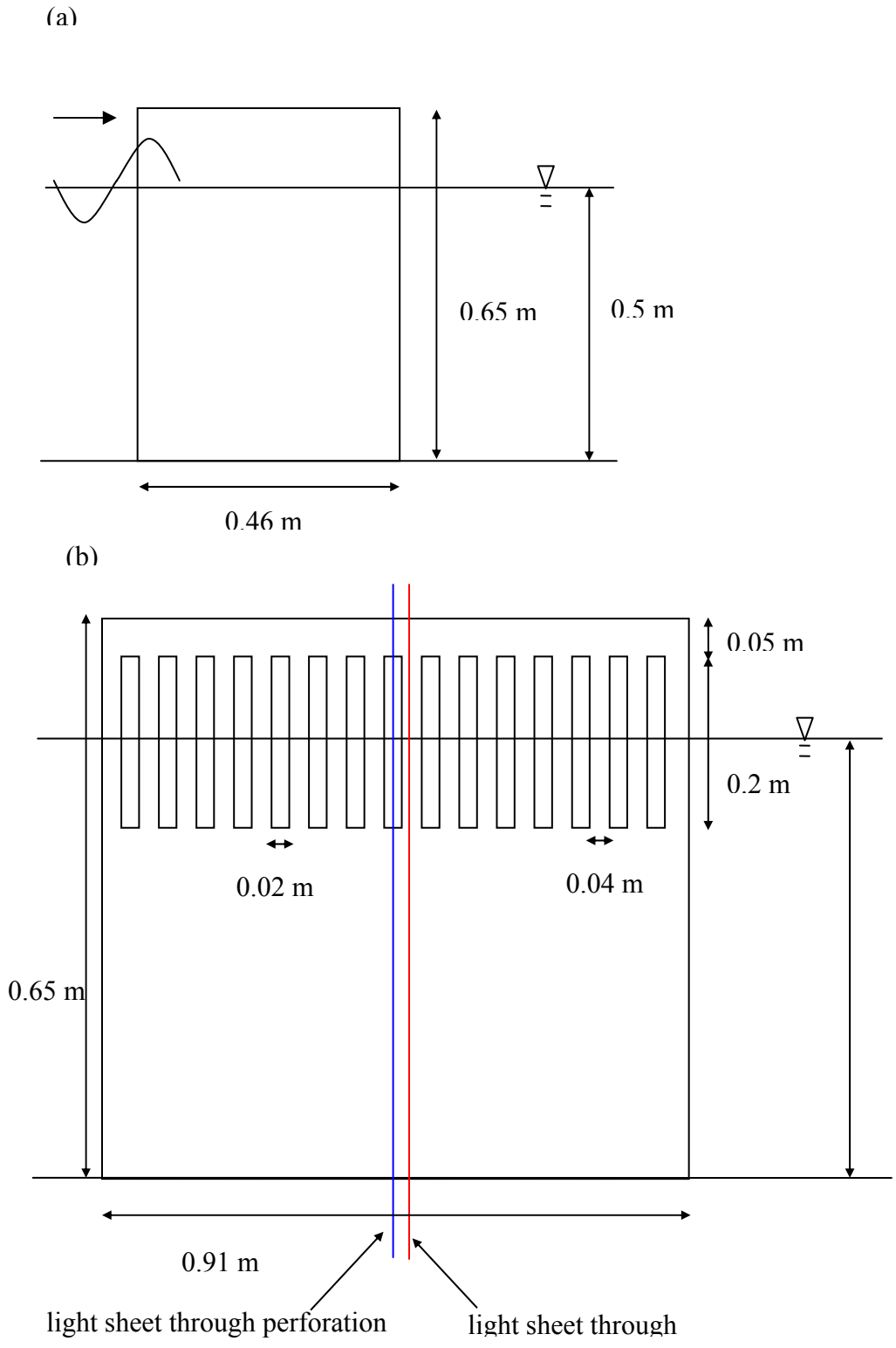

Fig. 2.2. Breakwater model schematic. (a) Side view. (b) Light sheets.

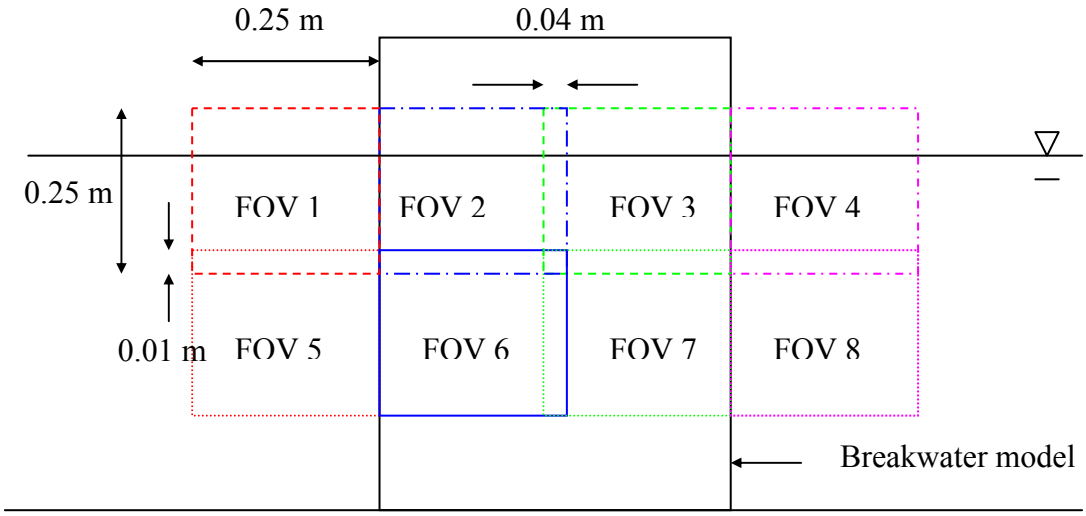

Fig. 2.3. Arrangement of field of view.

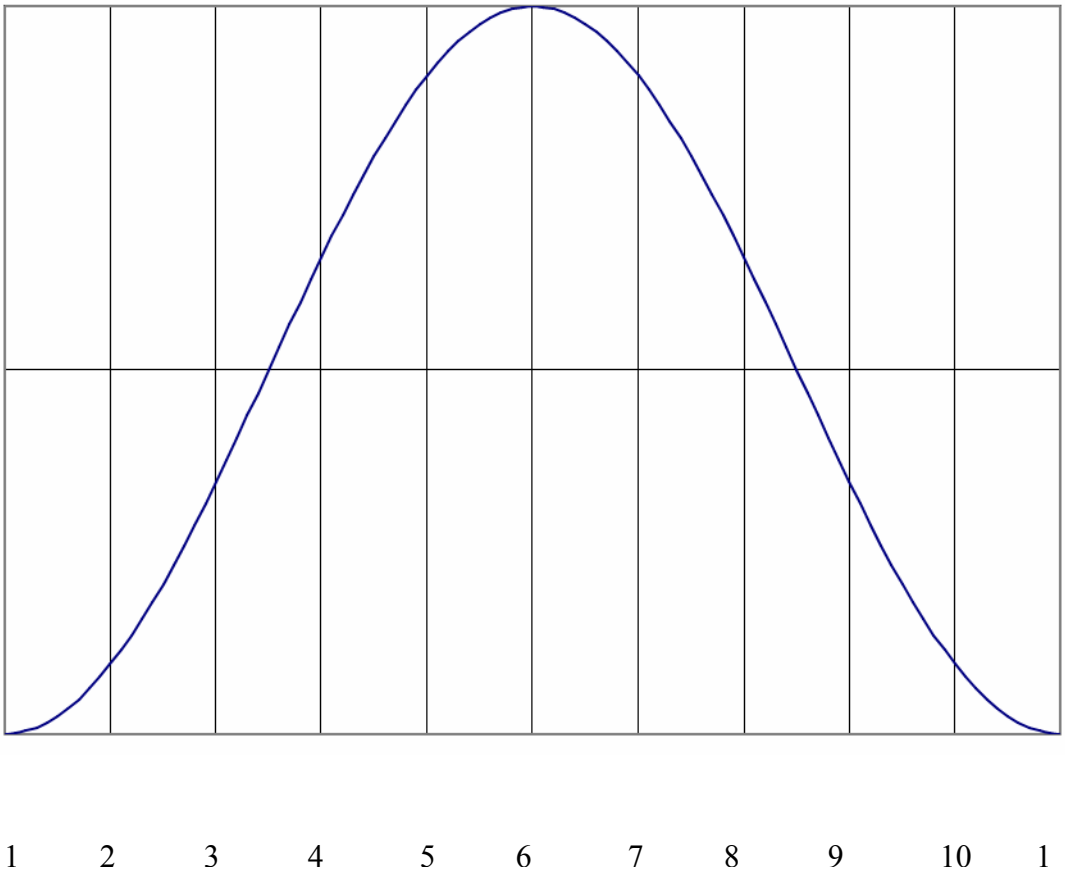

Fig. 2.4. Locations of phases in one wave corresponding to PIV velocity measurements.

Table 2-1

Wave conditions

Wave condition	Wave Period T (s)	Wave Height H_i (cm)
1	1.0	4.0
2	1.0	6.0
3	1.0	8.0
4	1.0	10.0
5	1.6	8.0
6	2.0	8.0
7	2.5	8.0

2.1 Wave maker

The wave generator is a Sea Sim Rolling Seal absorbing Wave maker (RSW 90-85), a dry back, aluminium space frame, and PVC cased, modular, hinged flap wave maker. The flap is sealed by a low friction rolling seal and is driven by a precision, electronically commutated synchronous servomotor, while being hydrostatically balanced using an automatic near constant force, pneumatic control system (Sea Sim Rolling Seal Absorbing Wave maker Manual, Data sheet RSW 382). The analog signal needed to create the required motion of the wave maker was introduced by a PC with a data acquisition board (National Instruments AT-MIO-16E-2) which generates analog output DC voltage and was controlled by a National Instrument LabVIEW program (see figure 2.5). The LabVIEW programme was made in such a way that it controlled the wave maker, the laser and the cameras simultaneously, thus the PIV measurements could be synchronized and precisely controlled.

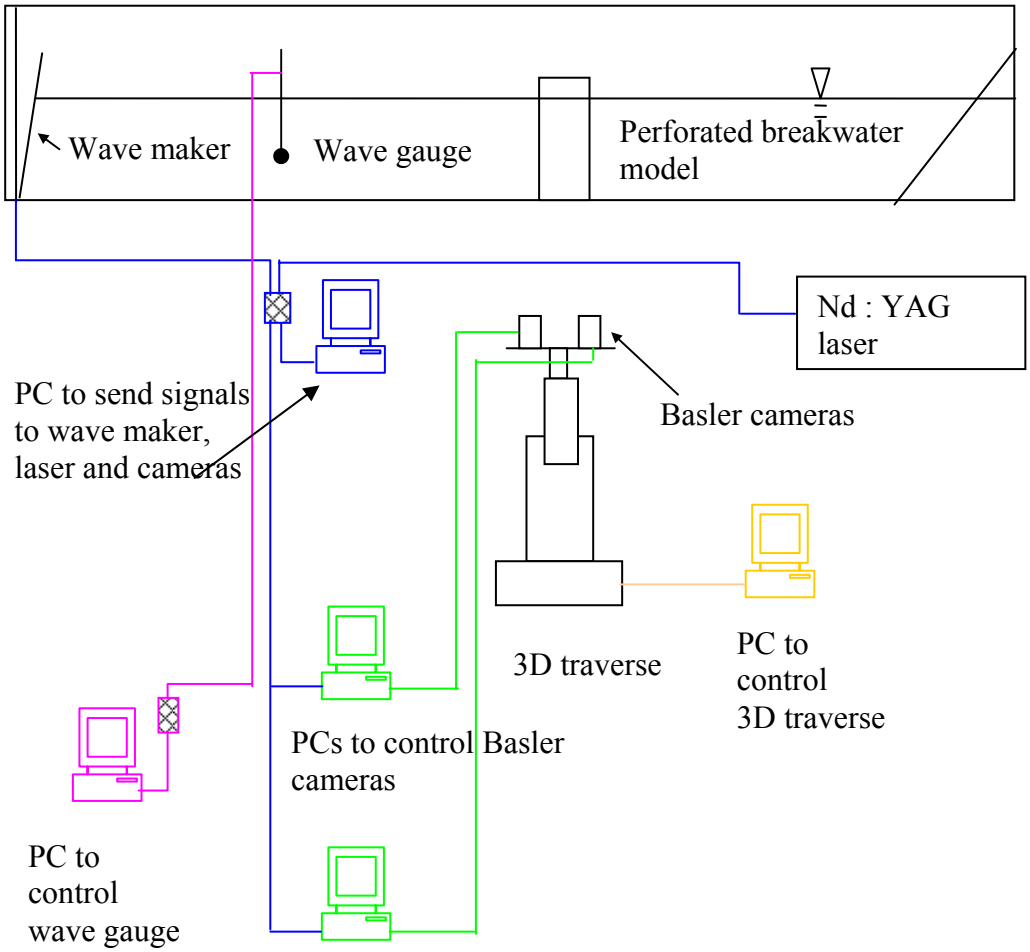

Fig. 2.5. Experimental setup.

2.2 Wave elevation data

The incoming wave height, reflected wave height and the transmitted wave height were measured using double-wire resistant-type wave gauges. An eight channel conditioner was used to generate excitation signal for the wave gauges. The return signal from the wave gauges was converted to voltage and sent to a data acquisition board (SN: CB-68LP) housed in a PC controlled by LabVIEW. The gauges were calibrated by comparing the wave gauge voltage output and the wave gauge sensor position. The accuracy of the wave gauge is ±1 mm. The incoming wave height and the transmitted wave height were directly measured (see figure 2.6). In order to measure the reflected wave height, the input time signal for the wave maker was modified (the number of waves was reduced), as a result the incoming number of waves reduced in such a way that the reflected wave was not effected by the incoming wave at the measuring location (see figure 2.7). Considering the time series of the measured wave elevation, it is possible to easily extract the incoming wave height and the reflected wave height (see figure 2.8). The elevation measurement was taken at 25 Hz for 100 seconds. Each test was repeated for three times, and the average value for all three trials was calculated.

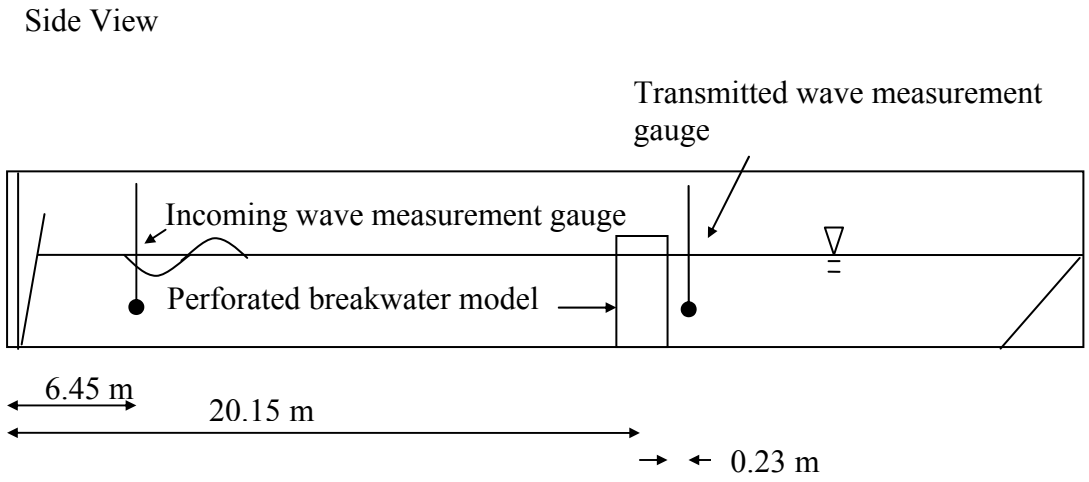

Fig. 2.6. Incoming and transmitted wave measurement gauge locations.

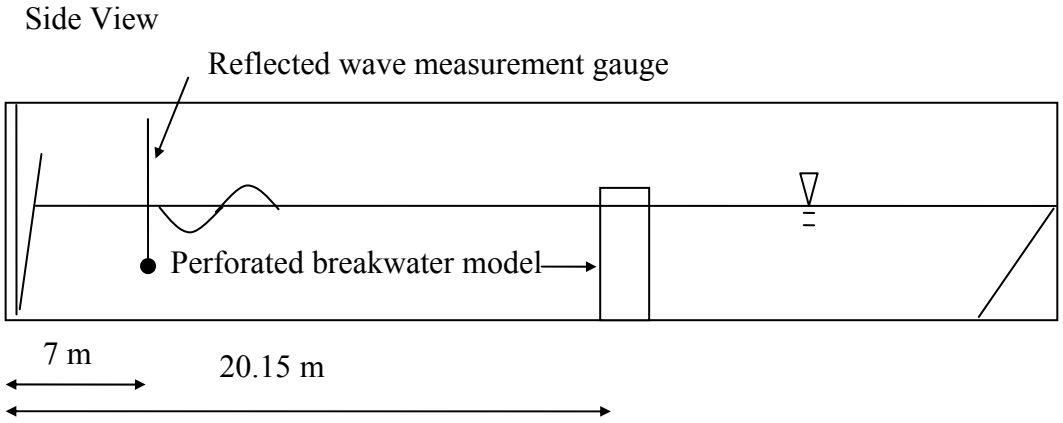

Fig. 2.7. Reflected wave measurement gauge location.

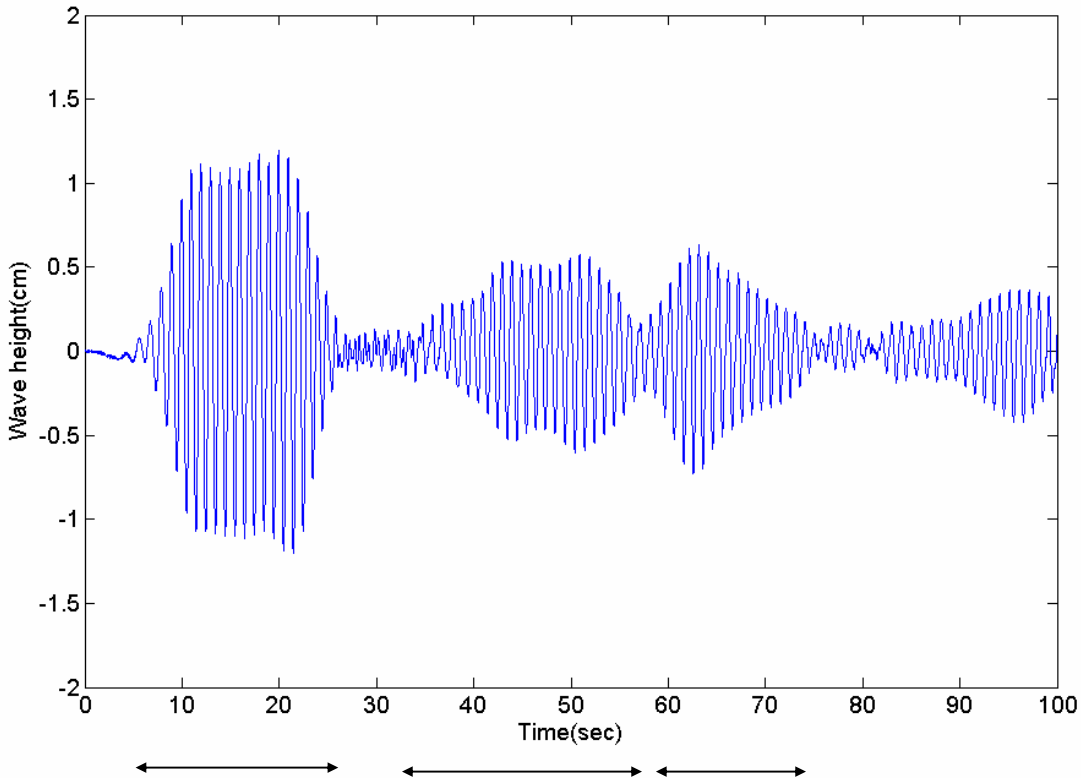

Fig. 2.8. Example of measured reflected wave elevation data.

2.3 Particle image velocimetry technique

Lack of experimental techniques suitable for measuring instantaneous whole field flow measurements was one of the major drawbacks in understanding the physics of the flows. The traditional velocity measurement techniques such as Laser Doppler Velocimetry (LDV) is a single point technique which can provide time series data of one or more velocity components of a single point, and cannot extract the time dependent structures of flows. The recently developed Particle Image Velocimetry (PIV) method has the potential to meet these challenges of measuring whole field, instantaneous velocity. PIV has its roots in flow visualization technique. The basic principle of estimating the velocity field is by measuring the motion of particles scattered in the flow. To use the PIV technique, the flow field is made visible by introducing carefully chosen small particles, which are called seeding particles. It is assumed the particles follow motion of the flow. The tracers are then illuminated by introducing a thin laser light sheet pulsing twice within a short time interval with dark background. The time tagged images of the particles are recorded electronically. The mean displacement during the short time interval is calculated using statistical correlation methods, it implicitly tracks the motion of a group of particles (in a small area called interrogation area) and extracts the mean velocity. The velocity can be calculated by measuring the motion of small particles in the fluid and by applying the definition of the velocity

$$\vec{U}(x,t) = \left[\vec{x}(t+\Delta t) - \vec{x}(t)\right] / \Delta t \qquad (2\text{-}1)$$

Where $\vec{x}(t+\Delta t)$ and $\vec{x}(t)$ are the locations of the particle at time *t* and *t+dt* respectively, and *dt* is a small time interval.

Post processing is generally applied to remove the stray vectors among the calculated velocity vectors and to interpolate the missing vectors.

2.4 Illumination

A Spectra Physics Nd: YAG laser was used as the illumination source. It offers two lasers in a single head, driven by a single compact power supply. The laser contains a crystal harmonic generator that is used to generate the frequency doubled 532 nm green light from the original 1064 nm invisible light. The laser has a maximum energy output of 400 mJ/pulse in the 532 nm wavelength and a pulse duration of 6 ns. The lasers can each pulse at a rate of 10 Hz, so that 20 pulses are generated per second. In the present study the time duration in between the pulses was kept at 3 ms.

2.5 Light sheet optics

The light sheet optics (see figure 2.9) consists of two cylindrical lenses (CSV025AR 14, PCC CYL LENS, UVFS, 19 x 50.8 x -25.4 FL and CKVS22-C, ValuMax PCC CYL LENS, 25.4 x 50.8 x -38.1FL), two circular mirrors and a flat

rectangular mirror. The cylindrical lenses have negative focal lengths and were used to diverge the laser beam into a thin light sheet.

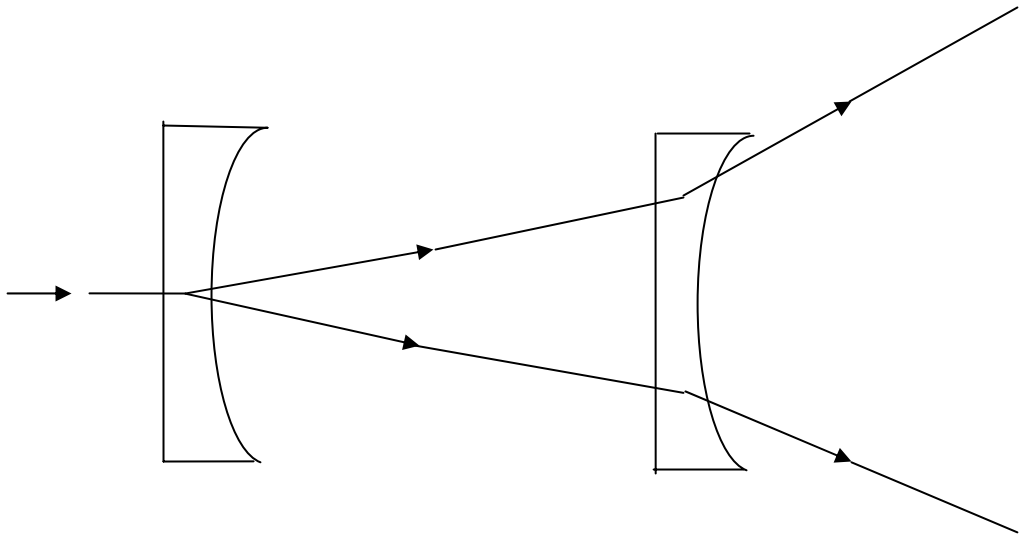

Fig. 2.9. Light sheet optics.

2.6 Seeding particles

The seeding particles used in the PIV experiments were Vestosint 2157 Natural made by Degussa-Huls company in Germany. The particles have a mean diameter of 57 μm and a specific gravity of 1.02. For each run, the seeding particles were introduced at

the measurement location and the water was stirred manually to mix the particles, followed by 5-6 minutes of waiting before starting the wavemaker.

2.7 Image recording

Two Basler A202K (1004 pixels H, 1004 pixels V), 10 bit, max frame rate 48 frames/sec cameras with Nikkon 50 mm lenses were used to capture the images. Focusing, aperture setting, illumination condition, particle image size and intensity were adjusted according to the required quality by inspecting the image shown in computer monitor. Camera aperture was set to f/4. Two frame single pulse method was used in recording the images (see figure 2.10). The input signal is shown in figure 2.10. The high and low signals indicate opening and closing of the camera shutter respectively. The input signal controls the shutter speed and the framing rate and it was set to have a single pulse on each frame.

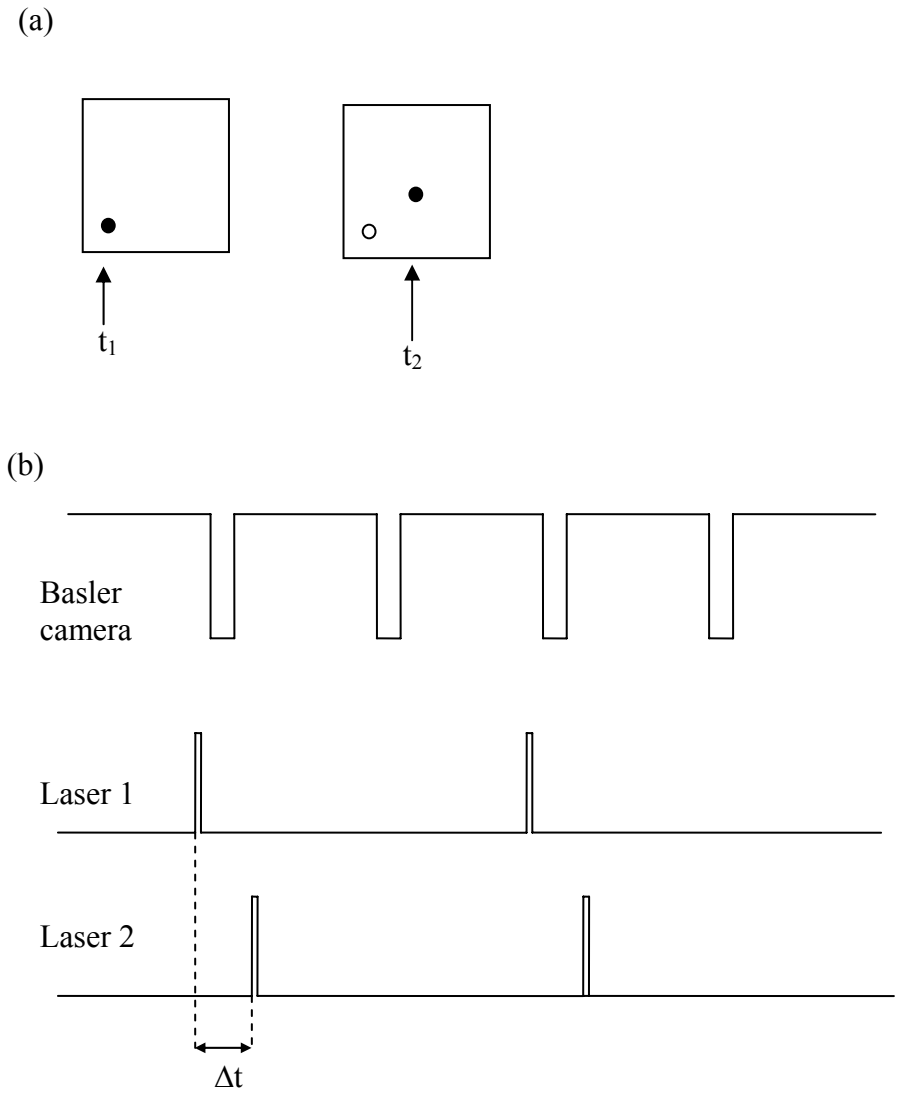

Fig. 2.10. Two frame / single - pulsed method. (a) Image recording technique. (b) Image recording trigger signals.

2.8 3D traverse

A Dantec Measurement 3D traverse (SN 199, EO No 55883) was used to move the cameras to the required positions. The movement is controlled by a PC software, 'Flow'. The resolution is 12.5 μm and the ranges are X-600mm (horizontal), Y-590mm (horizontal), Z-940mm (vertical).

2.9 Image processing

Image processing and post processing were done using MPIV toolbox (Mori & Chang, 2003) and DaVis 5.4.4, from LaVision (a commercial software). MPIV is a PIV toolbox written in Matlab. Davis is a stand-alone software product with a rich graphical user interface that supports image capturing functions, real time processing functions and post processing functions (La Vision, 2000). Statistical methods are used to compute the mean particle displacement in a small area called an interrogation area. Initially the velocity vectors were calculated for a 64 x 64 pixels interrogation area, then the calculated values were used and the velocity vectors were again calculated for a smaller area of 32 x 32 pixels. The cross correlation method was used with 50% overlap between interrogation areas.

The cross correlation,

$$R(\vec{s}) = \int I(\vec{x}) \cdot I'(\vec{x} + \vec{s})\ d\vec{x} \qquad (2\text{-}2)$$

Where $\vec{s}$ is a two dimensional displacement vector and I and I' are the image intensity field of the first and second interrogation area. R gives the correlation strength in displacements between the two interrogation areas (Raffel et al., 1998). The maximum displacement of s has to be less than one third of the width of the integration area in order to have enough particle pairs in the interrogation cell. Hence the particle maximum velocity was calculated based on linear wave theory and the time interval in between consecutive images was selected as 3ms. After the images were processed, post processing was applied. The first step was to filter the stray vectors using a median filter (Raffel et al., 1998). It compares the vector with average vector ± standard deviation from eight neighboring vectors for the validity of the vector when filtering, and the vectors, which are not valid, will be removed. Once the bad vectors are removed the spaces were filled using kriging interpolation. It calculates the required vector considering the nine neighboring vectors with a weighting function, which depends on the overlap areas with the respective vector. Finally the smoothing of vectors was applied. Smoothing also considers the nine neighboring vectors.

By repeating the experiments velocity field, vorticity, turbulence intensity and the turbulent kinetic energy were calculated and presented for each phase and for each wave condition. Performing phase average, the phase average velocity field, phase average vorticity field, the phase average turbulence intensity and the phase average turbulent kinetic energy for each wave condition were calculated and presented. Depth average, horizontally average and spatially average turbulent kinetic energy for each wave condition is presented and discussed. The generation, evolution and dissipation of

the vortices were investigated. The energy balance considering the wave elevation data and velocity data are discussed.

CHAPTER III

WAVE ELEVATION DATA AND EFFICIENCY OF THE STRUCTURE

In order to find the effect of wave parameters (wave height and wave period) on the efficiency of the structure, thirteen different wave conditions were tested. All the wave conditions represent intermediate depth waves. The incoming wave height (H_i), reflected wave height (H_r) and transmitted wave height (H_t) were measured for each test (see Appendix B for measured data). The measurements were taken at 25 Hz for 100 seconds. Each test was repeated three times. The average of the three tests was calculated. The incoming wave height, calculated reflected and transmitted wave heights are given in table 3-1.

Table 3-1

Calculated reflected and transmitted wave heights for different wave conditions

Wave Period, T (Sec)	Incoming wave height, H_i (cm)	Reflected wave height, H_r (cm)	Transmitted wave height, H_t (cm)
1.0	2.0	0.907	0.648
1.0	4.0	1.724	1.213
1.0	6.0	2.602	1.877
1.0	8.0	3.675	2.397
1.0	10.0	4.817	2.594
1.2	4.0	1.257	1.366
1.2	8.0	2.813	3.387
1.6	4.0	1.518	1.491
1.6	8.0	3.974	3.315
2.0	4.0	1.745	1.388
2.0	8.0	4.311	3.078
2.5	4.0	1.954	0.983
2.5	8.0	4.328	2.121

Applying linear wave theory, the wave number k was calculated iteratively,

$$\omega^2 = g\, k \tanh(kh) \tag{3.1}$$

where,

$\omega = 2\pi / T$

g – gravitational acceleration (m^2/sec)

h – water depth (m)

The wavelength, L was calculated assuming linear wave theory as,

$$L = (g\, T^2 / 2\pi) \tanh(kh) \tag{3.2}$$

The reflection coefficient K_r is defined as,

$$K_r = H_r / H_i \tag{3.3}$$

The transmission coefficient K_t is defined as,

$$K_t = H_t / H_i \tag{3.4}$$

Applying the energy balance equation for the system,

$$E_i = E_r + E_t + \varepsilon \tag{3.5}$$

where,

E_i - incoming wave energy

E_r - reflected wave energy

E_t - transmitted wave energy

ε - dissipated wave energy

Hence,

$\varepsilon = E_i - E_r - E_t$

Applying linear wave theory, per wavelength, per unit crest width

(Dean and Dalrymple (1992))

$$E_i = 1/8\ \rho\ g\ (H_i)^2 \quad (3.6)$$

$$E_r = 1/8\ \rho\ g\ (H_r)^2 \quad (3.7)$$

$$E_t = 1/8\ \rho\ g\ (H_t)^2 \quad (3.8)$$

$$\varepsilon = 1/8\ \rho\ g\ (H_i)^2 - 1/8\ \rho\ g\ (H_r)^2 - 1/8\ \rho\ g\ (H_t)^2 \quad (3.9)$$

$$\varepsilon\ /\ 1/8\ \rho\ g\ (H_i)^2 = 1 - K_r^{\,2} - K_t^{\,2} \quad (3.10)$$

The calculated reflection coefficient, transmission coefficient and dissipated energy with respect to incoming energy are shown in table 3-2.

Table 3-2

Calculated reflection coefficient, transmission coefficient and dissipated energy

T (Sec)	H_i (cm)	H_r (cm)	H_t (cm)	L (m)	B/L	h/L	H/L	k (1/m)	kh	kA	K_r	K_t	Energy Dissipation
1.000	2.000	0.907	0.648	1.513	0.304	0.330	0.013	4.153	2.076	0.042	0.454	0.324	0.689
1.000	4.000	1.724	1.213	1.513	0.304	0.330	0.026	4.153	2.076	0.083	0.431	0.303	0.722
1.000	6.000	2.602	1.877	1.513	0.304	0.330	0.040	4.153	2.076	0.125	0.434	0.313	0.714
1.000	8.000	3.675	2.397	1.513	0.304	0.330	0.053	4.153	2.076	0.166	0.459	0.300	0.699
1.000	10.000	4.817	2.594	1.513	0.304	0.330	0.066	4.153	2.076	0.208	0.482	0.259	0.701
1.200	4.000	1.257	1.366	2.048	0.225	0.244	0.020	3.068	1.534	0.061	0.314	0.342	0.785
1.200	8.000	2.813	3.387	2.048	0.225	0.244	0.039	3.068	1.534	0.123	0.352	0.423	0.697
1.600	4.000	1.518	1.491	3.078	0.149	0.162	0.013	2.041	1.021	0.041	0.380	0.373	0.717
1.600	8.000	3.974	3.315	3.078	0.149	0.162	0.026	2.041	1.021	0.082	0.497	0.414	0.582
2.000	4.000	1.745	1.388	4.056	0.113	0.123	0.010	1.549	0.774	0.031	0.436	0.347	0.689
2.000	8.000	4.311	3.078	4.056	0.113	0.123	0.020	1.549	0.774	0.062	0.539	0.385	0.562
2.500	4.000	1.954	0.983	5.239	0.088	0.095	0.008	1.199	0.600	0.024	0.488	0.246	0.701
2.500	8.000	4.328	2.121	5.239	0.088	0.095	0.015	1.199	0.600	0.048	0.541	0.265	0.637

The maximum energy dissipation is 79% and occurs for wave condition, T = 1.2 sec, H_i = 4 cm whereas the minimum energy dissipation is 56% and occurs for T = 2 sec, H_i = 8 cm. For more than 75% of the tested cases, the energy dissipation is above 69%. Thus the structure is very effective in energy dissipation.

The variations of K_r, K_t and energy dissipation with B/L for different wave heights were examined (see figure 3.1).

From the results it is clear that reflection, transmission and energy dissipation depends on the parameter B/L. Since B is a constant the variations show the effect of variation of wave period, T. The pattern of variations of K_r, K_t and energy dissipation for both H_i = 4 cm and H_i = 8 cm are similar, while the magnitudes of K_r and K_t are higher for H_i = 8 cm compared to H_i = 4 cm while the magnitude of energy dissipation (with respect to incoming wave energy) is lower for H_i = 8 cm compared to H_i = 4 cm.

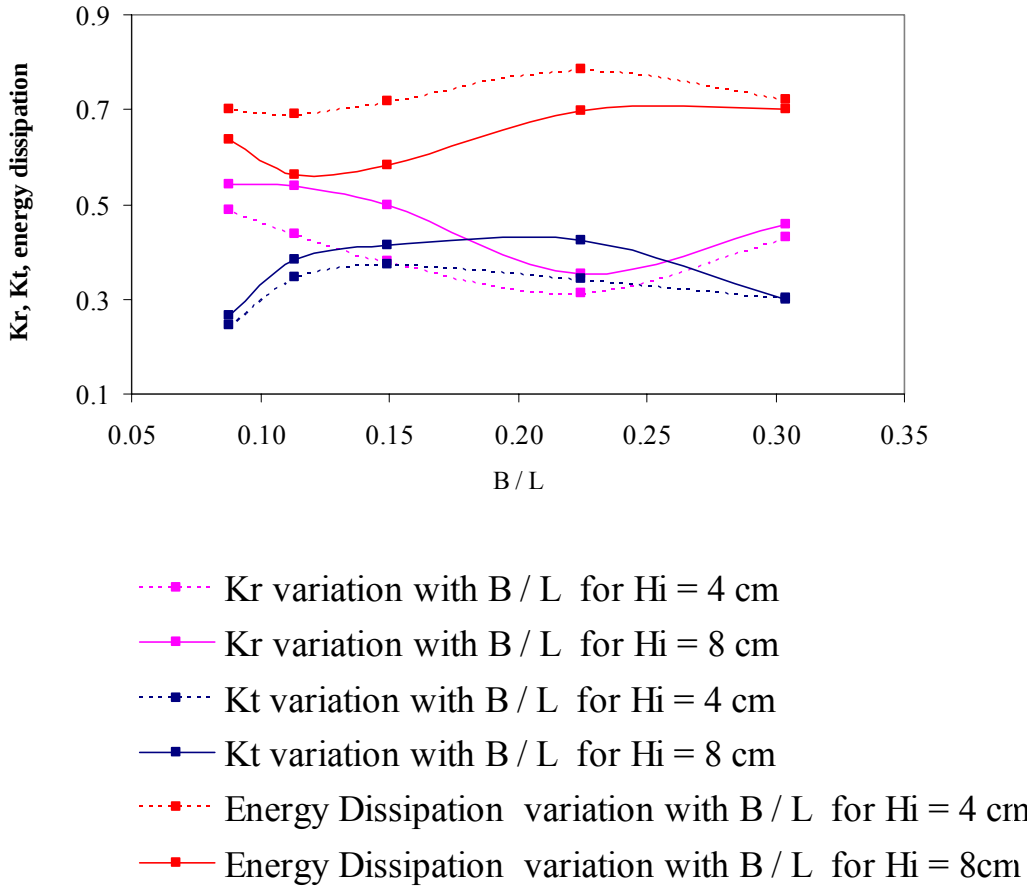

Fig. 3.1. Variation of K_r, K_t and energy dissipation with *B/L*.

The reflection coefficient decreases with increasing *B/L* till about 0.225, then it starts increasing. The minimum reflection coefficient occurs at $B/L \approx 0.2 - 0.25$. This agrees well with Kondo (1979), Suh et al., (2001) and Hagiwara (1984). Fugazza and Natale (1992) showed analytically that for regular waves, the resonance inside the chamber is important for reflection and the reflection is minimum for $B/L = (2n + 1) / 4$ ($n = 0,1,2,3$ ….) in which *B* is the width of the structure and *L* is the wave length. Suh et al. (2001) concluded that, for practical interest, due to the width limit, the fundamental mode (i.e., $n = 0$) is more important.

> They also concluded that the minimum reflection occurs at a point somewhat smaller than the theoretical value due to inertia effect. They concluded that a partial standing wave forms in front of the perforated wall due to wave reflection from the breakwater. If there is no perforated wall, the node would occur at a distance of about L/4 from the back wall of the wave chamber, and hence the largest energy loss might occur at this point because there is no inertia resistance. However, in reality there exists inertia resistance at the perforated wall, which decreases the length of the wave, thus slowing it; consequently, the location of the node will move towards the breakwater, and the distance to the point of maximum energy loss becomes less than L/4; thus, the minimum reflection occurs at a

value of B/L smaller than 0.25 (Suh et al., 2001).

The transmission coefficient increases with increasing *B/L* till about *B/L* ≈ 0.125, then starts decreasing with increasing *B/L*. The variation of transmission coefficient agrees with Hagiwara (1984).

Energy dissipation pattern for H_i = 4 cm and H_i = 8 cm are same, but energy dissipation is higher for H_i = 4 cm for all *B/L* compared to H_i = 8 cm. Minimum energy dissipation is at *B/L* = 0.113. For the tested wave conditions, the energy dissipation lies between 56% and 78%. For more than 75% of the tested cases, the energy dissipation is above 69%. This means the structure is very effective in energy dissipation. For small waves (ex H_i = 4 cm), the energy dissipation does not change much with *B/L*, but for larger waves (ex H_i = 8 cm) the energy dissipation varies in a wider range with *B/L*, decreasing with *B/L* till *B/L* ≈ 0.115 then increasing. For larger *B/L* (ie small *L* or smaller *T*) the energy dissipation is higher. For small wave conditions (small *T* and small H_i) the structure is more effective in energy dissipation than for large wave conditions (large *T* and large H_i).

Fewer vortices form for small waves compared to larger waves. For small waves most of the energy dissipation is due to inertia at the slots. For larger wave conditions, more small vortices form, hence the energy dissipation is due to turbulent kinetic energy dissipation. Even though the total energy dissipation per wavelength is higher for higher wave conditions the energy dissipation compared to incoming wave energy is higher for small wave conditions.

The variations of K_r, K_t and energy dissipation with kA for constant wave period were examined in order to study the effect of wave height on energy dissipation (see figure 3.2).

For a constant wave period, the reflection coefficient, transmission coefficient and energy dissipation does not change much with wave steepness (i.e. with wave height). For all five wave heights tested, the energy dissipation stays around 70%, whereas the reflection coefficient stays at 0.5 and the transmission coefficient, which represents the efficiency of the structure, stays at 0.3.

The variations of K_r, K_t and energy dissipation with kA were examined in order to study the effect of wave steepness (see figure 3.3).

All reflection coefficient, transmission coefficient and energy dissipation vary with kA. For kA less than 0.25 reflection coefficient, transmission coefficient and energy dissipation vary in a large range with kA, but for kA larger than 0.25 the above parameters stay constant.

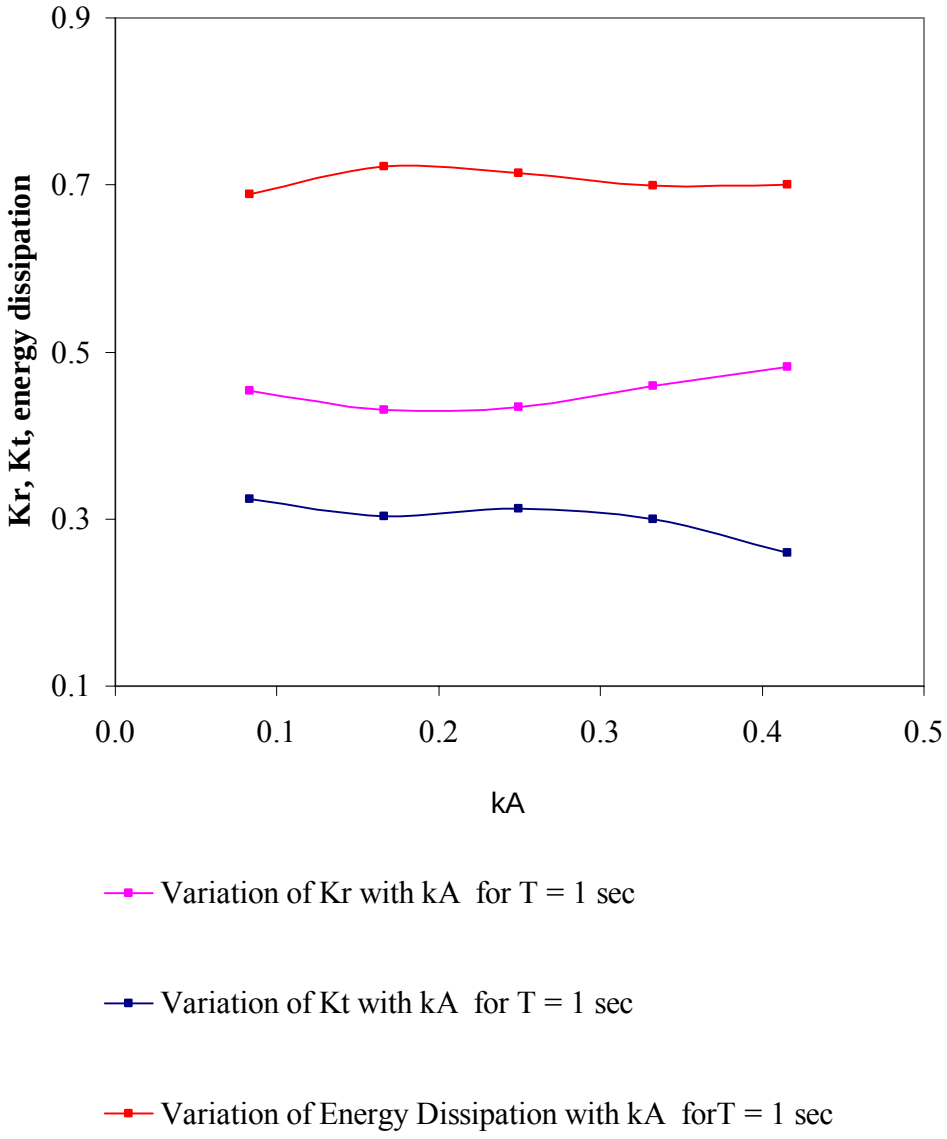

Fig. 3.2. Comparison of reflection coefficient, transmission coefficient and energy dissipation with wave steepness for constant wave period.

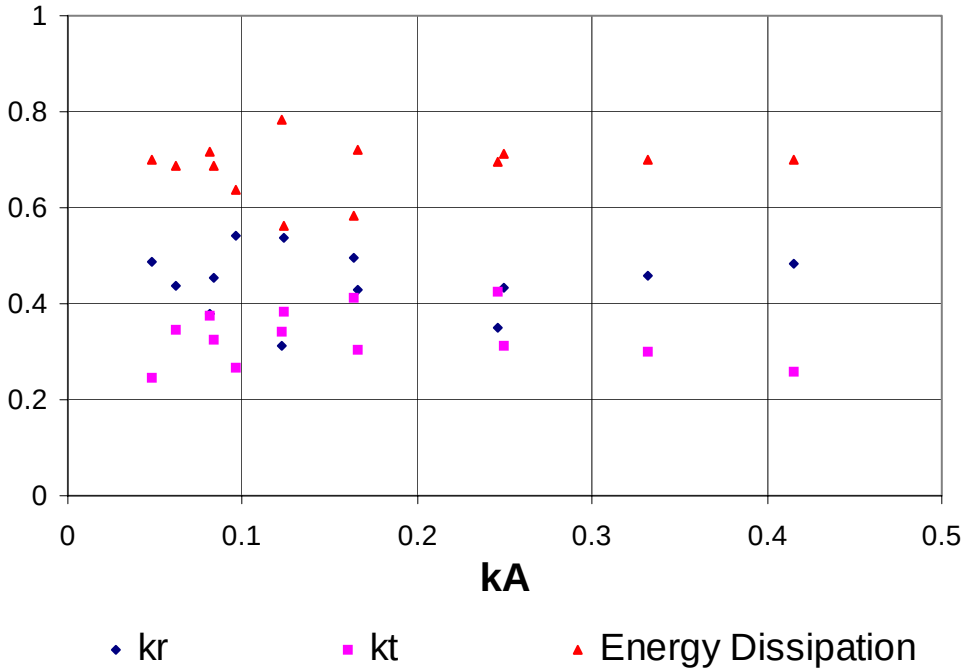

Fig. 3.3. Variations of reflection coefficient, transmission coefficient and energy dissipation with kA.

CHAPTER IV

VELOCITY FIELD IN THE VICINITY OF THE STRUCTURE

In order to find the effect of wave conditions on the flow around the structure, seven different wave conditions were selected (see table 4-1). All wave conditions represent intermediate depth wave conditions. Each test was repeated three times.

The images were analyzed using MPIV matlab tool box (Mori & Chang, 2003). For some of the images, MPIV did not give velocity vectors for some areas. For those cases DaVis 5.4.4, from LaVision (a commercial software for PIV) was used. Laser cannot penetrate through bubbles. For some tested wave conditions flow near free surface and near front wall gets very complex and bubbles form. Hence for those conditions images have some dark areas where no particles can be seen. In finding the correlation, Davis 5.4.4 has several options, one is 'Normalized'. In 'Normalized' option for normalization the average of the individual interrogation windows is used as reference. This means that even matching dark areas contribute to the correlation. Hence Davis 5.4.4 gives better results than MPIV for images which have dark areas due to no laser penetration.

Since the whole image is considered by the software program in interpolation function, it is required to first crop the image to give only the required area (the area below the water surface, where we need the flow velocity to be calculated) as input. After modifying the input image, either MPIV or DaVis was used to analyze the data as required (see figure 4.2).

Once the velocity vectors were calculated, the stray vectors were removed using median filter (Raffel et al., 1998) (see figure 4.3 a). In the median filter method the vector of interest is calculated as average vector ± standard deviation considering eight neighbouring vectors. The middle vector is compared with the calculated value and will be removed if not valid.

After removing the stray vectors, the spaces were filled using kriging interpolation and the velocity vectors were smoothed to remove sudden changes in velocity (see figure 4.3 b). Kriging is a minimum error-variance estimation algorithm. It calculates a value based on weighted combination of neighbouring points by minimizing the variance of the estimation errors (Deutsch C.V., & Journel, A.G., 1998). Smoothing was done using a weighted method based on eight neighbouring points. The weighted coefficients were calculated considering the overlap area with respect to the middle point (Chang, 1999).

A mask was applied to remove the vectors above the free surface. The final velocity field can be obtained after adding the area above the free surface (see figure 4.4).

The velocity vector field was calculated as mentioned for all the raw images for each FOV. In order to get a representative velocity map for a phase the average of all available instantaneous velocity fields for that particular phase was calculated. In order to get the complete velocity field for the desired area, eight FOV were added together (see figure 4.5). The phase averaged velocity field was calculated by taking the average

of the velocity matrices for the ten phases (see figure 4.6 and 4.7). This was done for all wave conditions.

Table 4-1

Wave conditions used in flow behaviour study

Wave condition	Wave Period (s)	Wave Height (cm)
1	1.0	4.0
2	1.0	6.0
3	1.0	8.0
4	1.0	10.0
5	1.6	8.0
6	2.0	8.0
7	2.5	8.0

Examples of images taken at time t and t+Δt are shown in Fig. 4.1.

(a)

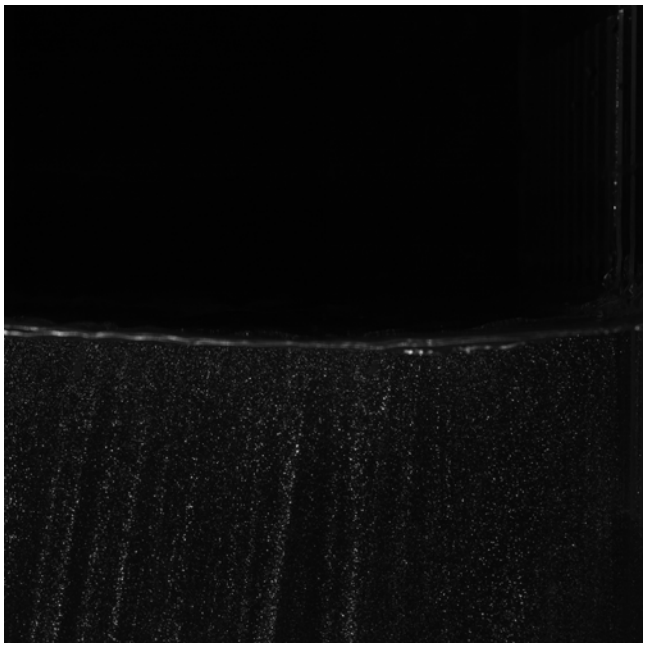

(b)

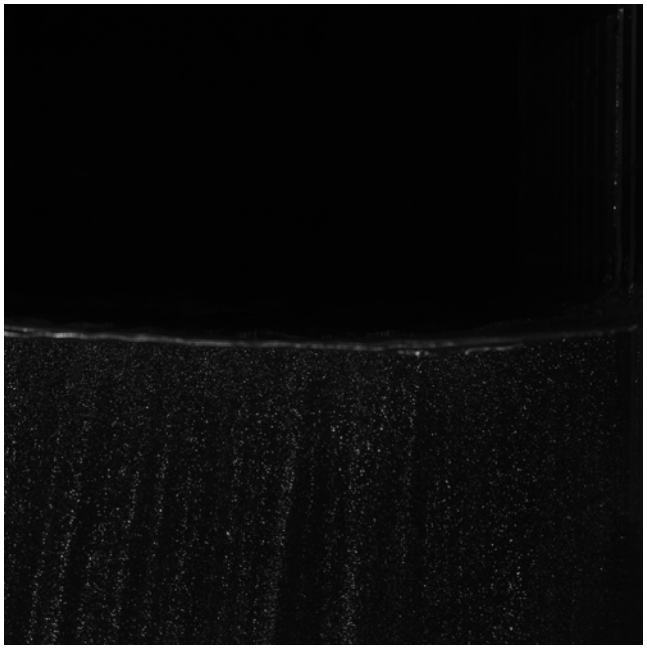

Fig. 4.1. (a) Raw image 1, image taken at t. (b) Raw image 2, image taken at $t+\Delta t$.

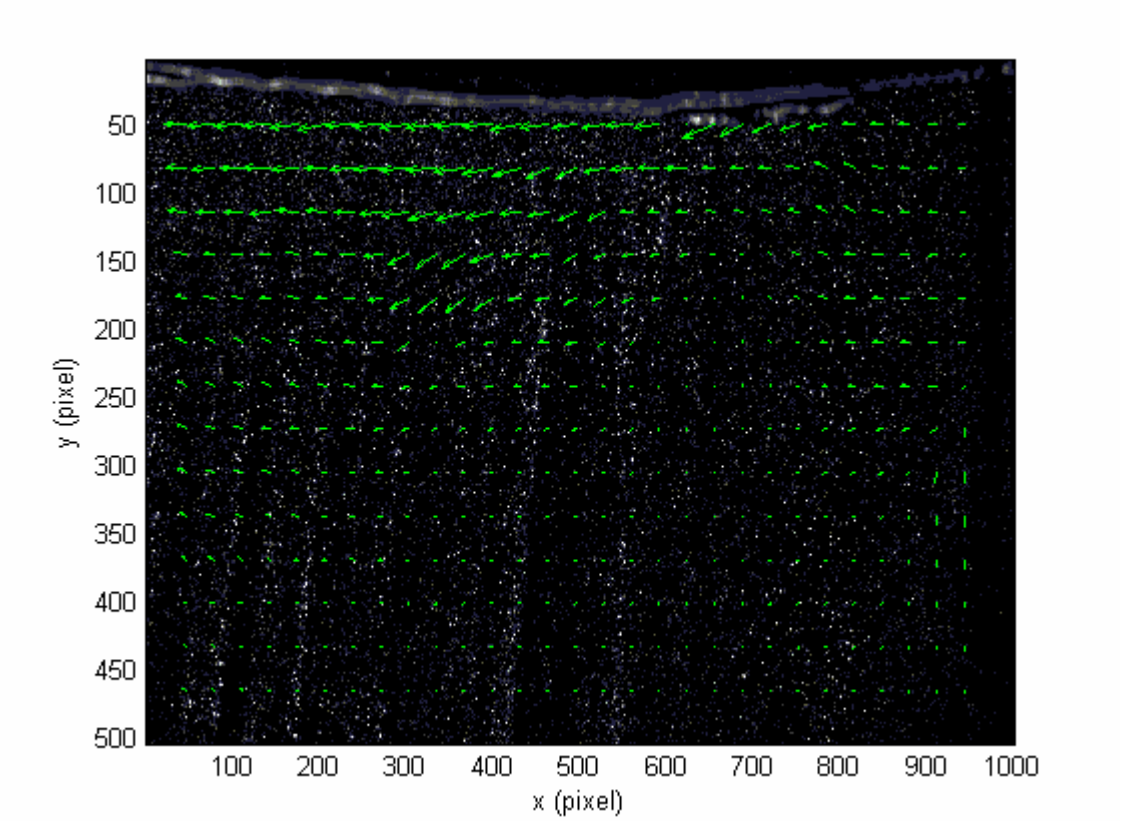

Fig. 4.2. Calculated velocity data using MPIV.

(a)

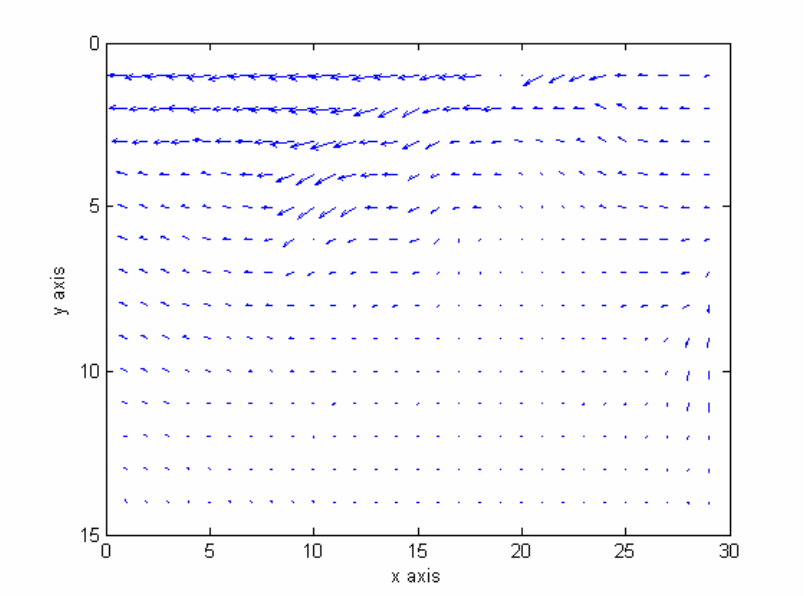

(b)

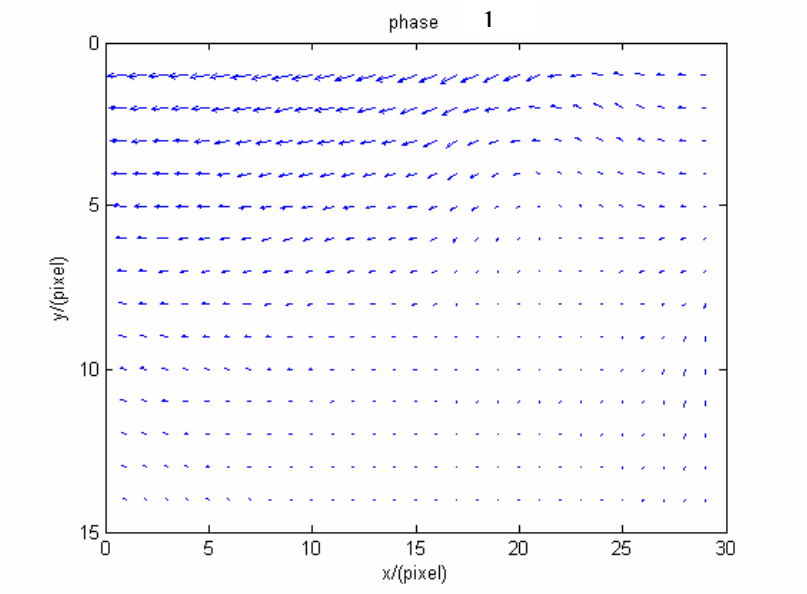

Fig. 4.3. (a) Velocity vector field after removing bad vectors using median filter. (b) Velocity vector field after applying kriging interpolation to fill the spaces and smoothing.

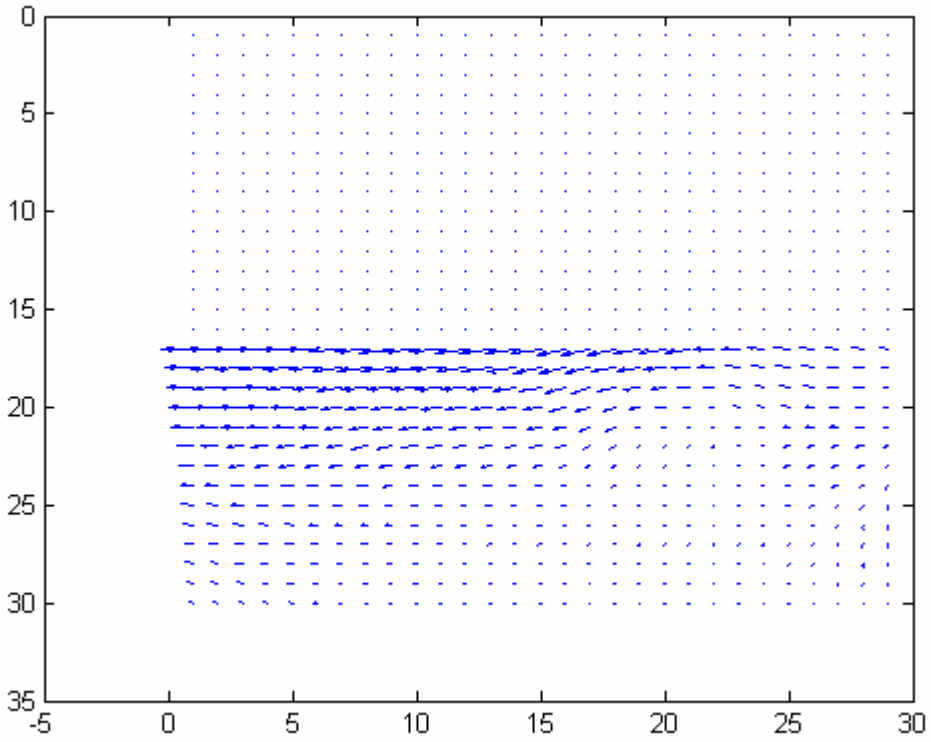

Fig. 4.4. Final velocity field (after adding the area above the free surface).

For each phase after calculating the velocity field for all eight FOV, they were added together to find the velocity field in the vicinity of the structure.

(a)

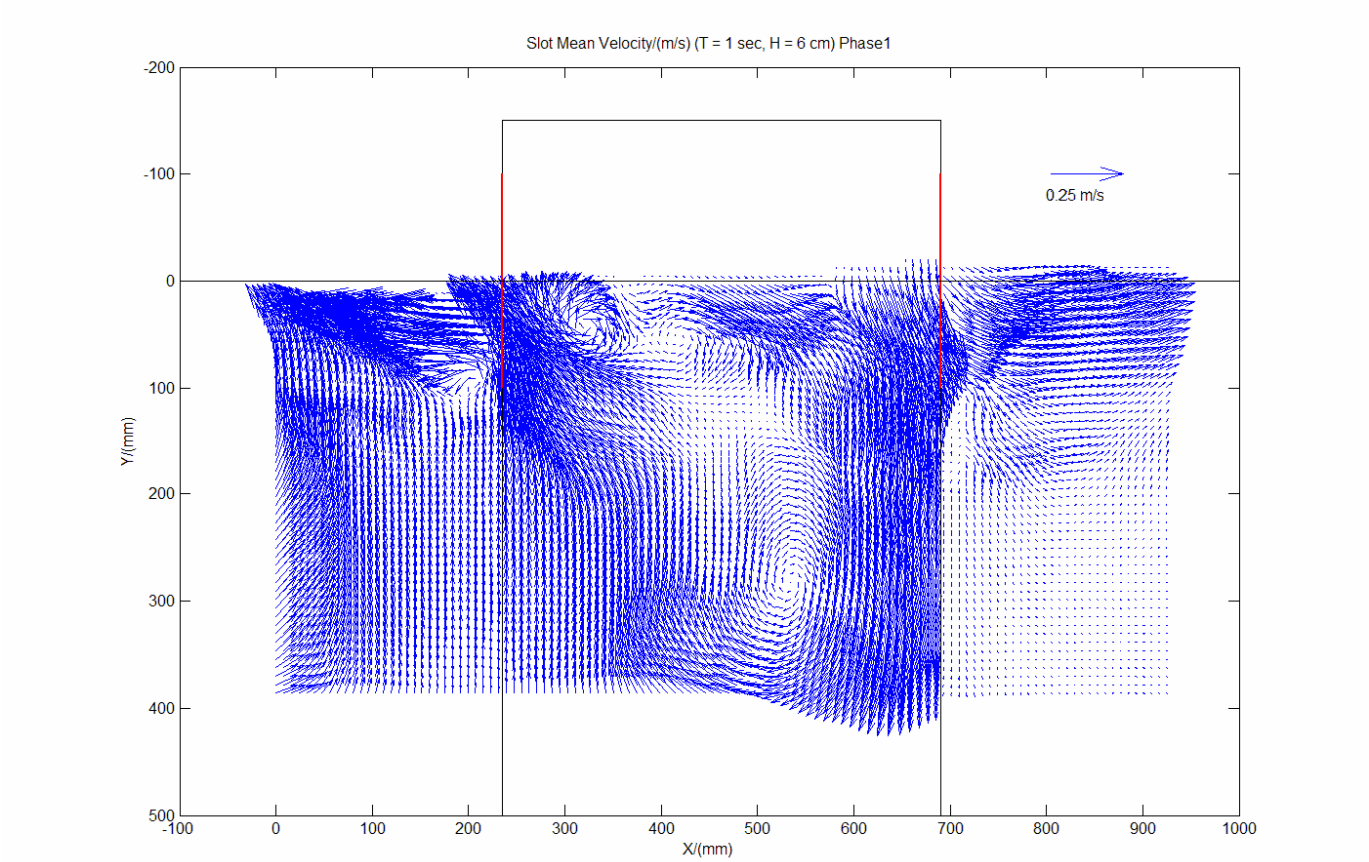

Fig. 4.5. Velocity fields through slot for wave condition, $T = 1$ sec $H_i = 6$ cm. (a) Phase 1. (b) Phase 2. (c) Phase 3. (d) Phase 4. (e) Phase 5. (f) Phase 6. (g) Phase 7. (h) Phase 8. (i) Phase 9. (j) Phase 10.

(b)

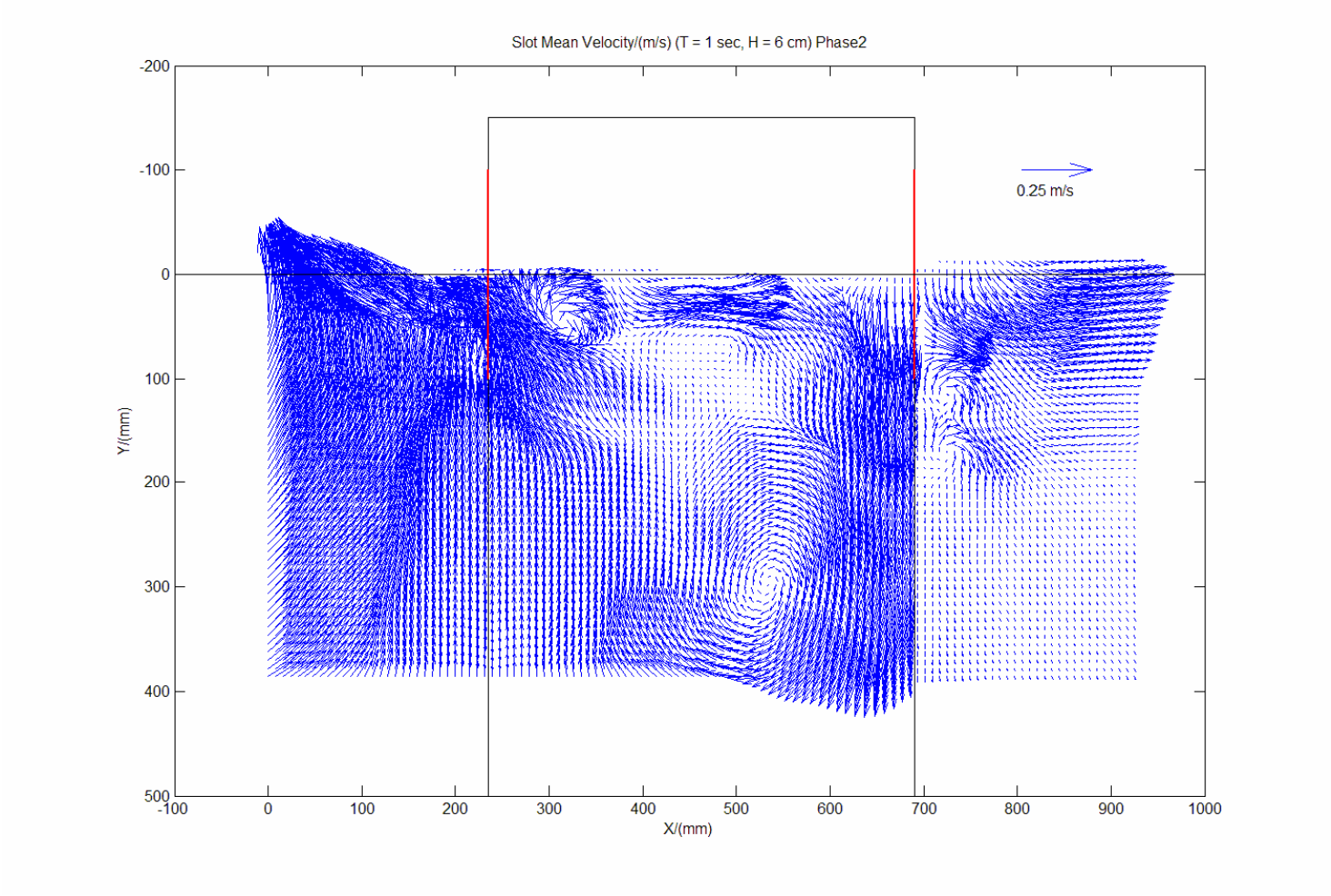

Fig. 4.5. continued.

(c)

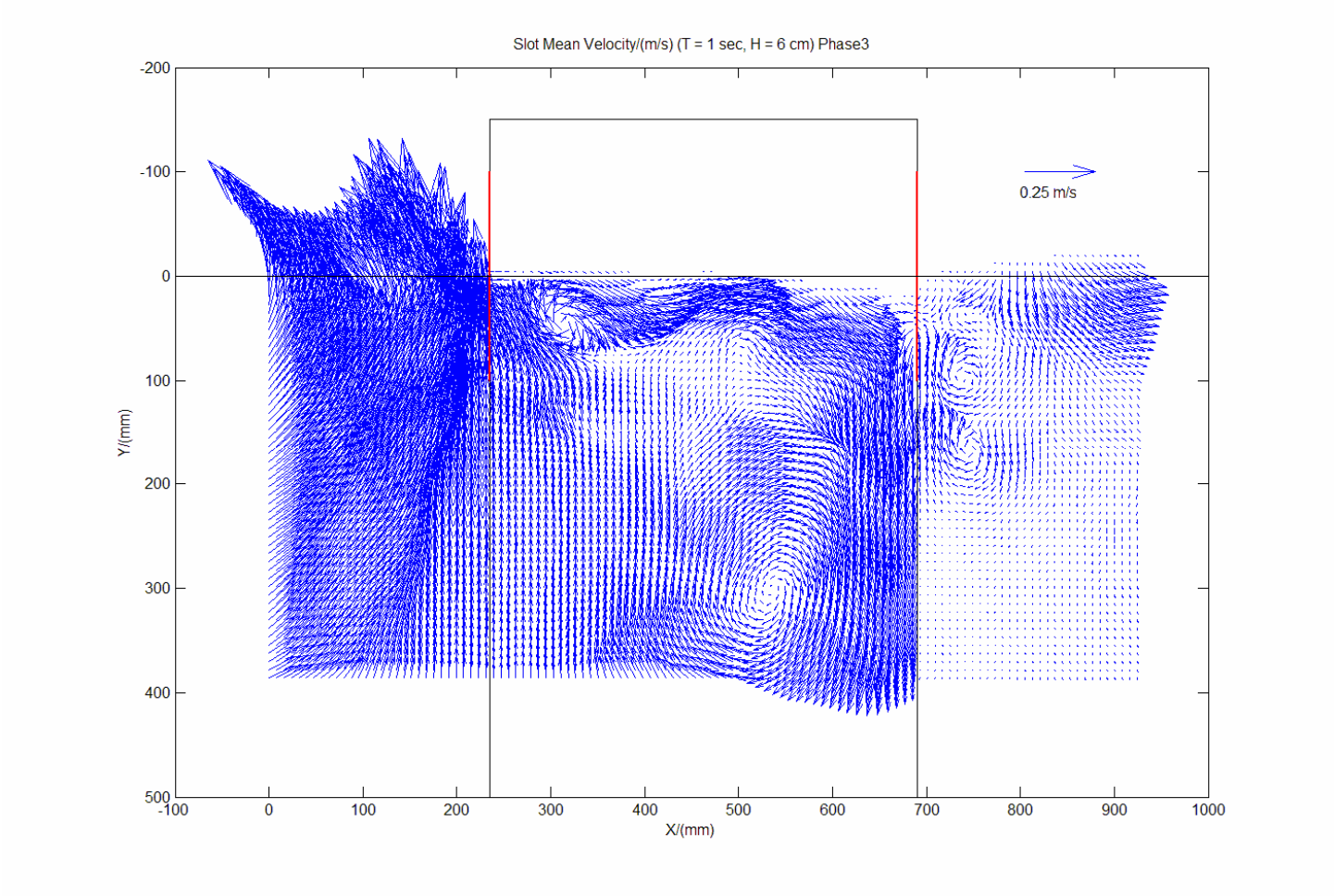

Fig. 4.5. continued.

(d)

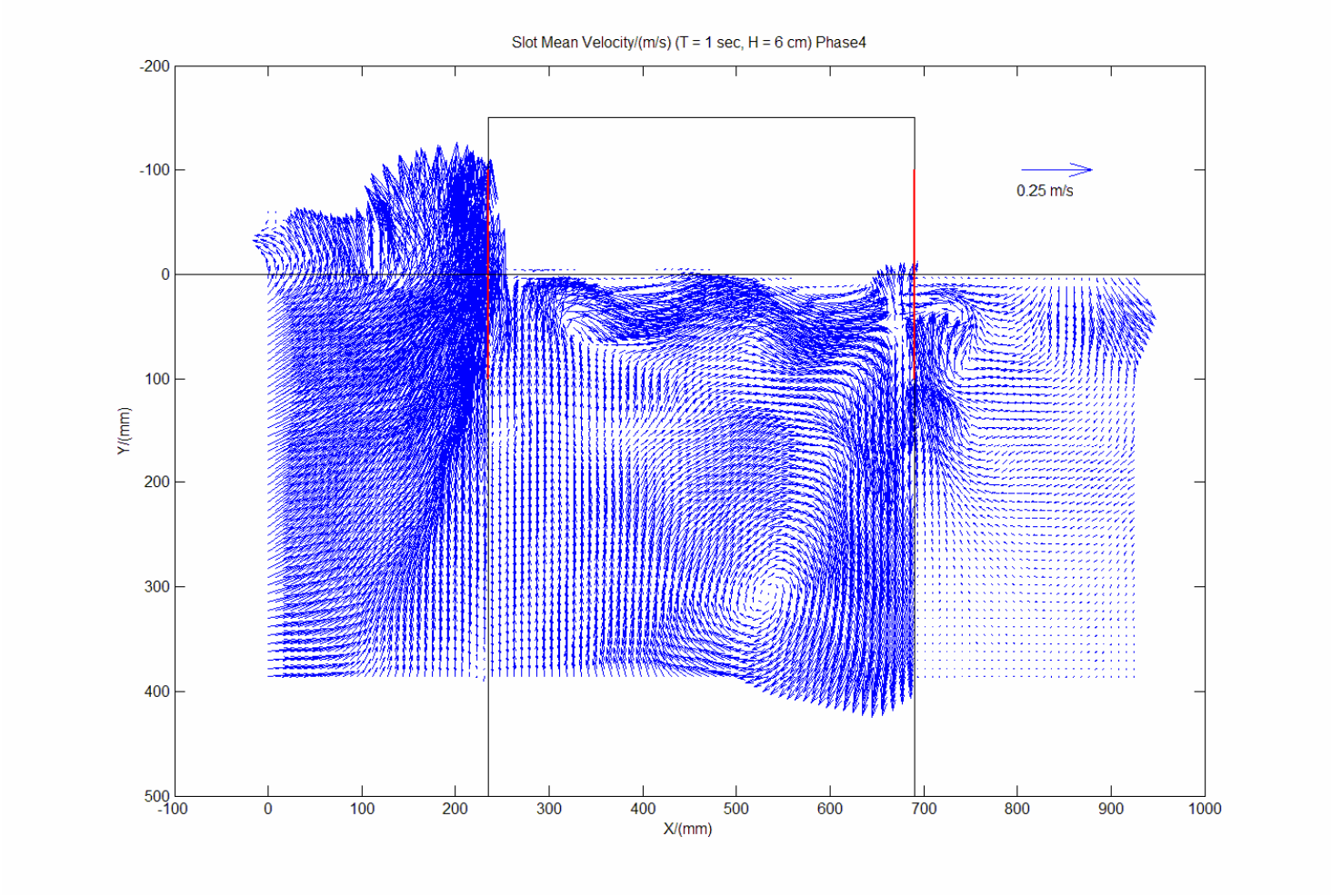

Fig. 4.5. continued.

(e)

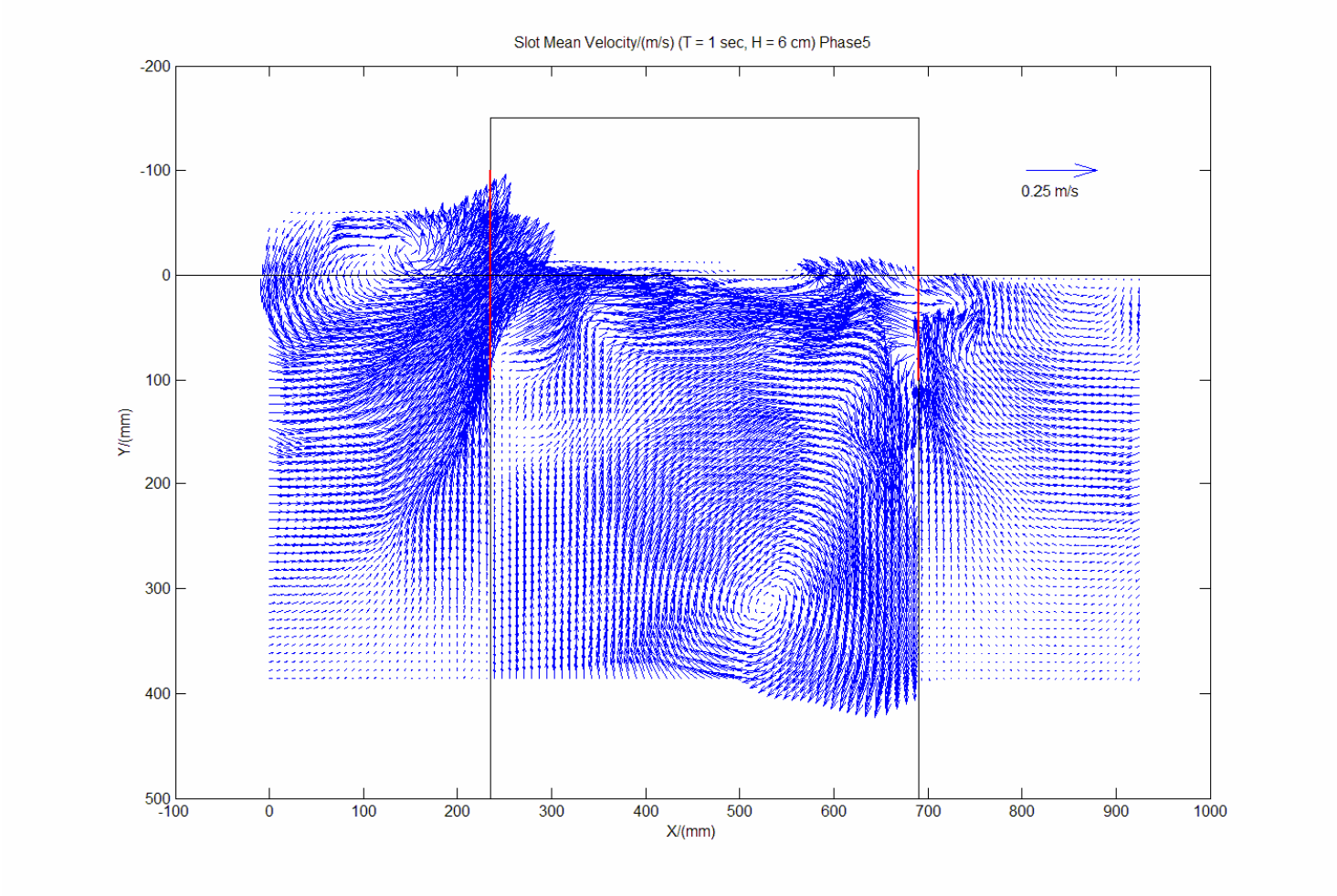

Fig. 4.5. continued.

(f)

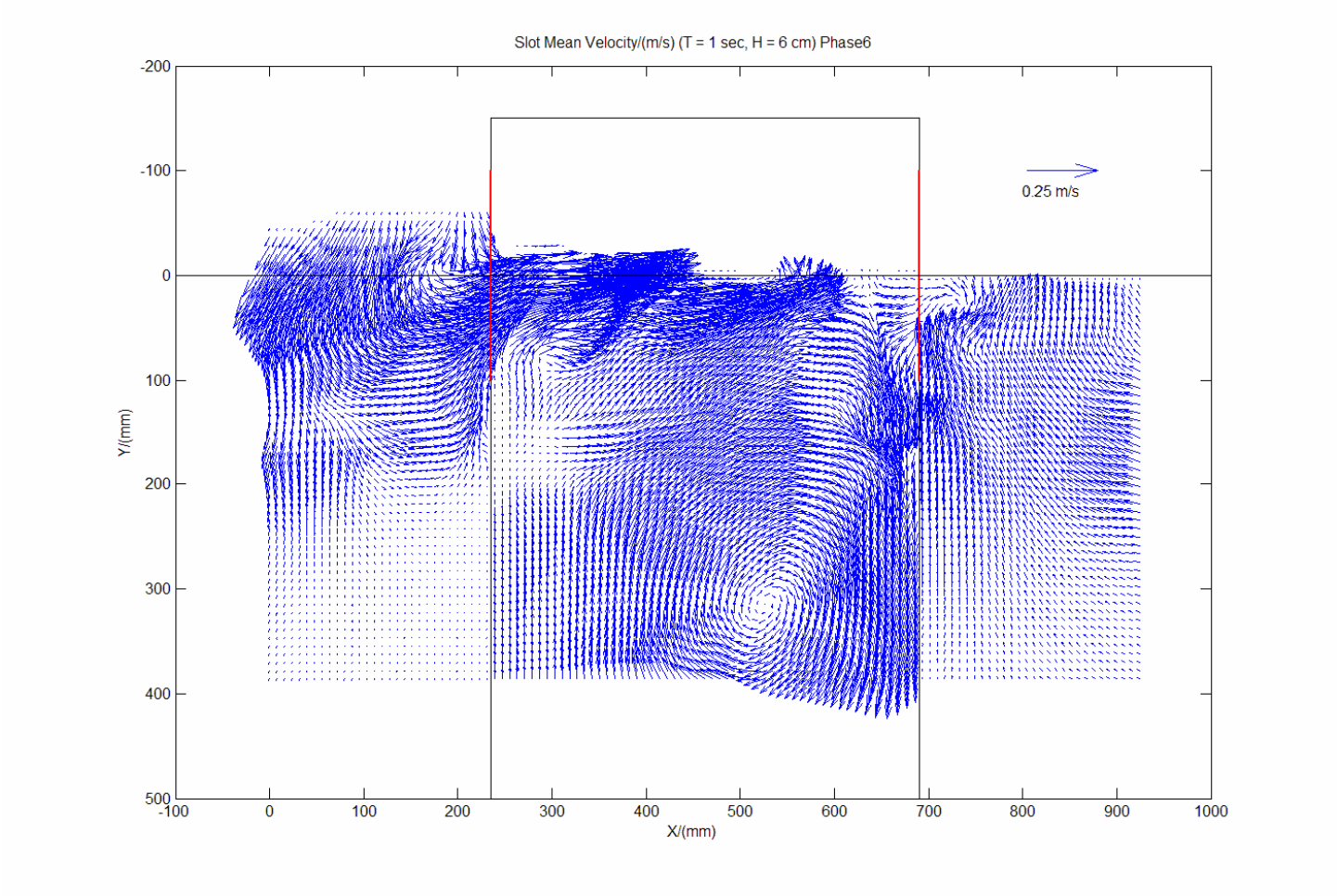

Fig. 4.5. continued.

(g)

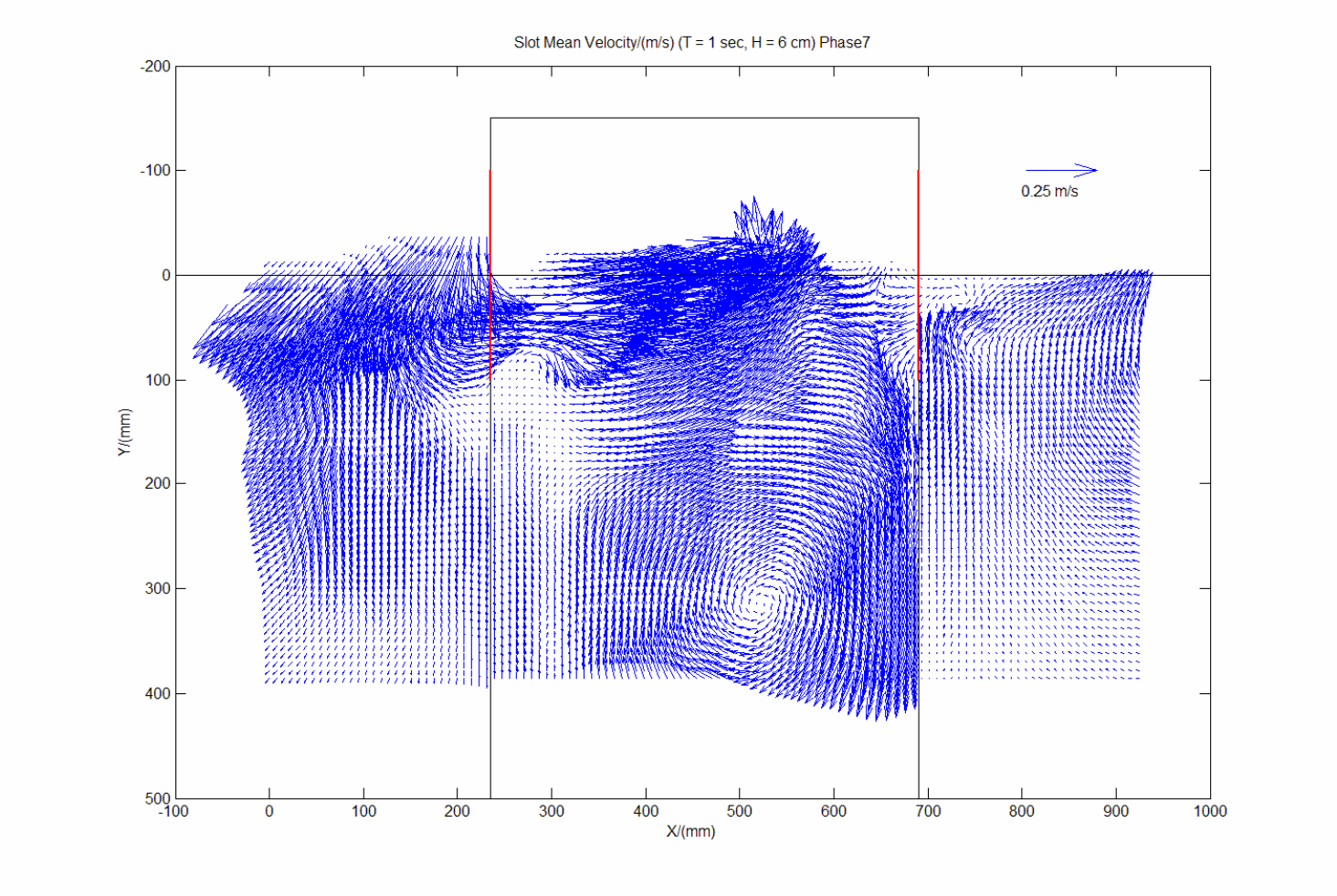

Fig. 4.5. continued.

(h)

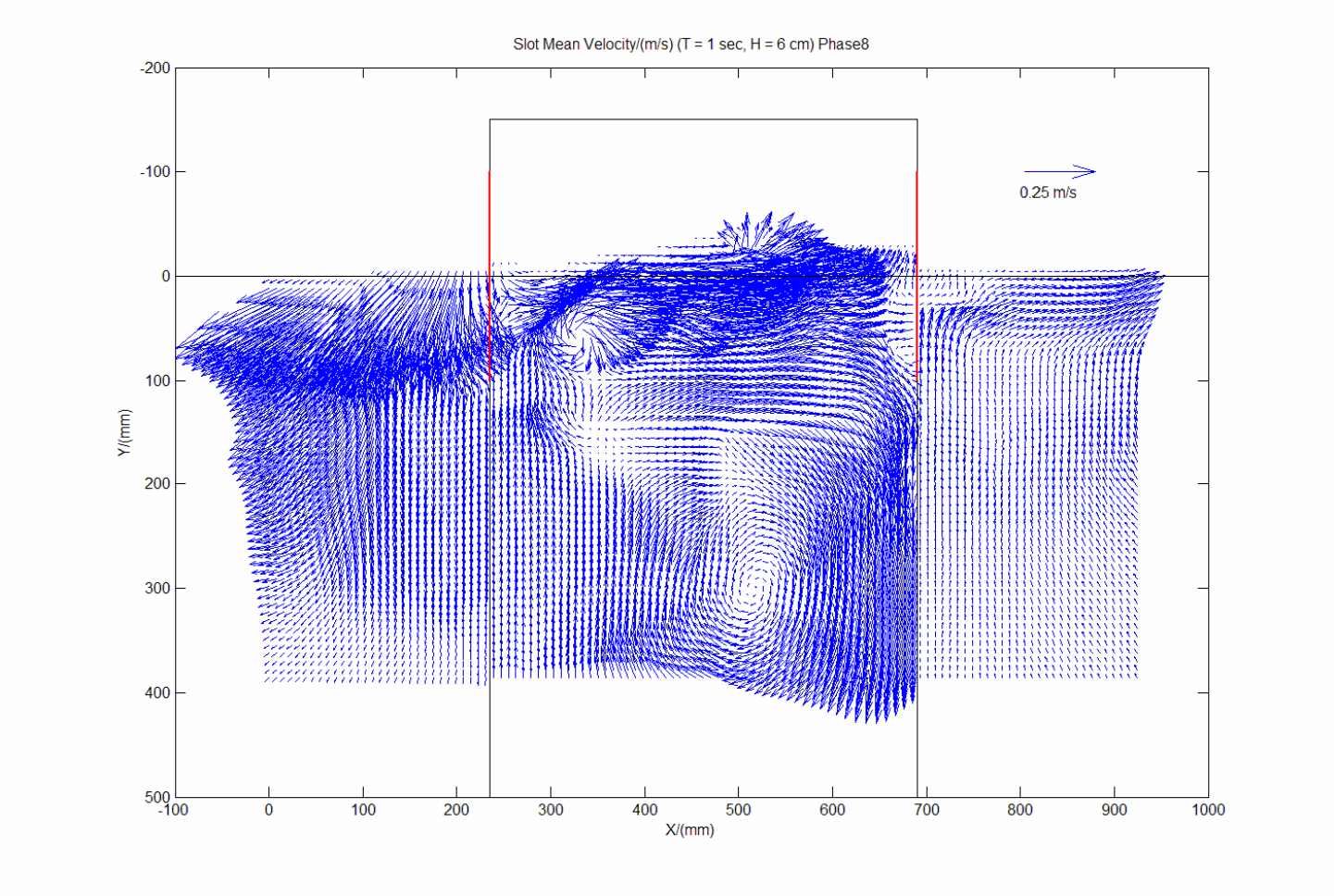

Fig. 4.5. continued.

(i)

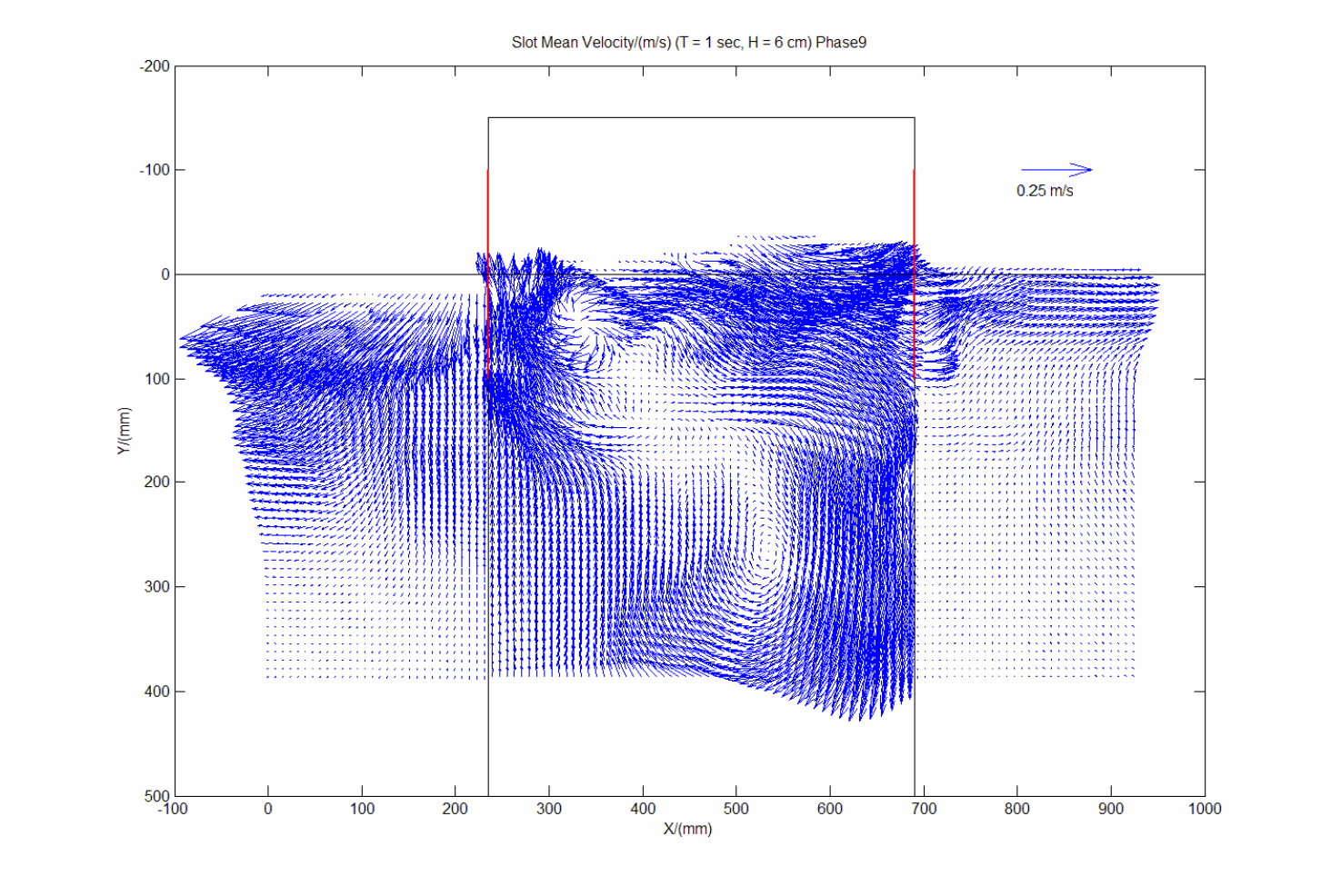

Fig. 4.5. continued.

(j)

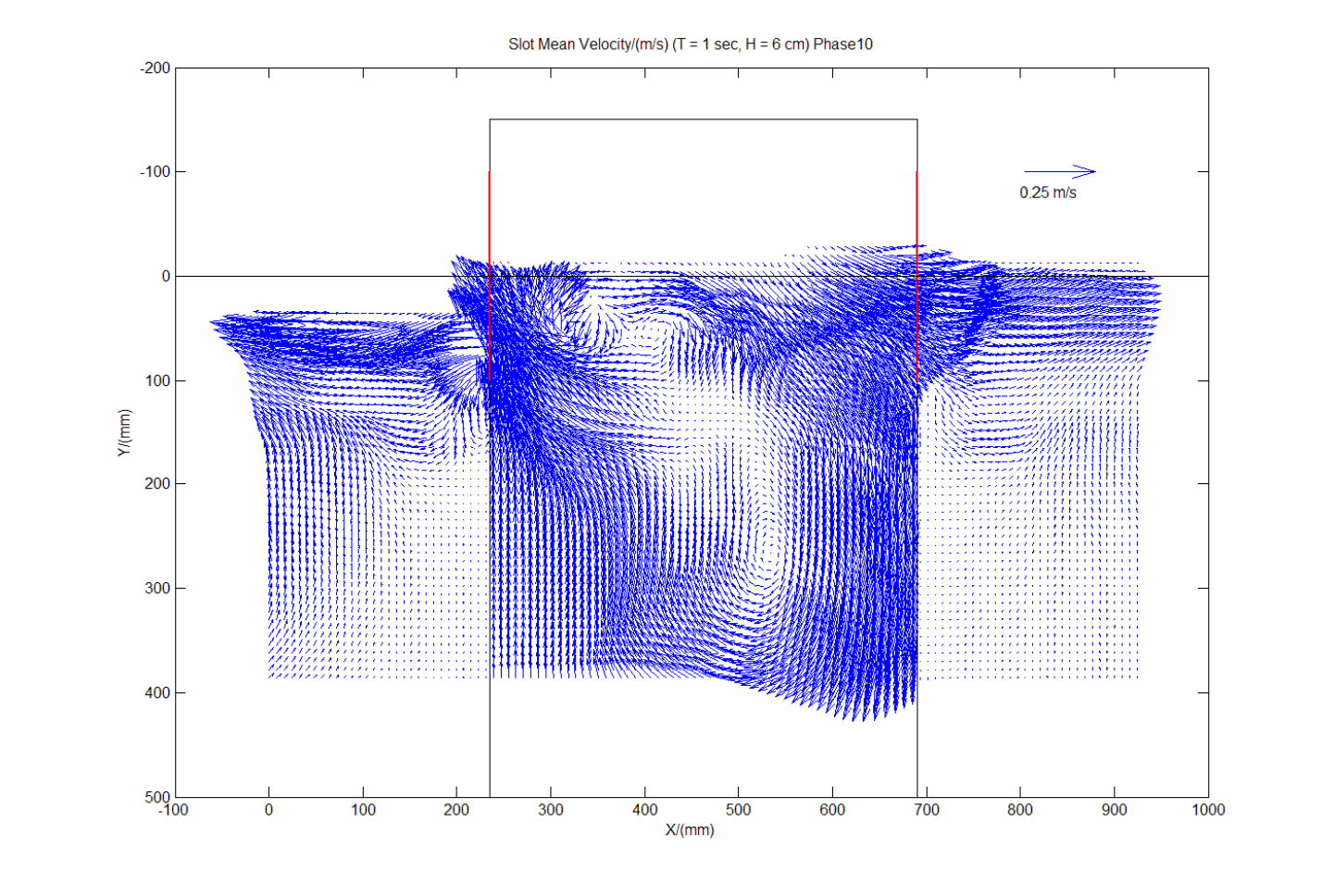

Fig. 4.5. continued.

4.1 Velocity field for light sheet through wall

For the light sheet through wall, for wave condition T = 1 sec and H_i = 4 cm, when the wave hits the structure due to the presence of wall, the water cannot flow smoothly. In the velocity maps this can be seen clearly. There is a clear discontinuity near both the front and back walls of the structure. Due to the presence of the wall the flow field near walls and near the free surface gets very complex, small vortices form with time near free surface. These vortices disappear and reappear with time. Due to entrapment of water inside chamber, the flow inside the chamber gets very complex, and violent. Inside the chamber the flow velocity near the free surface and below the free surface are comparable, where as for other areas, for most of the phases, higher velocity exists near the free surface. There is a large clockwise vortex inside the chamber, with its centre located near the back wall. With time the centre moves downward, stays stationary and then moves upward. The centre of the vortex moves with wave phase. The movement matches with wave, with trough (ex Phase 1) it moves downward and with crest (ex Phase 6) it moves upward. Since the amount of transmission wave is smaller compared to incoming wave the velocity field behind the back wall is smaller compared to velocity field in other areas. For all phases the velocity field behind the back wall is very small. The velocity in front of the front wall varies with phase. For all phases, the velocity inside the chamber is higher compared to other areas.

For the wave condition T = 1 sec, H_i = 6 cm, the flow pattern is same as that for the wave condition T = 4 sec and H_i = 4 cm, but the magnitude of the velocity is higher.

The effect of barrier wall can be seen clearly compared to wave condition T = 1 sec, and H_i = 4 cm. Flow near free surface and near the front wall gets very violent. Once the wave hits the structure more energy is reflected. Thus the reflected wave height increases when H_i increases (see table 3.2). Part of the incoming wave energy transmits through the front wall, it again suffers due to the presence of the back wall, and the flow inside the chamber gets complex. From the velocity maps, it is clear that when wave height increases, the transmitted wave energy from the front wall increases. Thus the transmitted wave height increases when H_i increases (see table 3.2), and flow velocity behind the back wall is larger compared to H_i = 4 cm. More small vortices form compared to H_i = 4 cm.

For the wave condition T = 1 sec, H_i = 8 cm, the flow pattern is same as for the wave condition T = 1 sec and H_i = 4, 6 cm, but the magnitude of the velocity is higher. The effect of the barrier wall can be seen clearly. Both reflected and transmitted wave heights are larger compared to T = 1 sec and H_i = 4, 6 cm and flow velocity behind the back wall is comparable with the velocity in other areas.

For the wave condition T = 1 sec, H_i = 10 cm, the flow pattern is the same as that for the wave condition T = 1 sec and H_i = 4, 6, 8 cm, except near walls but the magnitude of the velocity is higher. The effect of barrier wall can be seen clearly. Both reflected and transmitted wave heights are bigger compared to T = 1 sec and H_i = 4, 6, 8 cm and flow velocity behind the back wall is comparable with the velocity in other areas.

When the wave conditions get larger (T = 1.6, 2, 2.5 sec and H_i = 8 cm) the following is observed. Vortices appear behind the back wall for the first time at T = 1.6 sec. The velocity behind the back wall gets comparable to the velocity in other areas. The flow inside the chamber gets very complex. The velocity behind the back wall increases and the discontinuity of the velocity field near the walls appear clearly. The velocity field in front of the front wall, inside the chamber and near the free surface gets very complex. The centre of large vortex inside the chamber moves to the middle of the chamber, and with time the centre moves in a smaller area compared to smaller waves. The small vortices fade away quicker than it does for small waves. For T = 2 and 2.5 sec, many small vortices appear near the front wall, inside the chamber and near the back wall. The centre of the vortex inside the chamber moves in a smaller area and the flow inside the chamber becomes very complex.

4.2 Velocity field for light sheet through slot

For the light sheet through slot, flow transfers smoothly through walls, hence even for small wave conditions (ex T = 1 sec, H_i = 4 cm) clear continuity of velocity field can be seen near walls. The flow behind back wall is comparable to other areas. The flow near the free surface is violent compared to flow beneath. Small vortices form near the free surface with time. A large clockwise vortex appears inside the chamber. The centre of the vortex is closer to the back wall, the centre movement matches with wave, it moves downward with wave trough (ex Phase 1) and moves upward with crest

(ex Phase 6). For most of the phases the magnitude of the velocity is higher in flow near front wall and inside the chamber compared to flow behind back wall. More small vortices form near walls compared to light sheet through wall. Hence it can be seen that more energy is dissipated for light sheet through slot compared to light sheet through wall .

When wave conditions get larger (ex T = 1 sec, H_i = 6, 8, 10 cm) the velocity field for the light sheet through slot shows clear continuity near walls for all wave conditions. The magnitude of velocity is higher near the front wall and inside the chamber compared to the velocity near the back wall. When wave conditions get larger many small vortices appear in the vicinity of the structure, and flow behind the back wall becomes comparable to other areas.

For T = 1.6 sec for the first time small vortices form behind the back wall. For wave conditions T = 1.6, 2, 2.5 sec, H_i = 8 cm for many phases the velocity maps are similar to that with light sheet through wall except near walls.

For both light sheets, for small wave conditions (ex T = 1 sec, H_i = 4, 6, 8, 10 cm) the higher velocity appears near the front wall and inside the chamber. Behind the back wall the velocity is small. For higher wave conditions (ex T = 1.6, 2, 2.5 sec, H_i = 8 cm) the velocity behind the back wall is comparable with the velocity in front of front wall and inside the chamber. For all the wave conditions, the flow near the front wall and inside the chamber is more complex than the flow behind the back wall and for both light sheets, a big clockwise vortex appears inside the chamber. For most phases the velocity maps are the same for the two light sheets. Clear discontinuity can be seen near

walls for light sheet through wall. The flow field gets very complex near the front wall with time for both light sheets. More small vortices form with time for light sheet through slot compared to that for light sheet through wall. Vortices form behind the back wall for light sheet through slot, but no vortices form behind the back wall for light sheet through wall. The phase averaged velocity maps are almost same except near walls for the two light sheets.

After calculating the velocity field for each phase, the time average velocity field was calculated by taking the average of the ten phases for both light sheets (see figures 4.6 and 4.7).

(a)

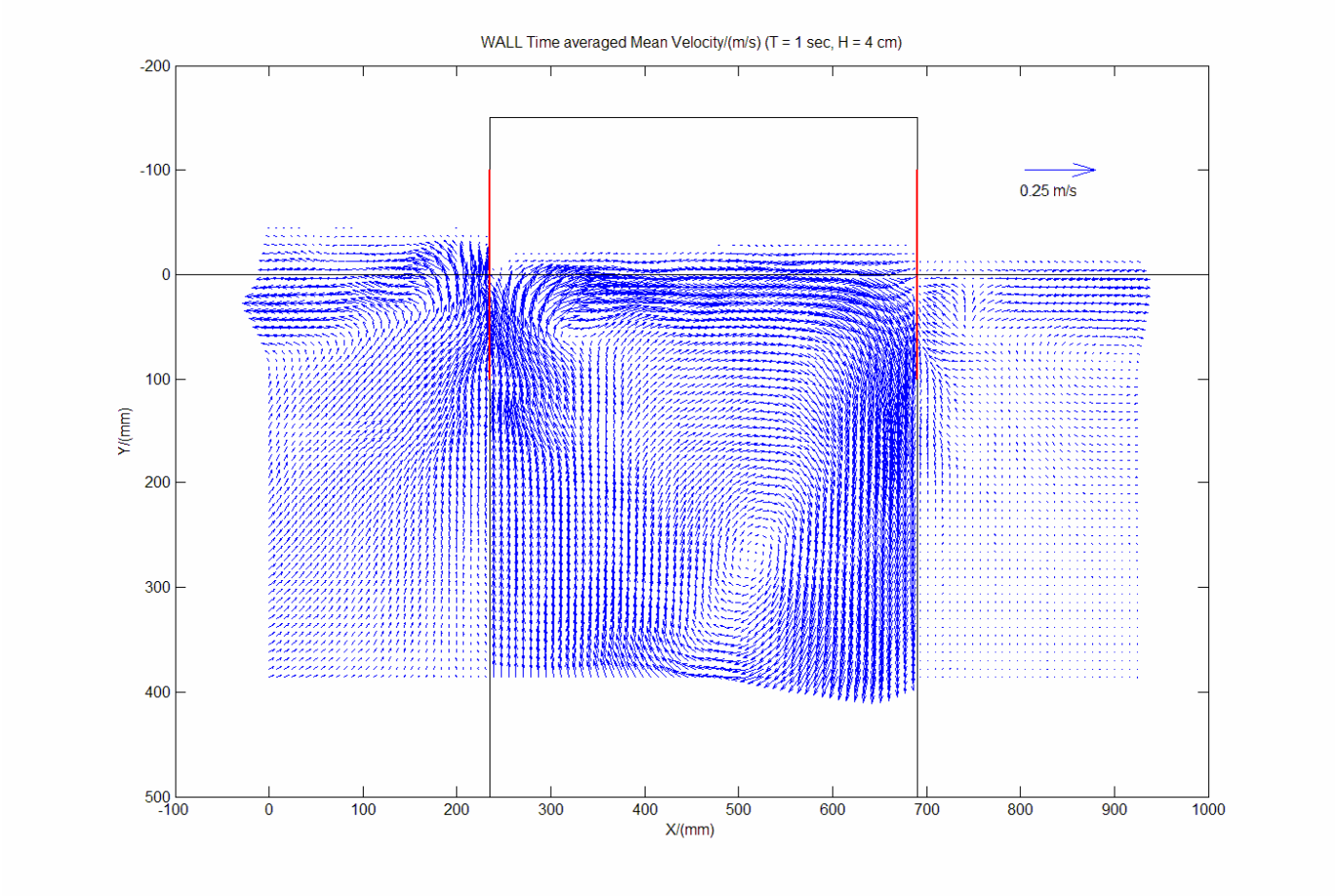

Fig. 4.6. Time averaged velocity fields through wall. (a) T = 1 sec, H = 4 cm. (b) T = 1 sec, H = 6 cm. (c) T = 1 sec, H = 8 cm. (d) T = 1 sec, H = 10 cm. (e) T = 1.6 sec, H = 8 cm. (f) T = 2 sec, H = 8 cm. (g) T = 2.5 sec, H = 8 cm.

(b)

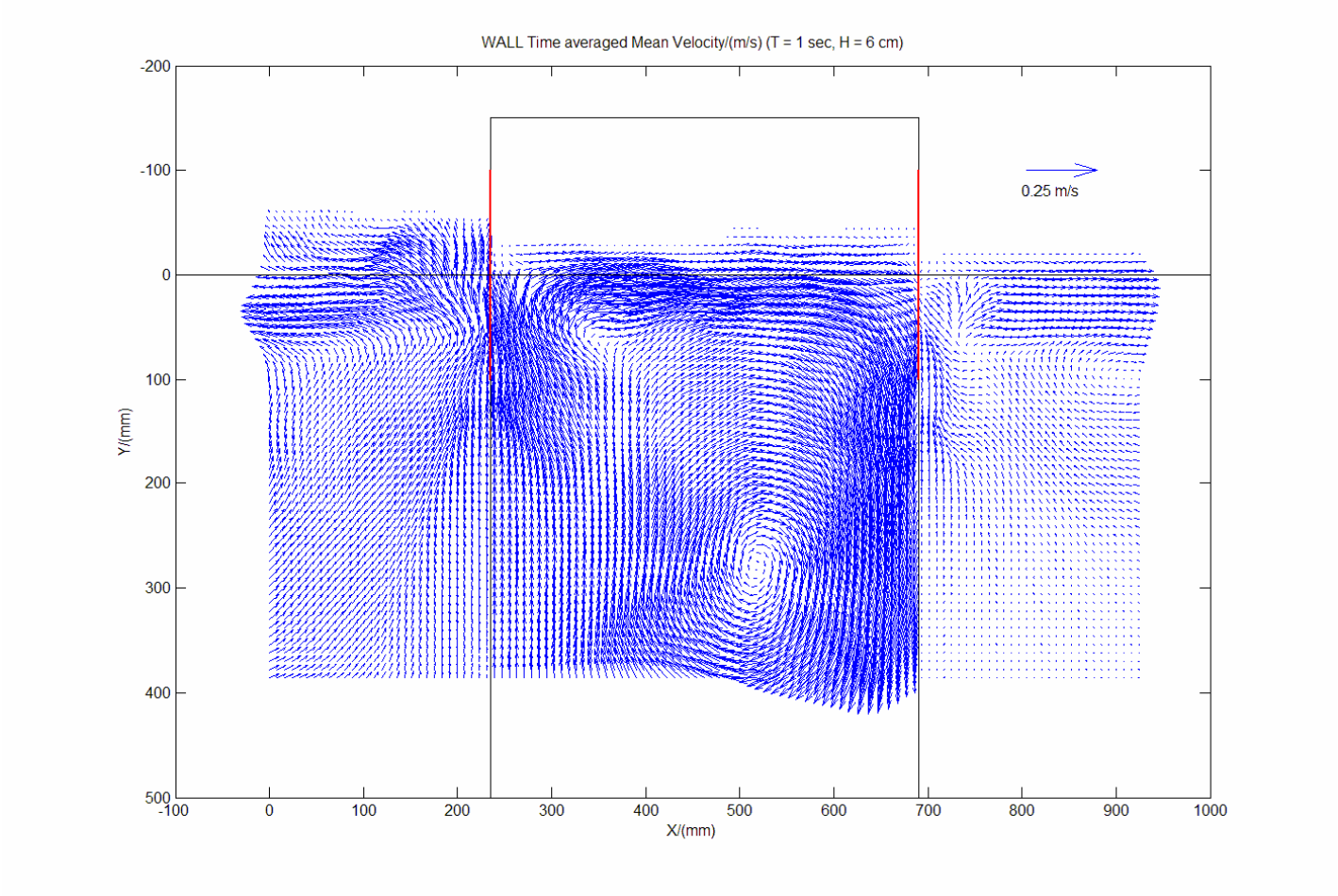

Fig. 4.6. continued.

(c)

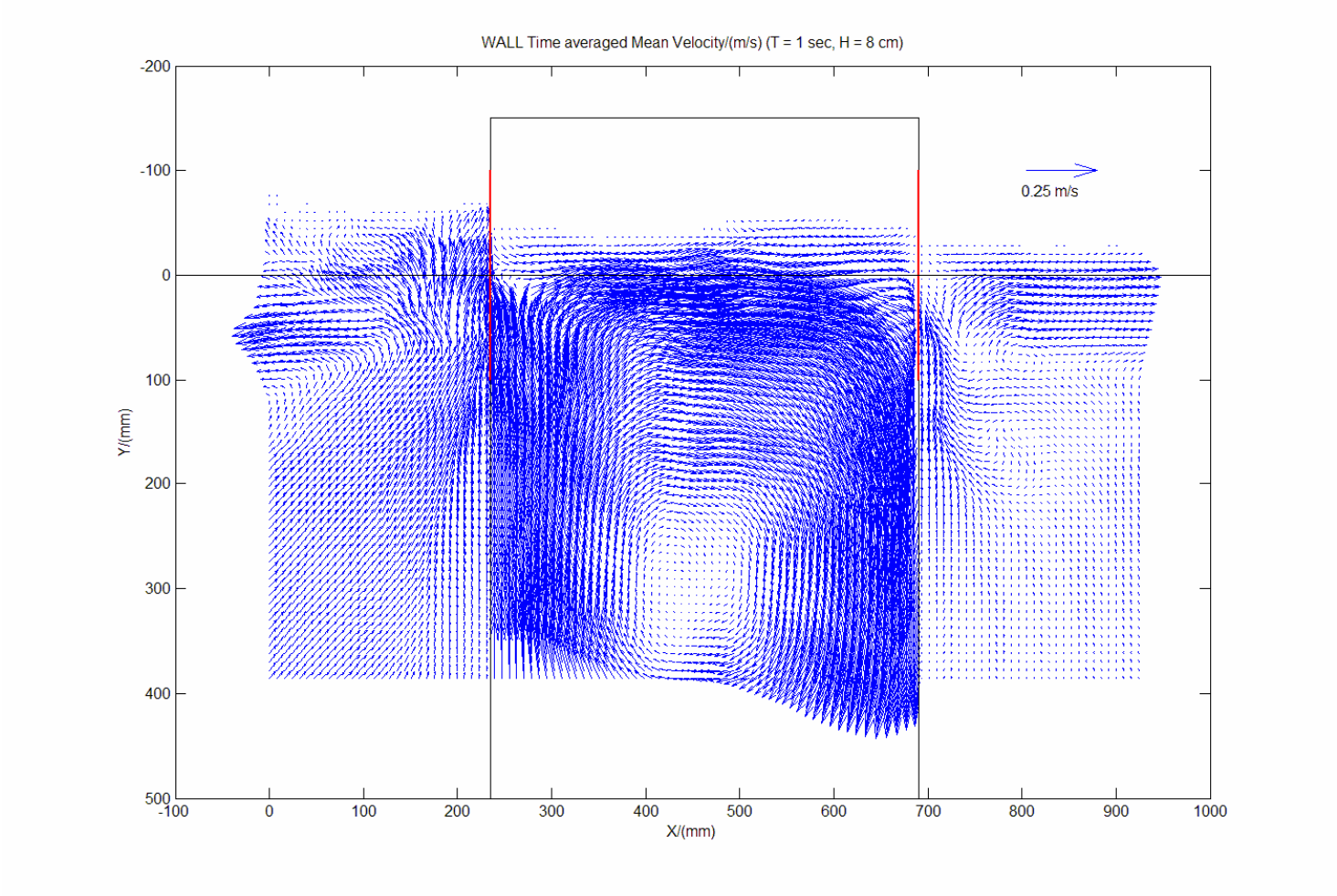

Fig. 4.6. continued.

(d)

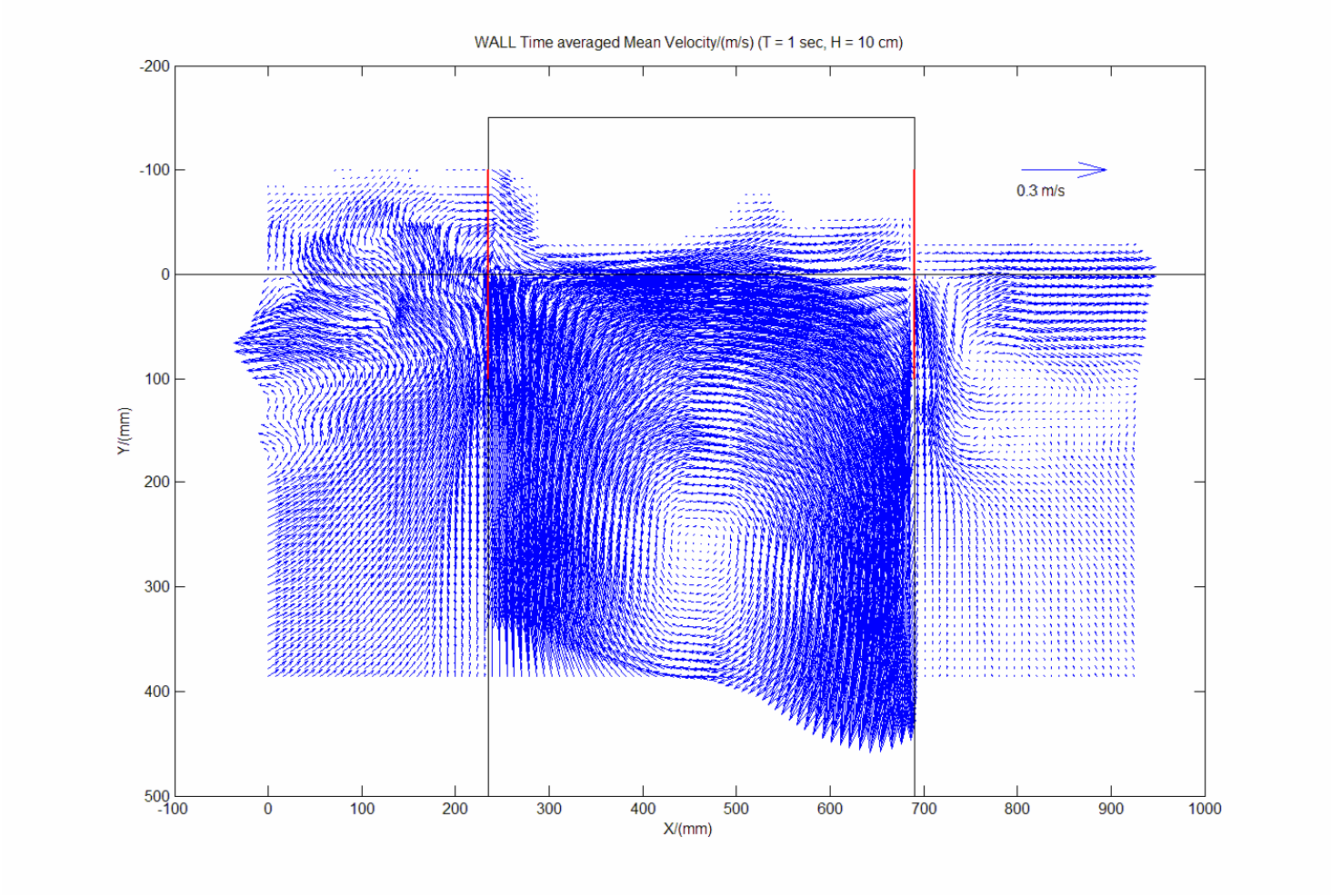

Fig. 4.6. continued.

(e)

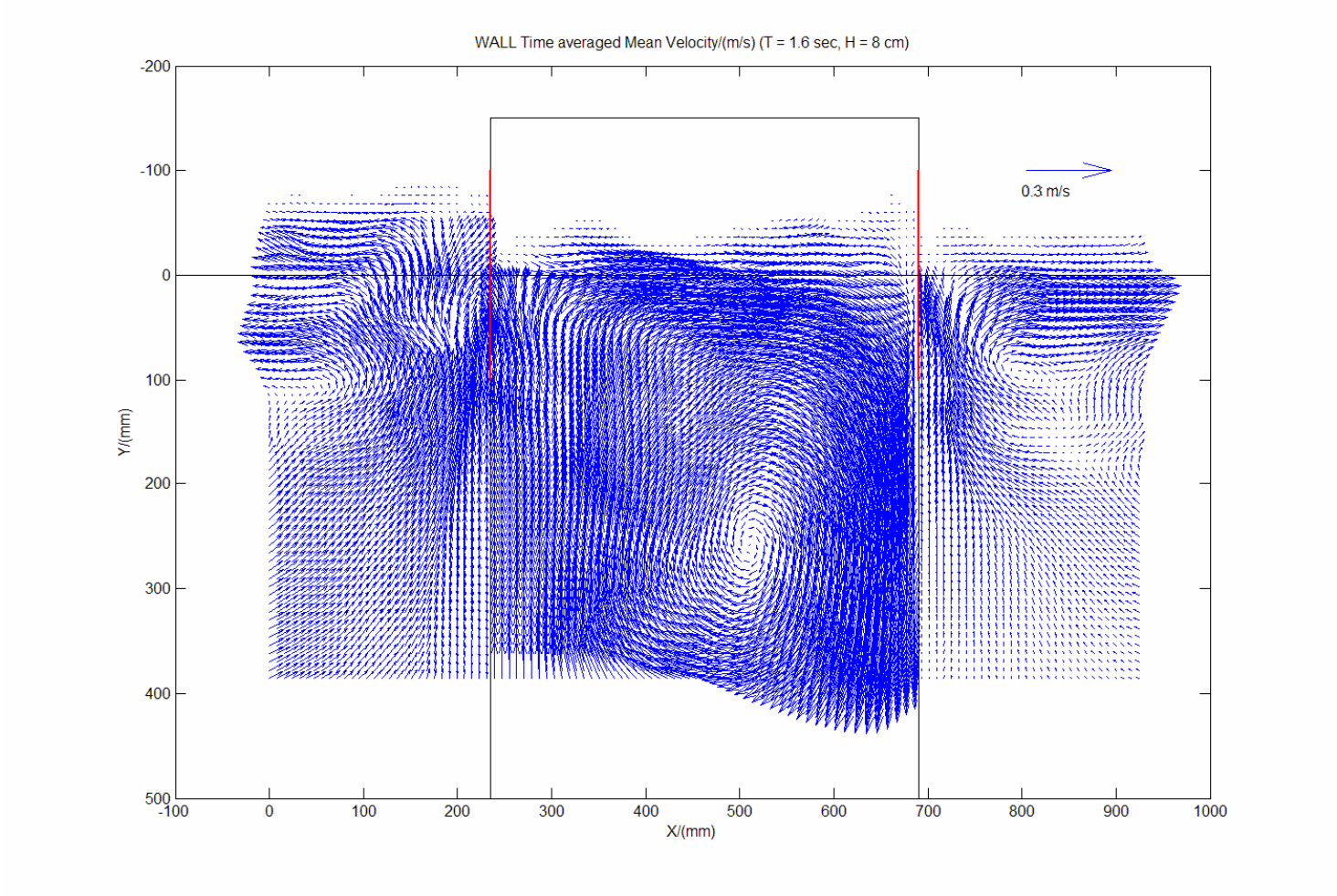

Fig. 4.6. continued.

(f)

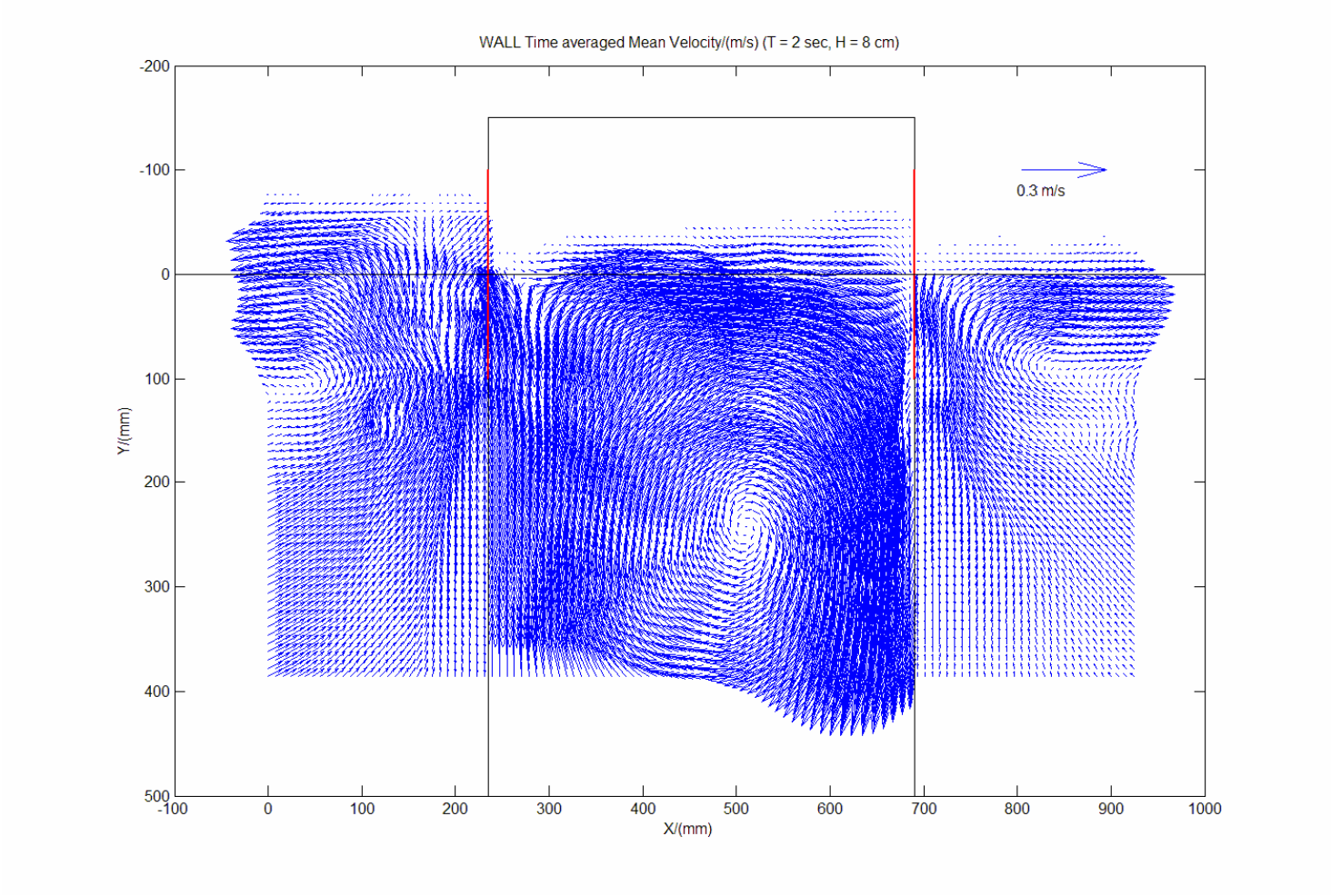

Fig. 4.6. continued.

(g)

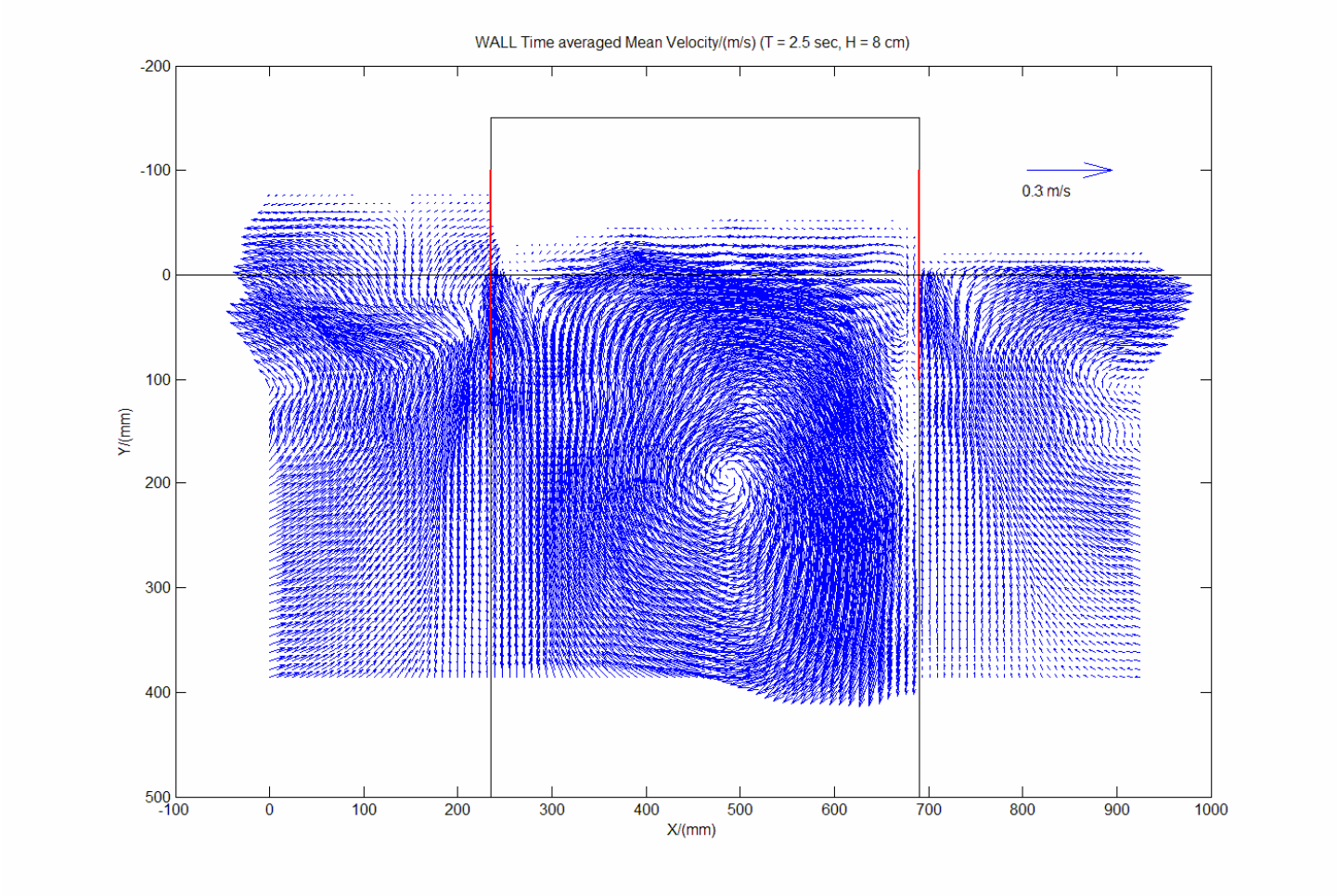

Fig. 4.6. continued.

(a)

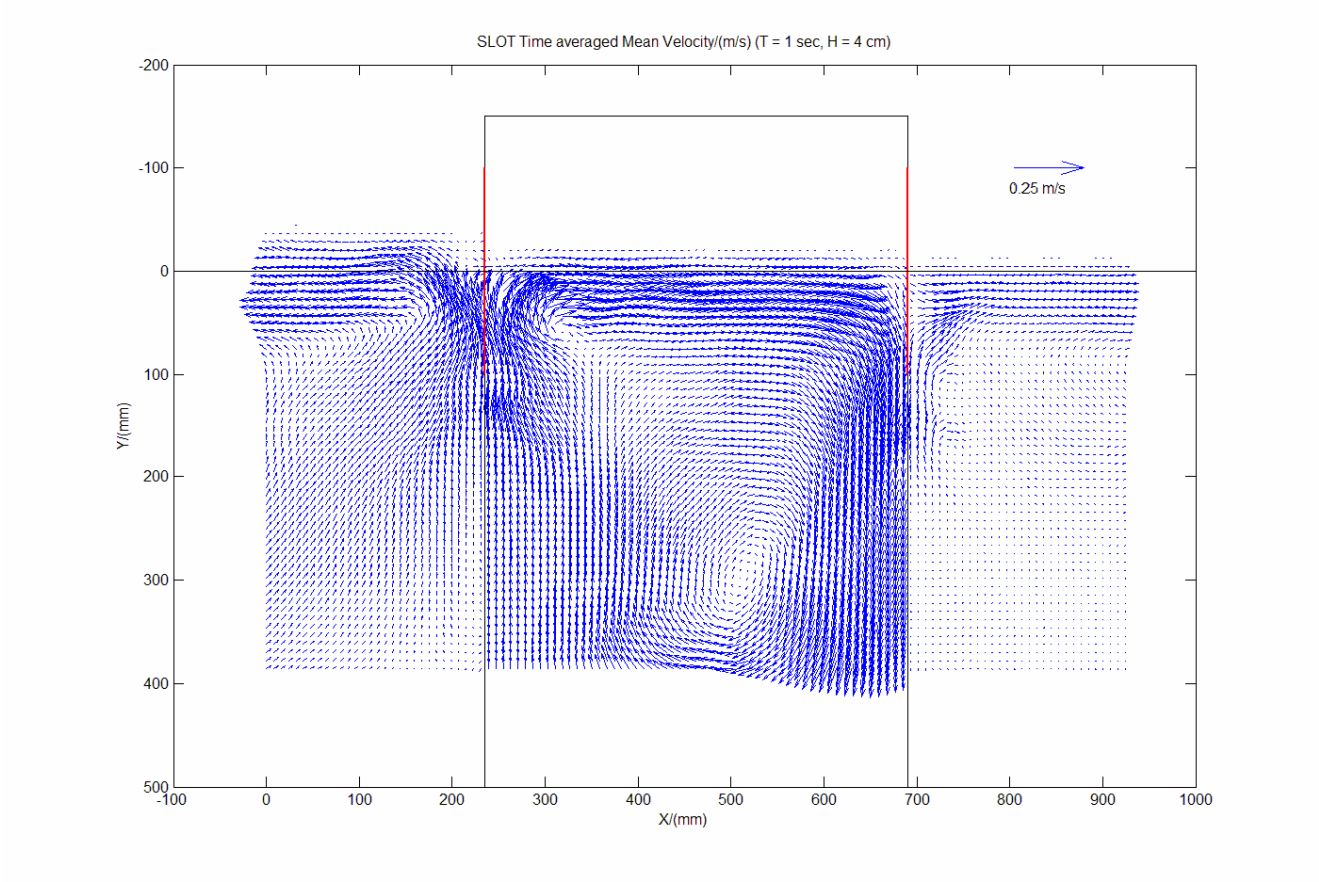

Fig. 4.7. Time averaged velocity fields through slot. (a) T = 1 sec, H = 4 cm. (b) T = 1 sec, H = 6 cm. (c) T = 1 sec, H = 8 cm. (d) T = 1 sec, H = 10 cm. (e) T = 1.6 sec, H = 8 cm. (f) T = 2 sec, H = 8 cm. (g) T = 2.5 sec, H = 8 cm.

(b)

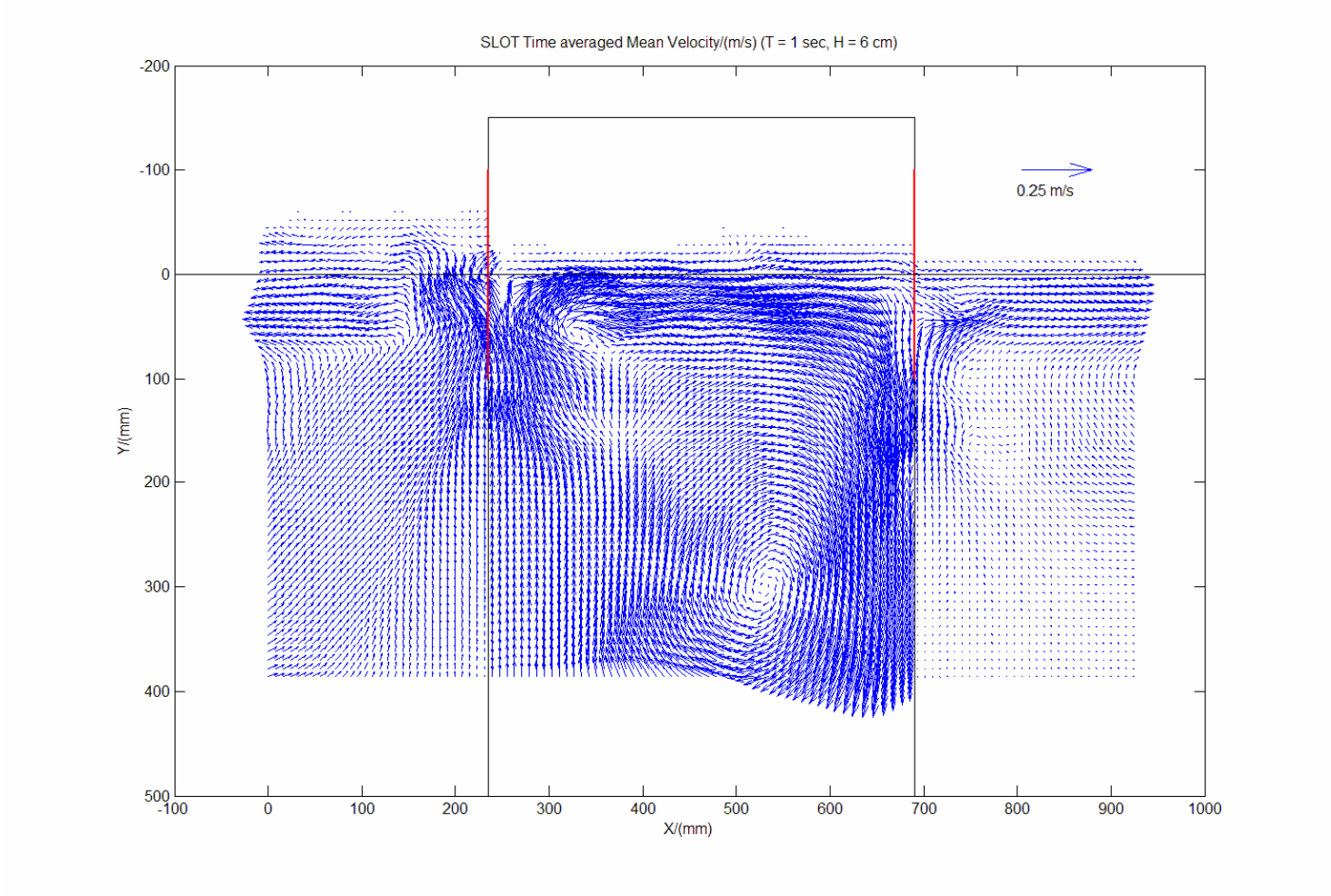

Fig. 4.7. continued.

(c)

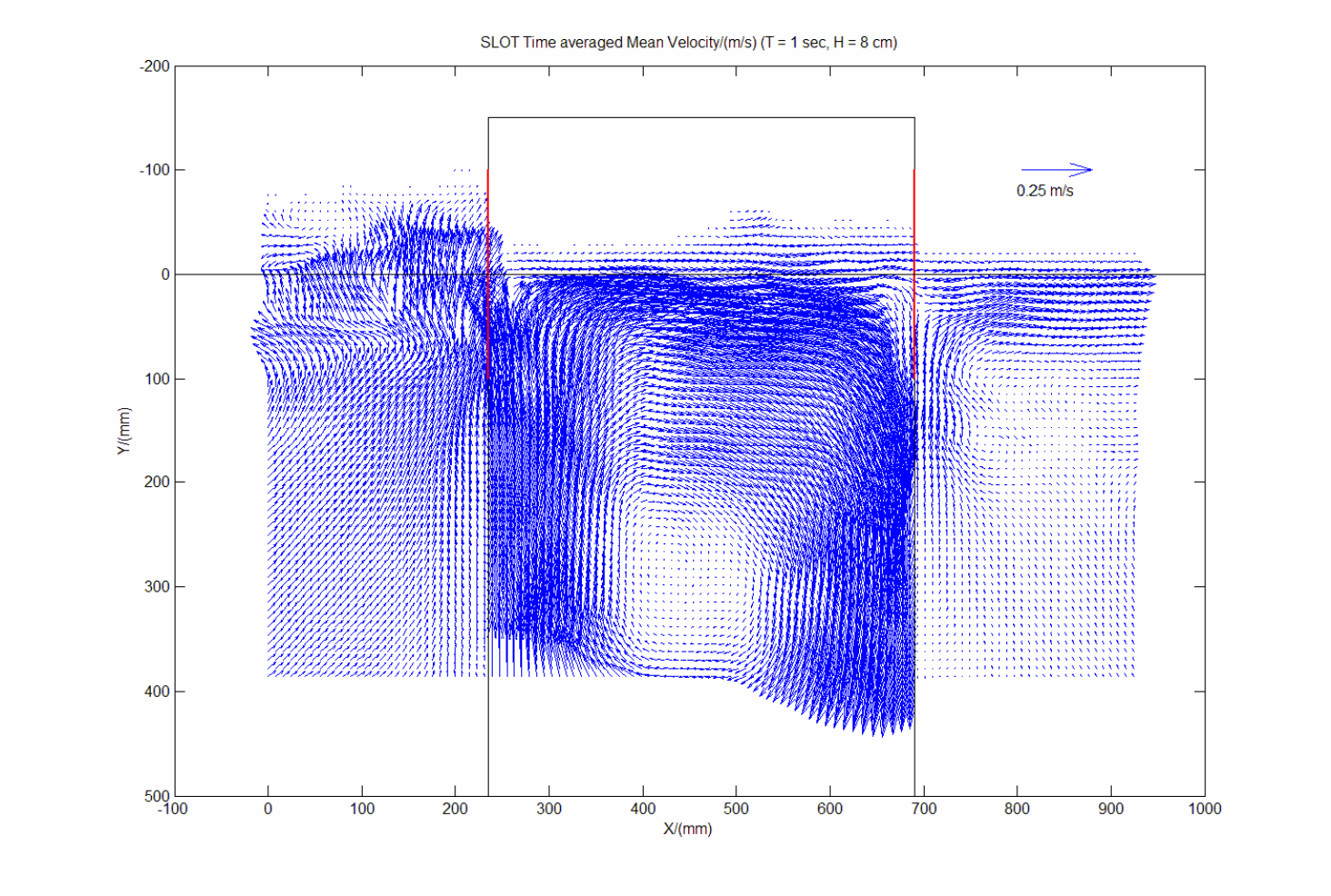

Fig. 4.7. continued.

(d)

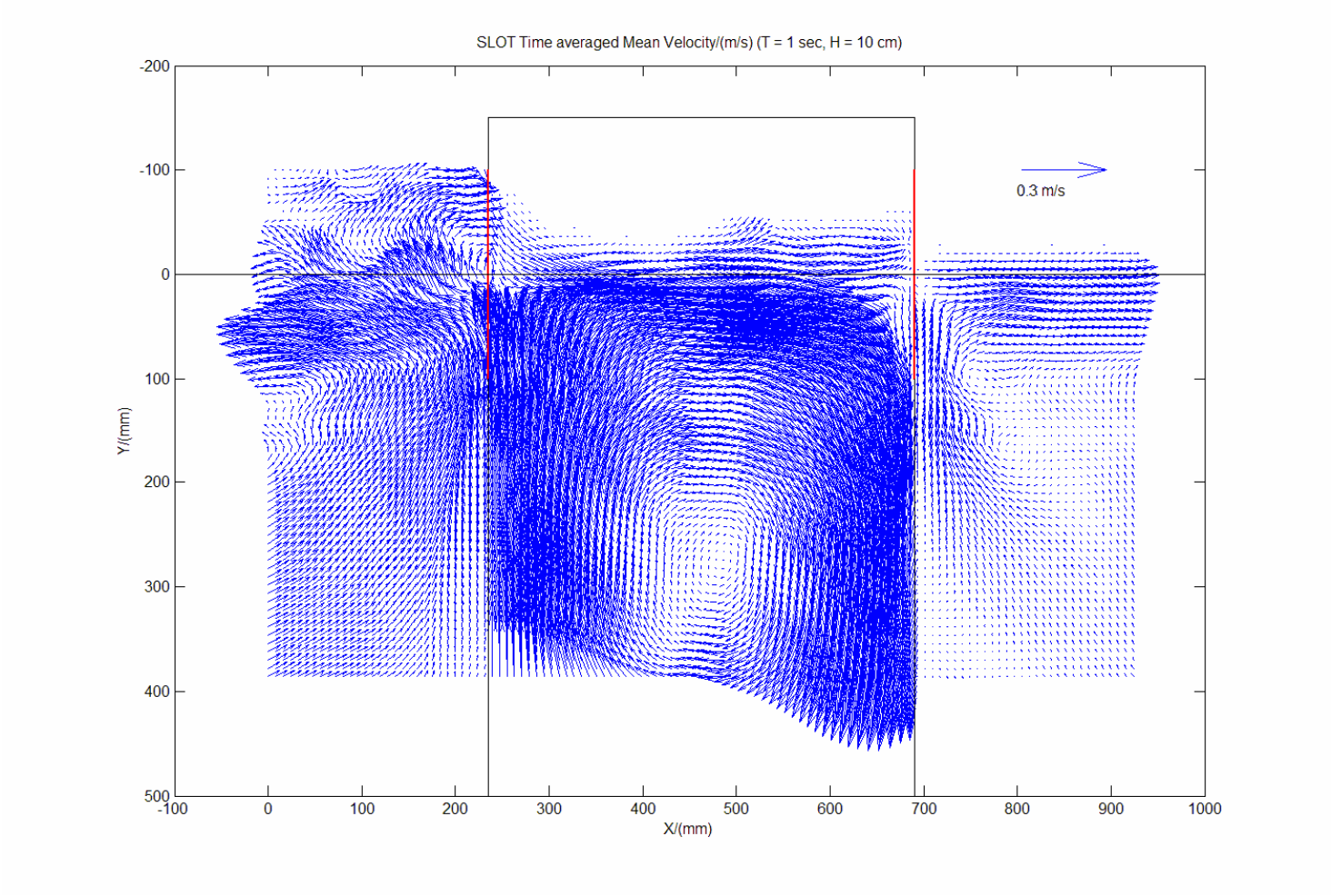

Fig. 4.7. continued.

(e)

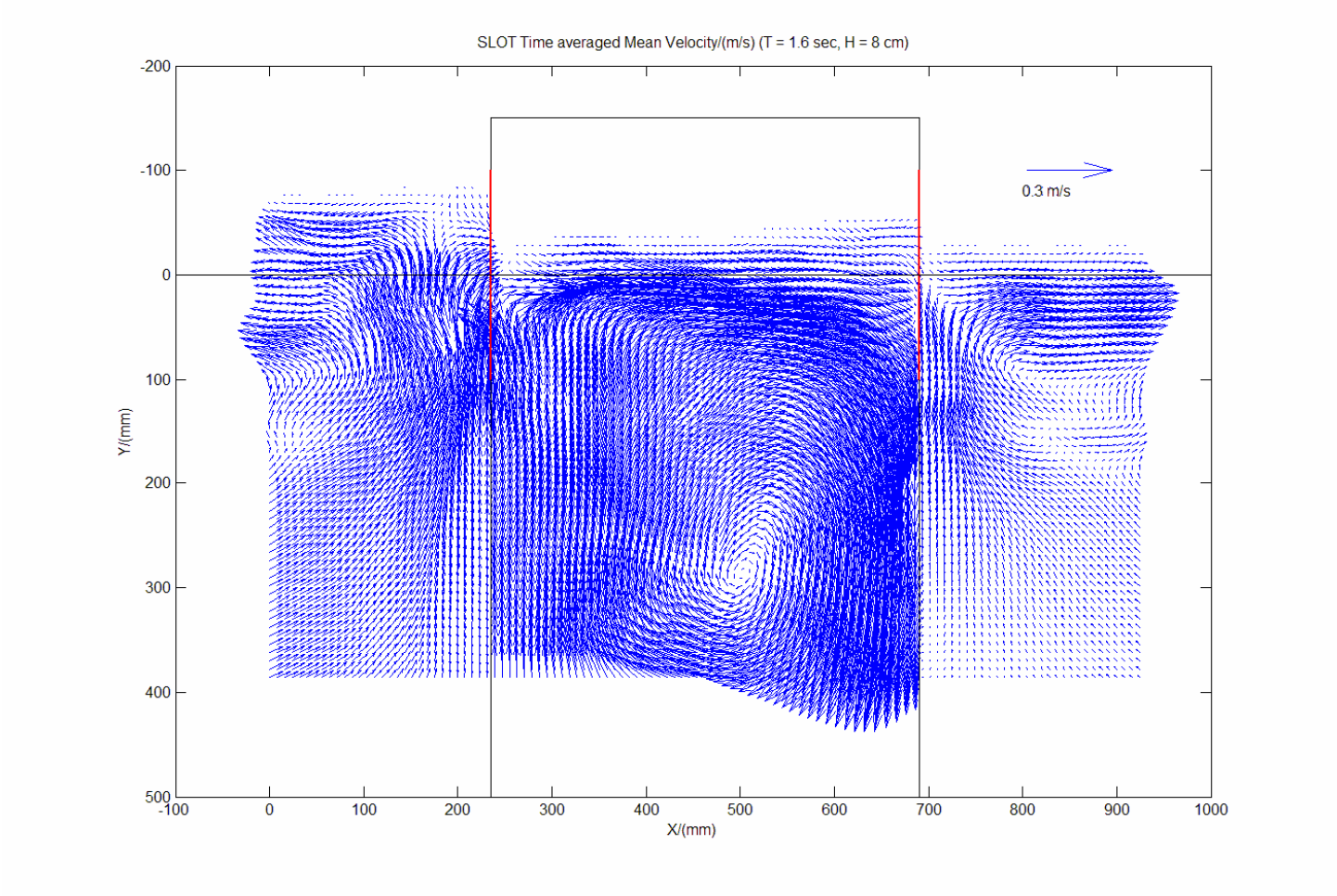

Fig. 4.7. continued.

(f)

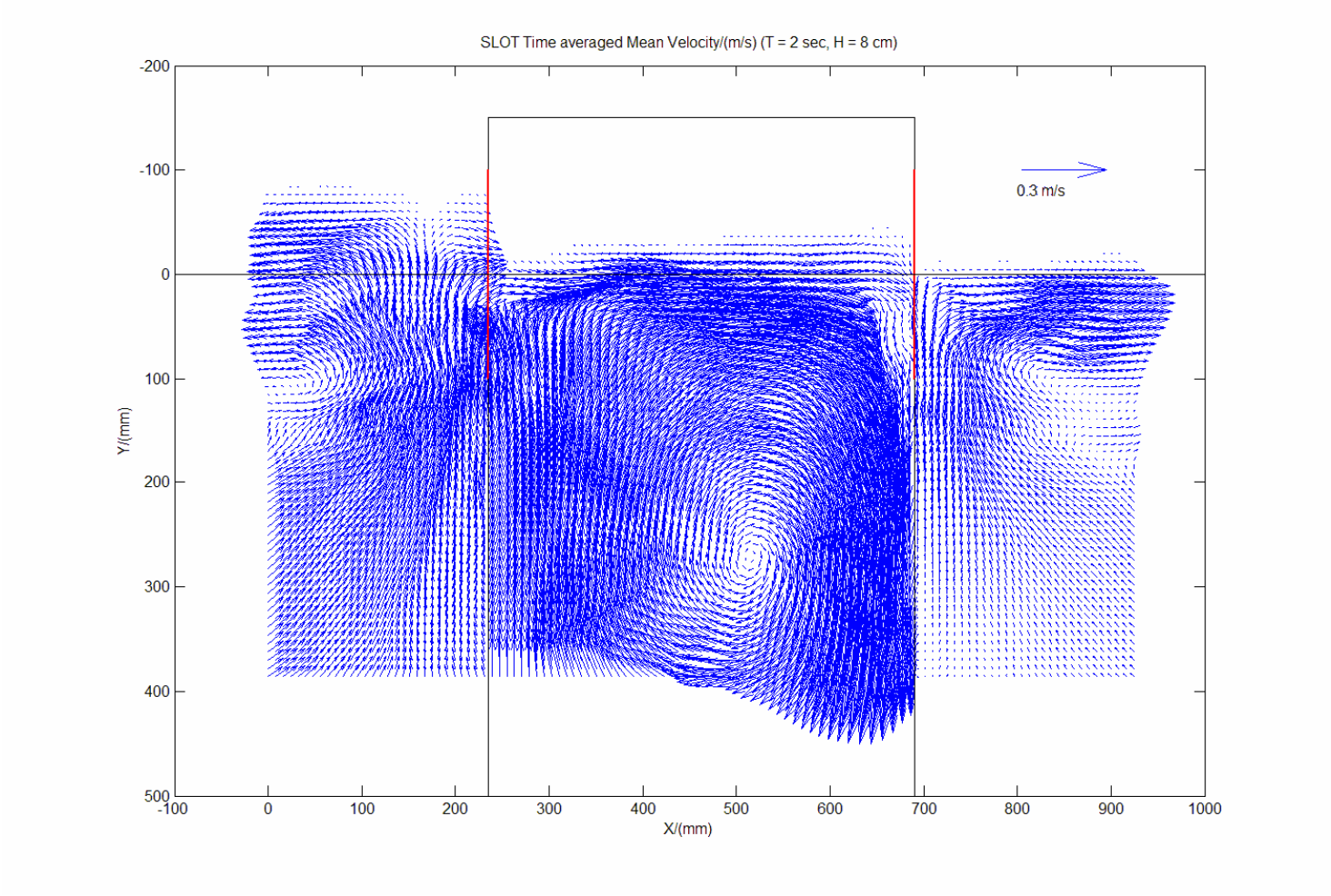

Fig. 4.7. continued.

(g)

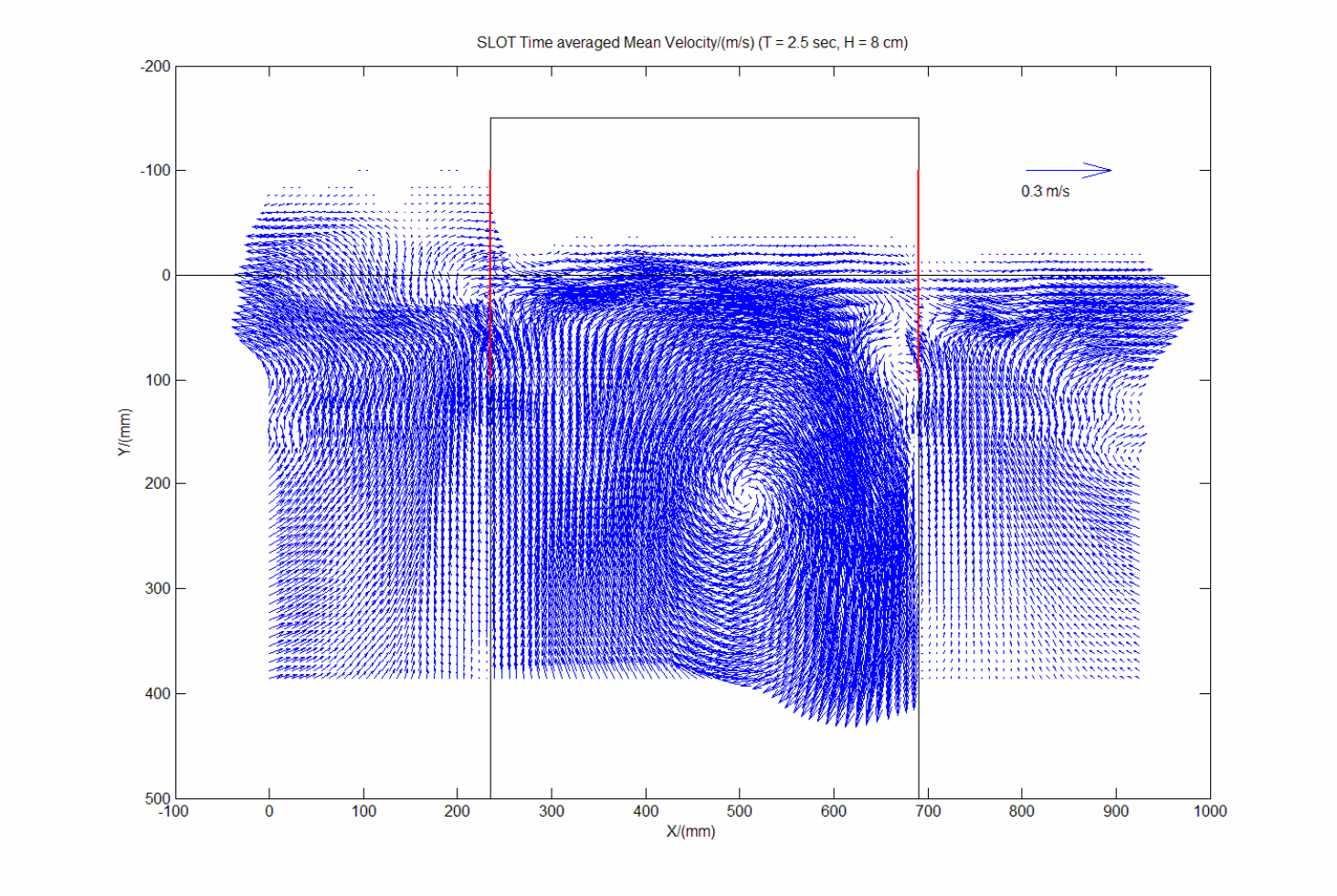

Fig. 4.7. continued.

CHAPTER V

VORTICITY FIELD IN THE VICINITY OF THE STRUCTURE

Once the velocity field was calculated for each phase and each wave condition, the vorticity field was calculated using the following equation (Raffel et al., 1998).

The vorticity at a point,

$$(\omega_Z)_{i,j} = \Gamma_{i,j} / 4\,\Delta X \Delta Y \qquad (5.1)$$

with

$$\begin{aligned}\Gamma_{i,j} = {} & 1/2\,\Delta X\,(U_{i-1,j-1} + 2\,U_{i,j-1} + U_{i+1,j-1}) \\ & + 1/2\,\Delta Y\,(V_{i+1,j-1} + 2\,V_{i+1,j} + V_{i+1,j+1}) \\ & - 1/2\,\Delta X\,(U_{i+1,j+1} + 2\,U_{i,j+1} + U_{i-1,j+1}) \\ & - 1/2\,\Delta Y\,(V_{i-1,j+1} + 2\,V_{i-1,j} + V_{i-1,j-1}) \qquad (5.2)\end{aligned}$$

Contour for the circulation calculation used in the estimation of the vorticity at point (i,j) is shown in figure 5.1.

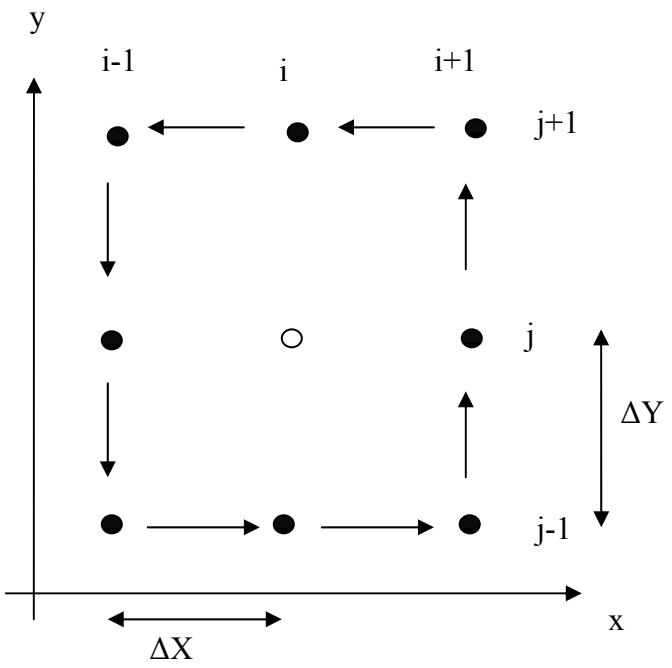

Fig. 5.1. Contour for the circulation calculation used in the estimation of the vorticity at point (i,j).

For wave condition T = 1 sec, H_i = 4 cm, for most of the phases the vorticity patterns are same for the two light sheets. For most of the phases there is a negative vorticity near front wall and a positive vorticity near back wall. For light sheet through slot the magnitude of vorticity is larger. A clear discontinuity of vorticity variation can be seen near walls even for small wave conditions (T = 1 sec, H_i = 4 cm) for light sheet through wall. The vorticity breaks in to small parts and fades away with time. Phase average vorticity maps are diferent for two light sheets and the magnitude of phase averaged vorticity is higher for light sheet through slot.

For wave conditions T = 1 sec, H_i = 6, 8, 10 cm, T = 1.6, 2, 2.5 sec, H_i = 8 cm for most of the phases the vorticity patterns are same for the two light sheets. For light sheet through slot, vorticity spreads in a wider area than that for light sheet through wall. Similar to wave condition T = 1 sec, H_i = 4 cm for most of the phases there is a negative vorticity form near front wall where as a positive vorticity form near back wall. For light sheet through slot the magnitude of vorticity is bigger. A clear discontinuity of vorticity variation can be seen near walls for light sheet through wall. Phase average vorticity maps are different and the magnitude of phase average vorticity is higher for light sheet through slot.

For the light sheet through wall, for small wave conditions (T = 1 sec, H_i = 4 cm) small vortices appear near free surface and near the front wall. With time the vortices spread in to a wider area, separate in to smaller parts and fade away. While the vortices disappear, small vortices form under the free surface, and move upward. When wave conditions get larger (T = 1.6, 2, 2.5 sec, H_i = 8 cm) many small vortices form in all the

areas. Most of the times, a negative vortex appears near the front wall and positive vortex appears near the back wall. With increasing wave conditions (T = 1.6, 2, 2.5 sec, H_i = 8 cm), the magnitude of the vortex gets larger; vortices appear in a wider area and vortices show a clear discontinuity near walls for the light sheet through wall.

For the light sheet through slot the vorticity pattern is the as same as that for the light sheet through wall except near walls, but it shows a continuity near walls.

For most wave conditions and for most phases, a negative vortex appears near front wall, whereas near the back wall a positive vortex appears. With time, the vortices seperate in to small vortices and fade away. When the vortices near the surface fade away small vortices form beneath the surface and move upward.

After calculating the vorticity field for each phase, the time average vorticity field was calculated by taking the average of the ten phases for each wave condition (see figures 5.2 and 5.3). The free surface is marked with a black colour line. There is a diffrence in water level in front and behind the front wall for the light sheet through slot, this can be due to the fact that the slot height is only one third of the structure height.

(a)

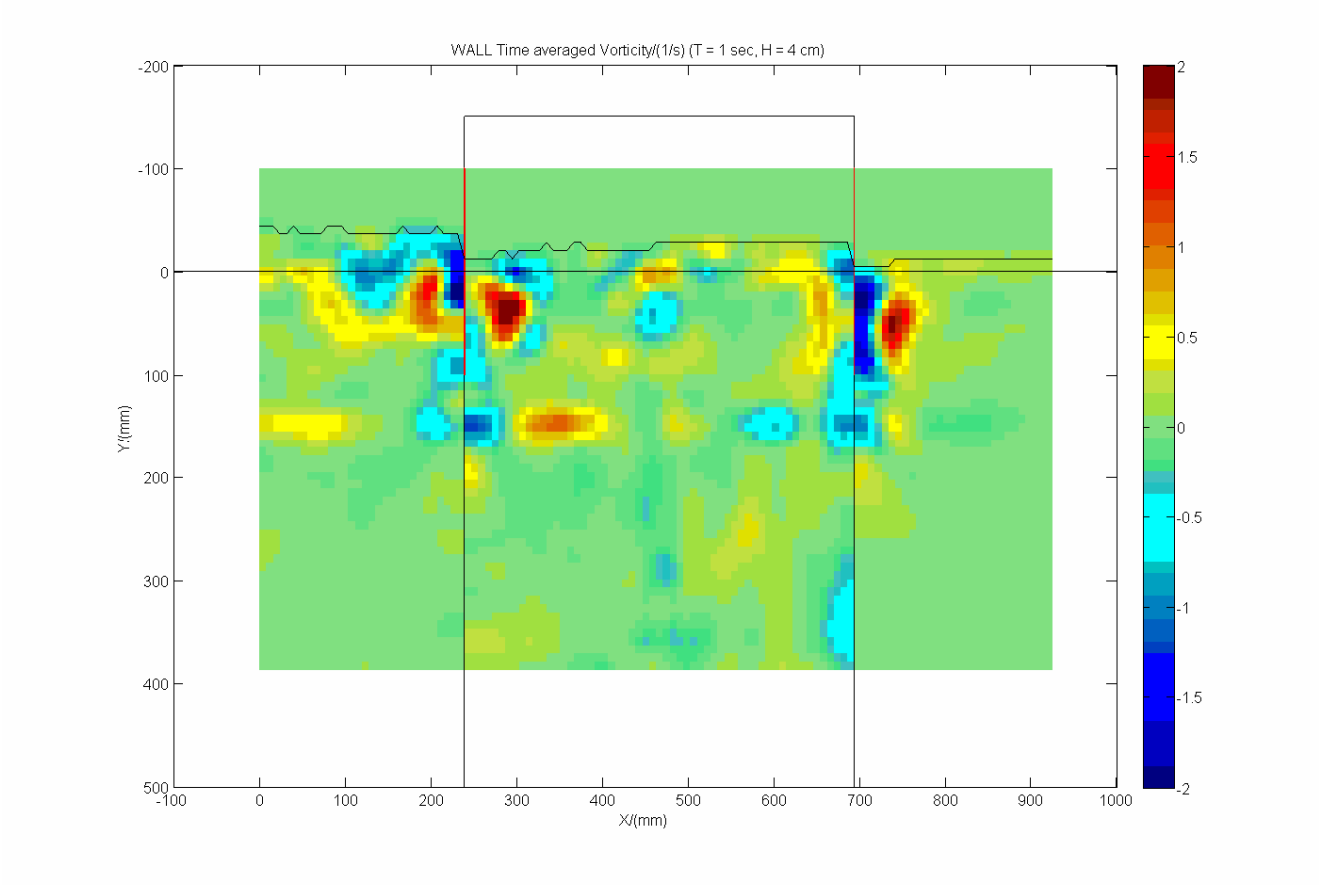

Fig. 5.2. Time averaged vorticity fields through wall. (a) T = 1 sec, H = 4 cm. (b) T = 1 sec, H = 6 cm. (c) T = 1 sec, H = 8 cm. (d) T = 1 sec, H = 10 cm. (e) T = 1.6 sec, H = 8 cm. (f) T = 2 sec, H = 8 cm. (g) T = 2.5 sec, H = 8 cm.

(b)

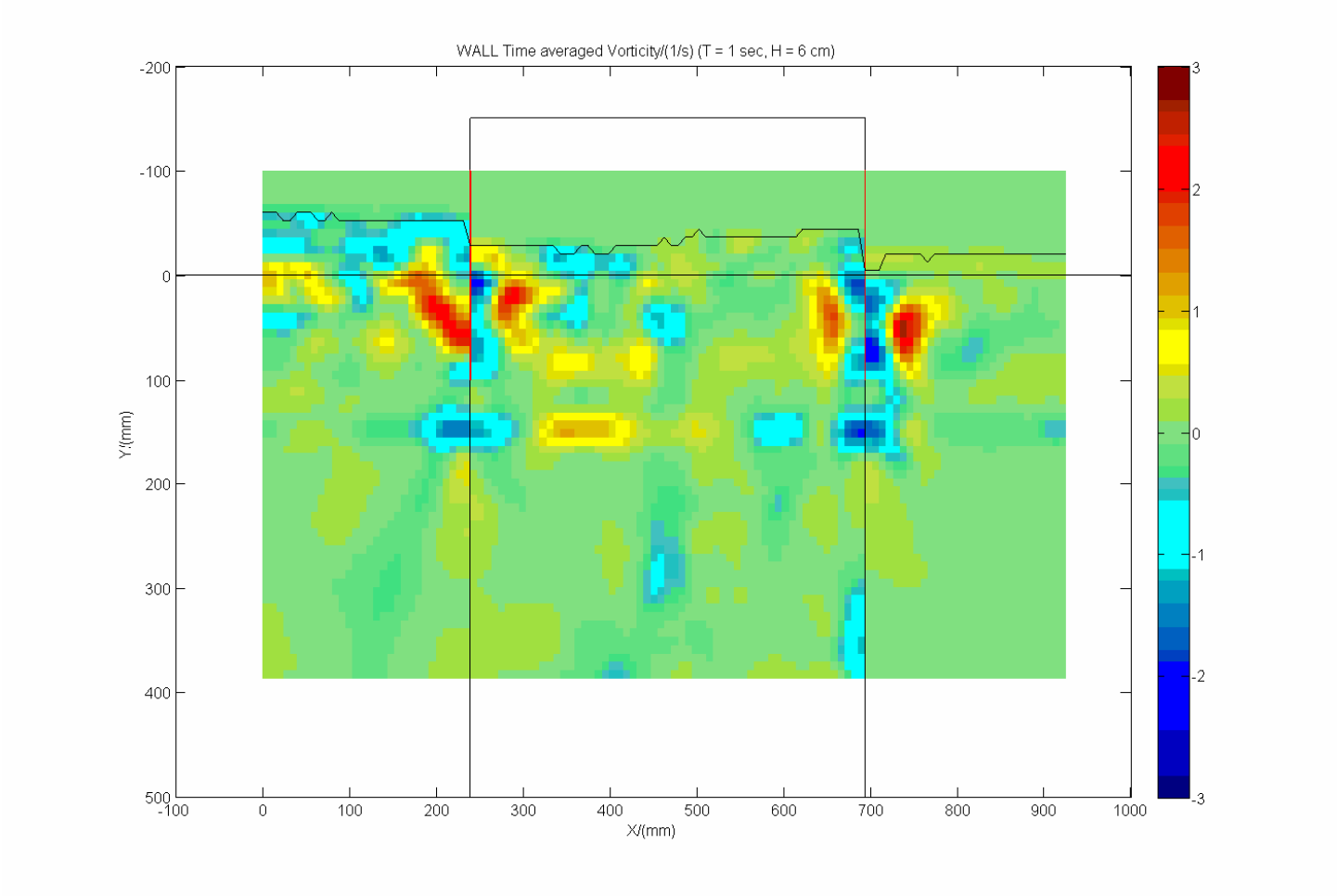

Fig. 5.2. continued.

(c)

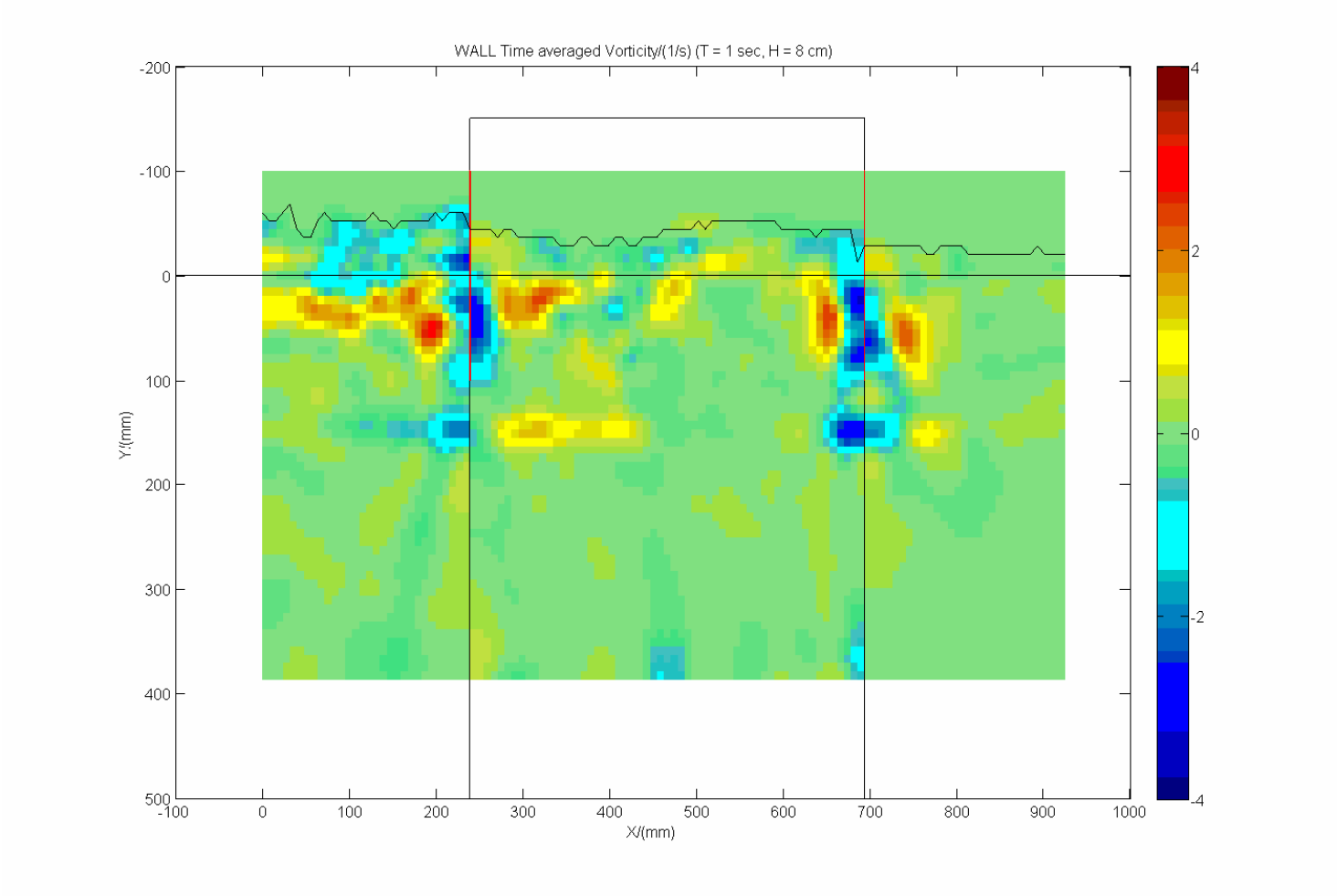

Fig. 5.2. continued.

(d)

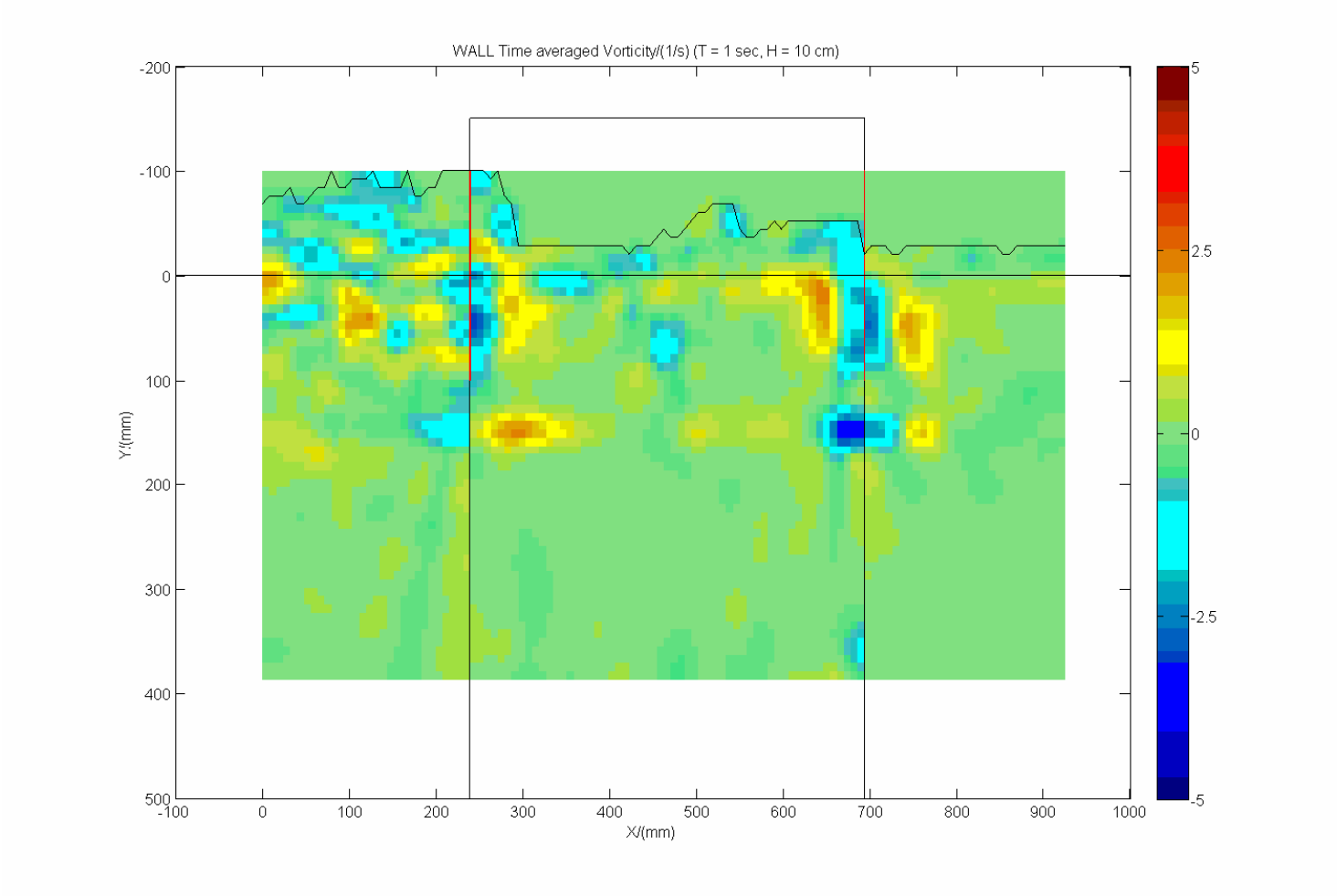

Fig. 5.2. continued.

(e)

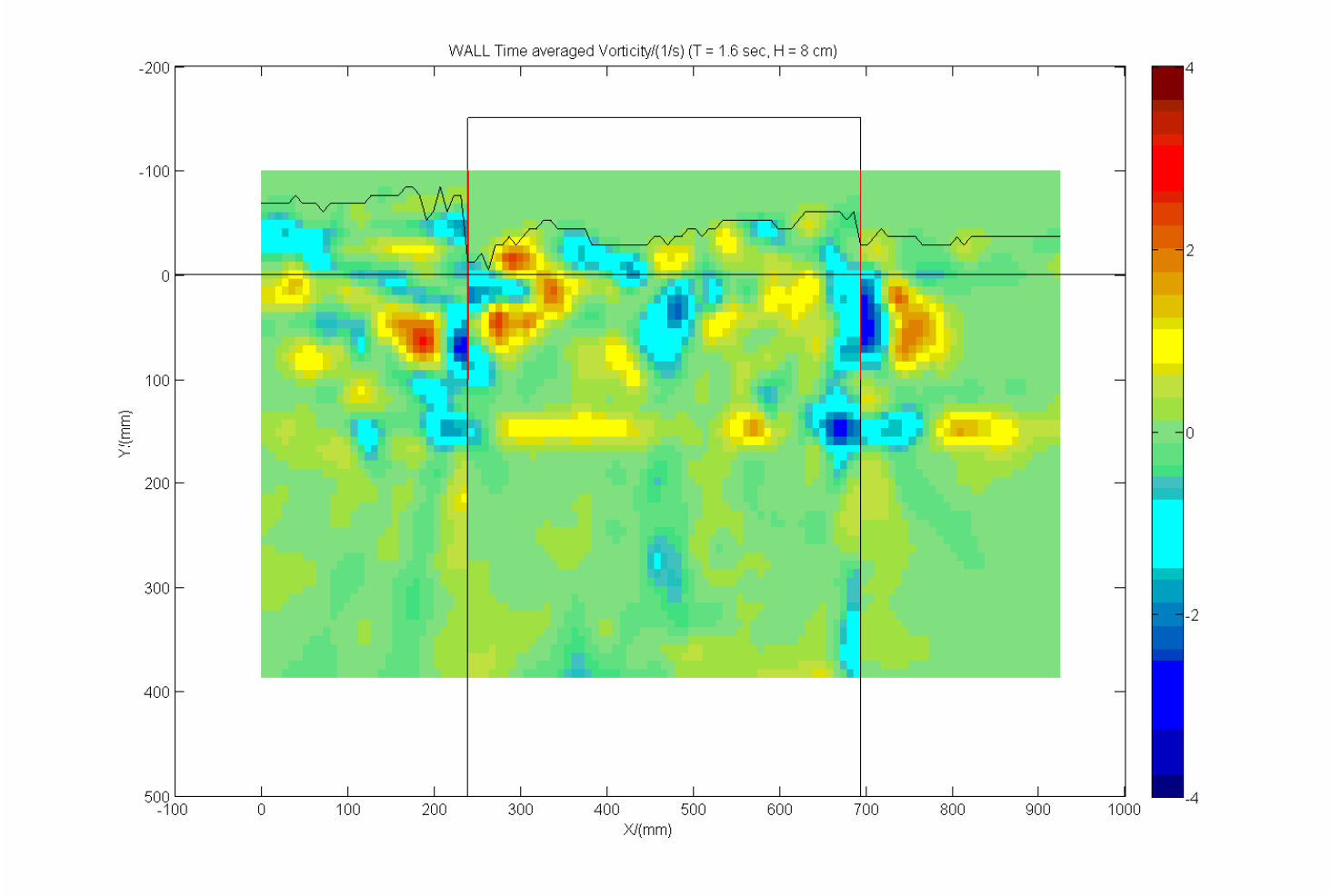

Fig. 5.2. continued.

(f)

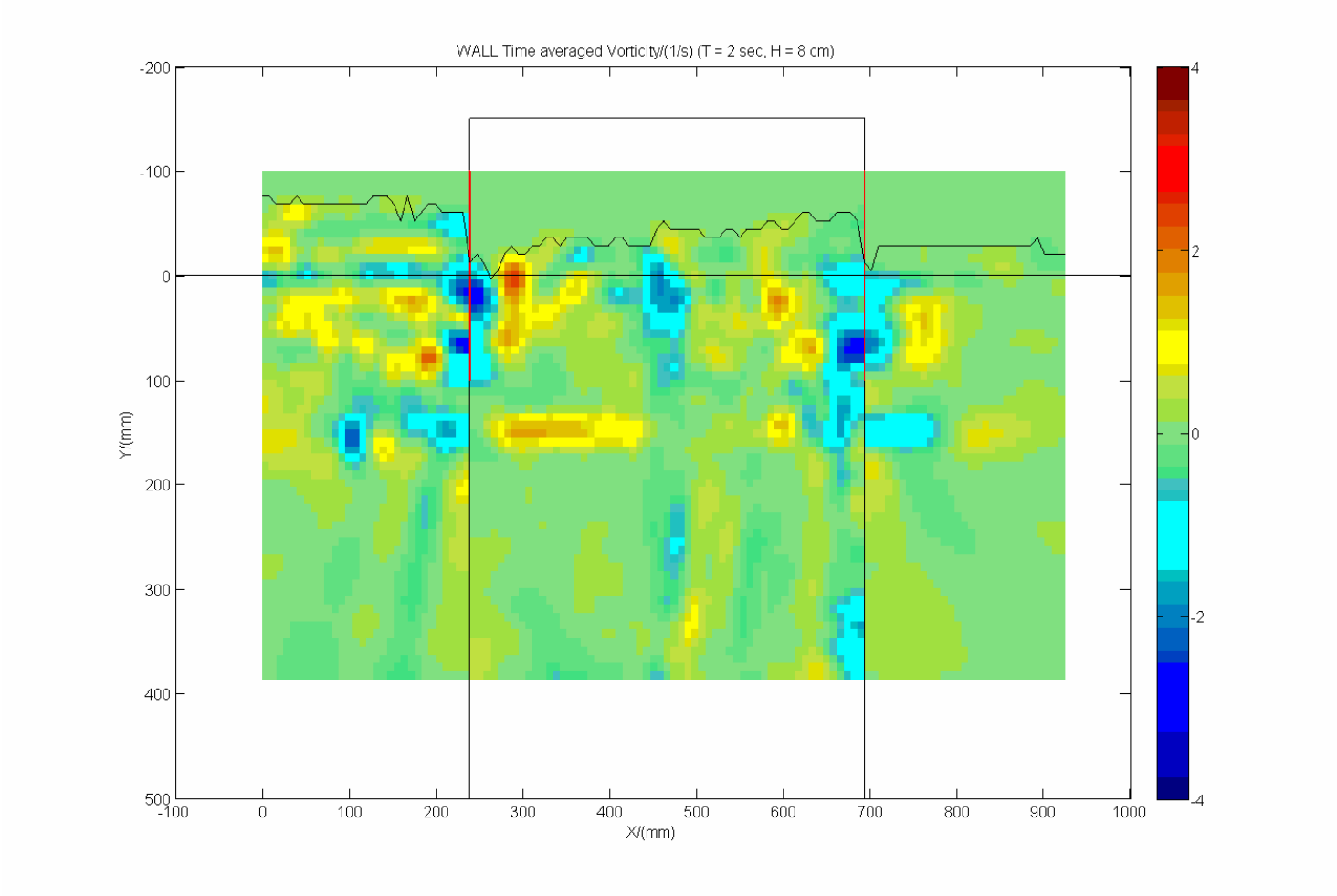

Fig. 5.2. continued.

(g)

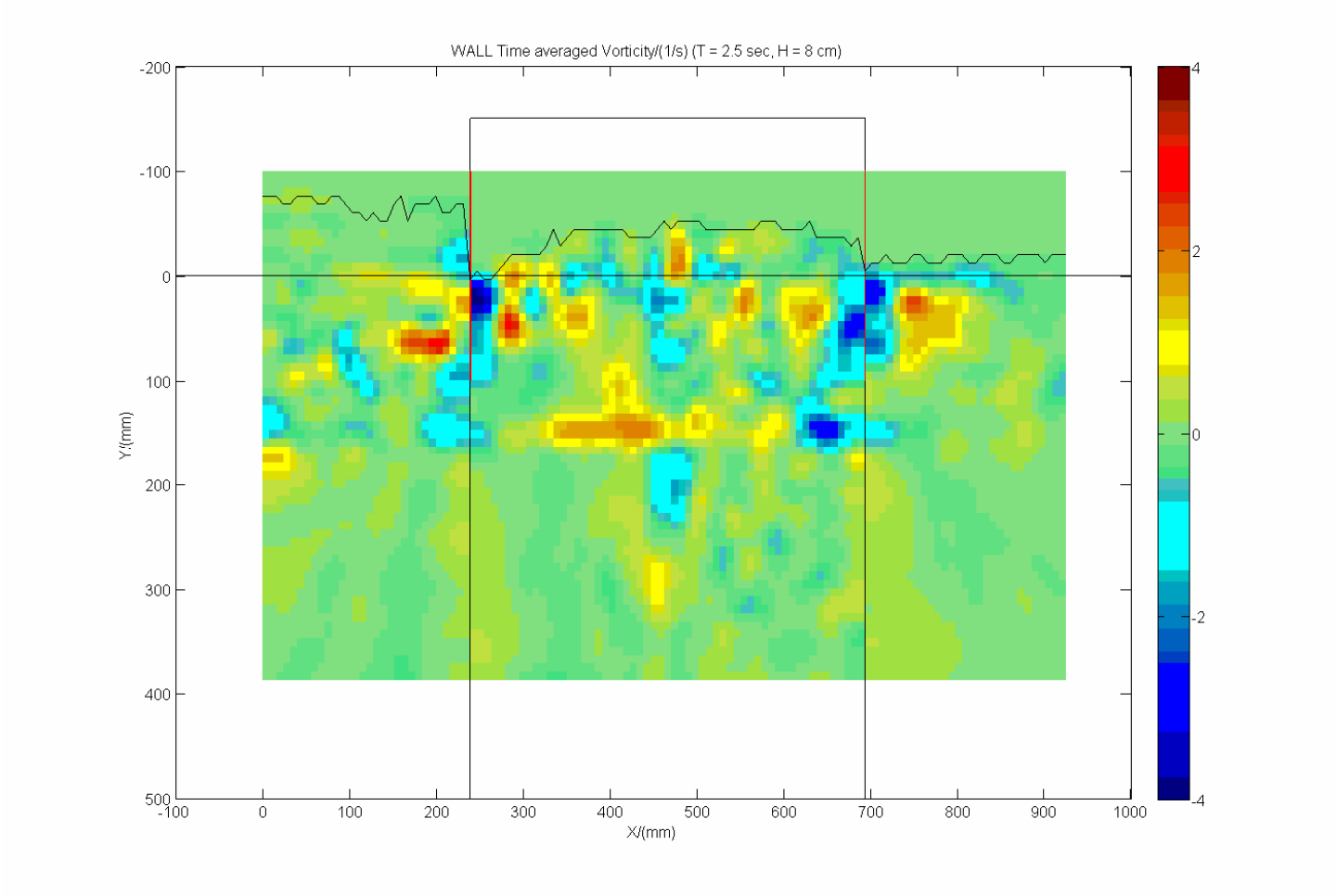

Fig. 5.2. continued.

(a)

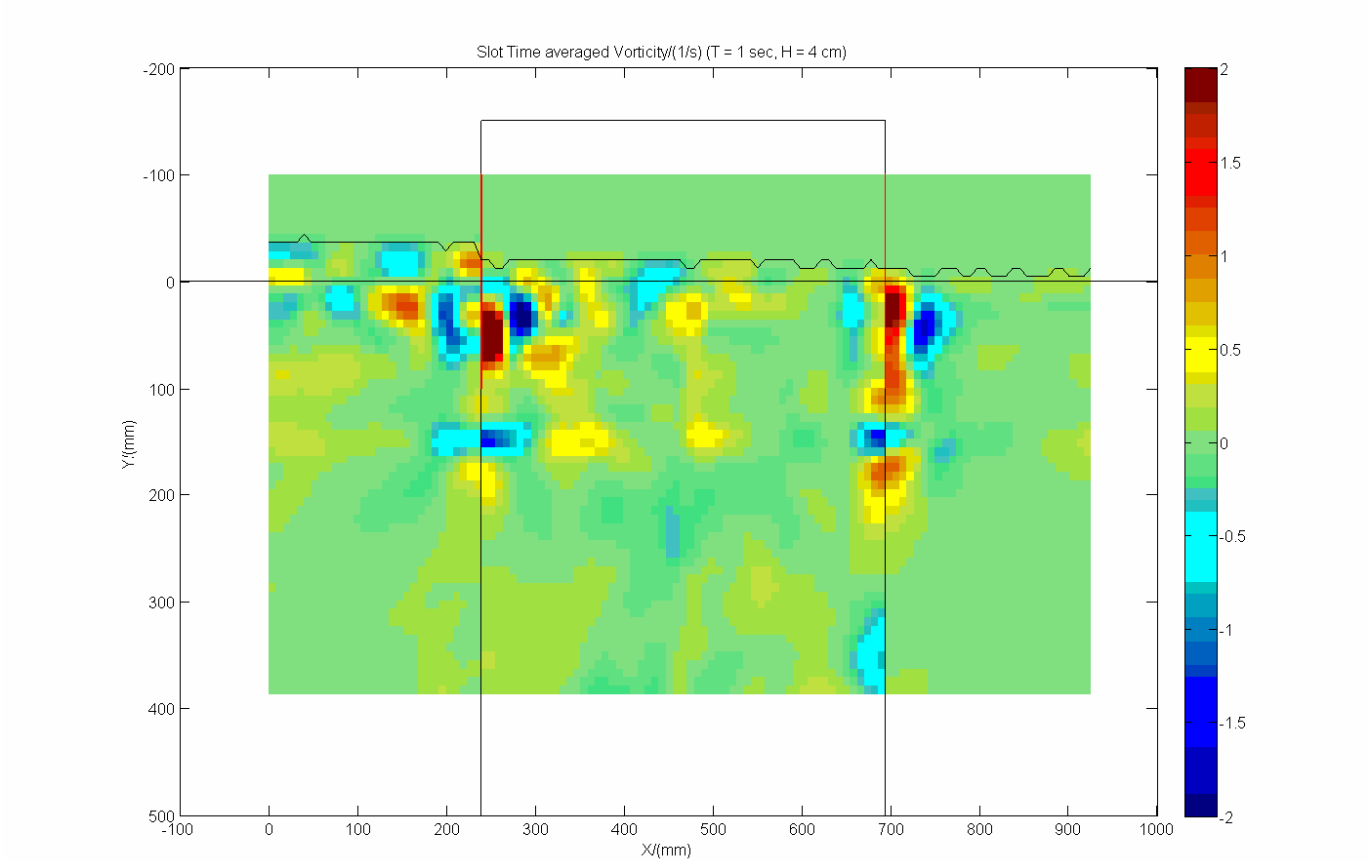

Fig. 5.3. Time averaged vorticity fields through slot. (a) T = 1 sec, H = 4 cm. (b) T = 1 sec, H = 6 cm. (c) T = 1 sec, H = 8 cm. (d) T = 1 sec, H = 10 cm. (e) T = 1.6 sec, H = 8 cm. (f) T = 2 sec, H = 8 cm. (g) T = 2.5 sec, H = 8 cm.

(b)

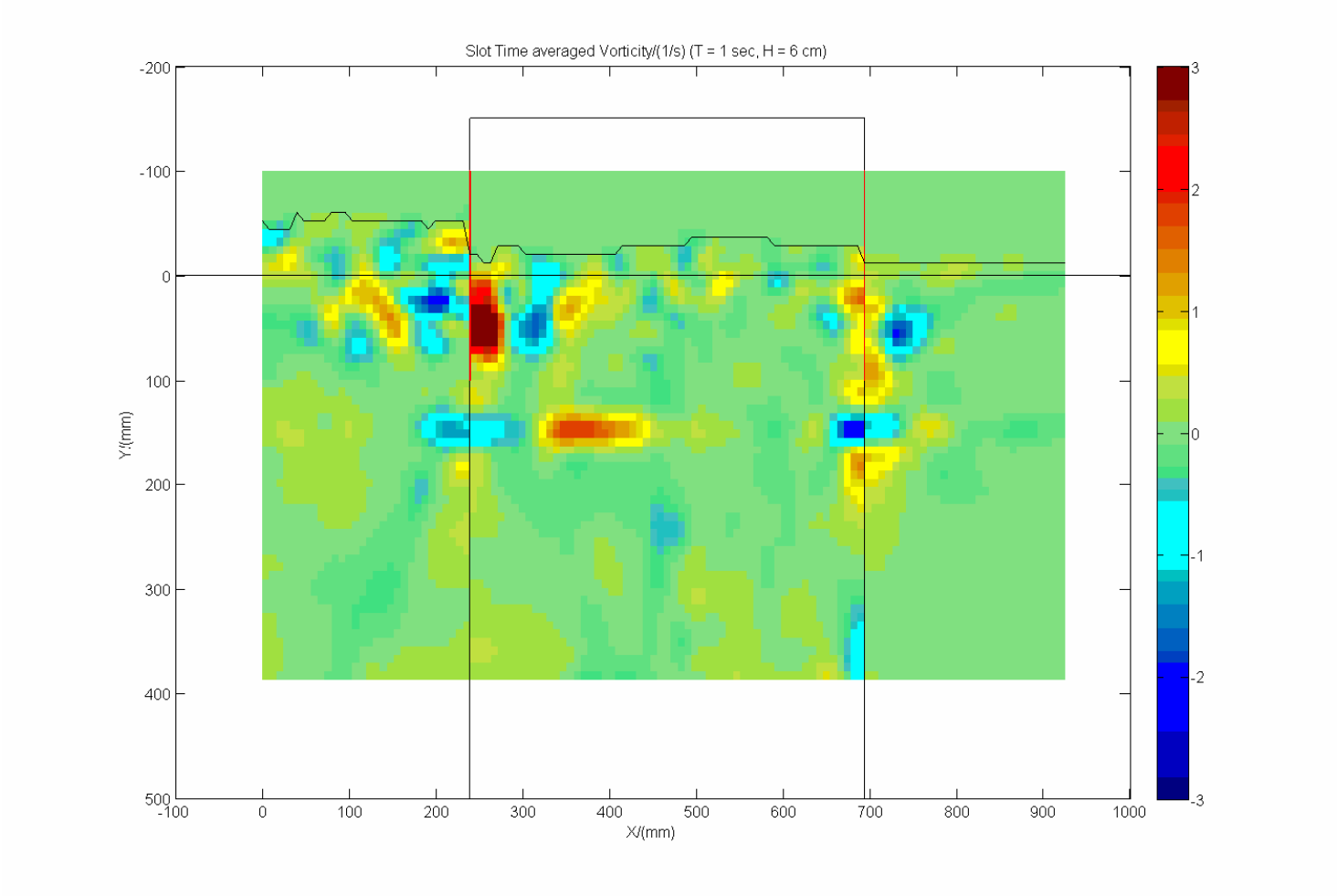

Fig. 5.3. continued.

(c)

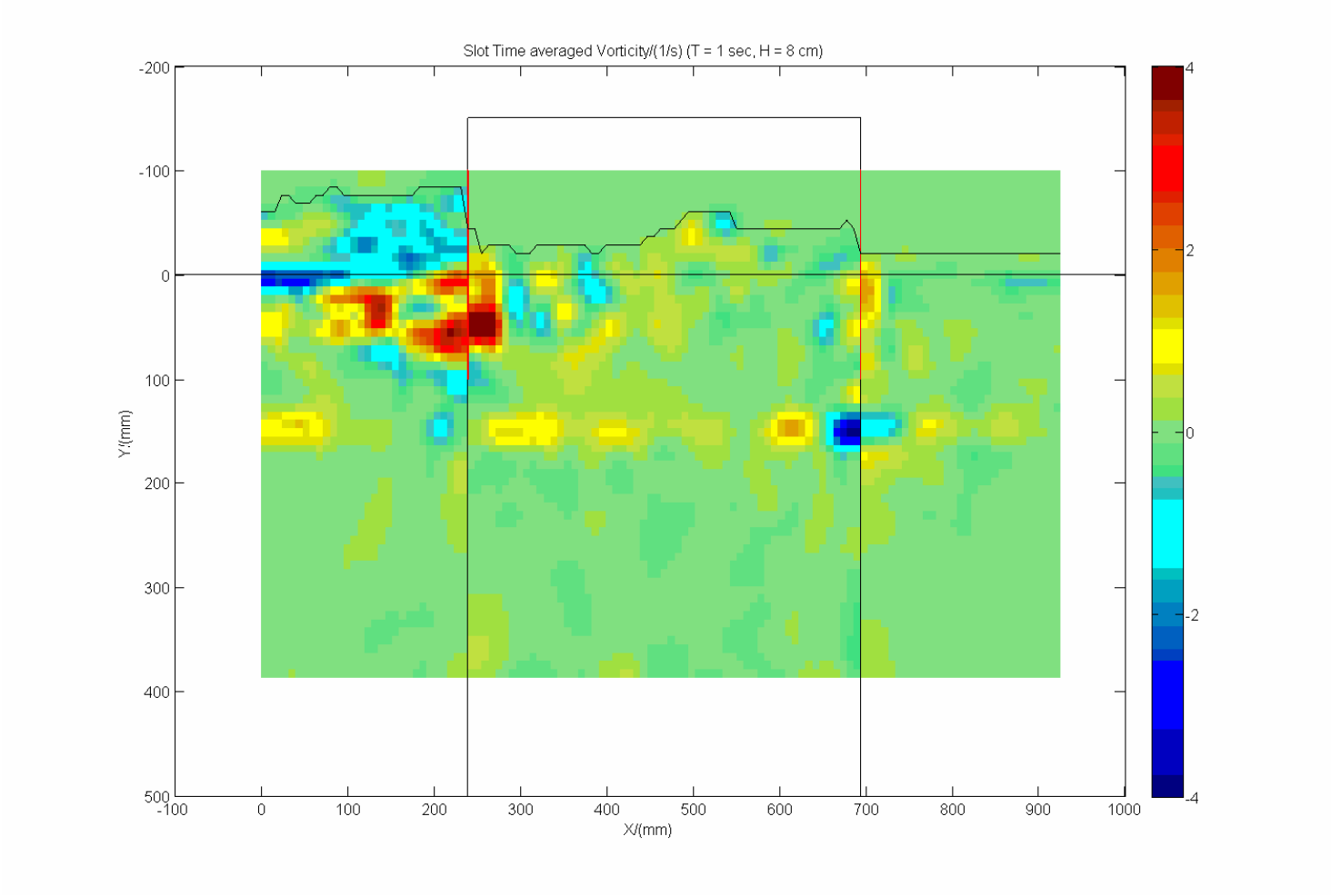

Fig. 5.3. continued.

(d)

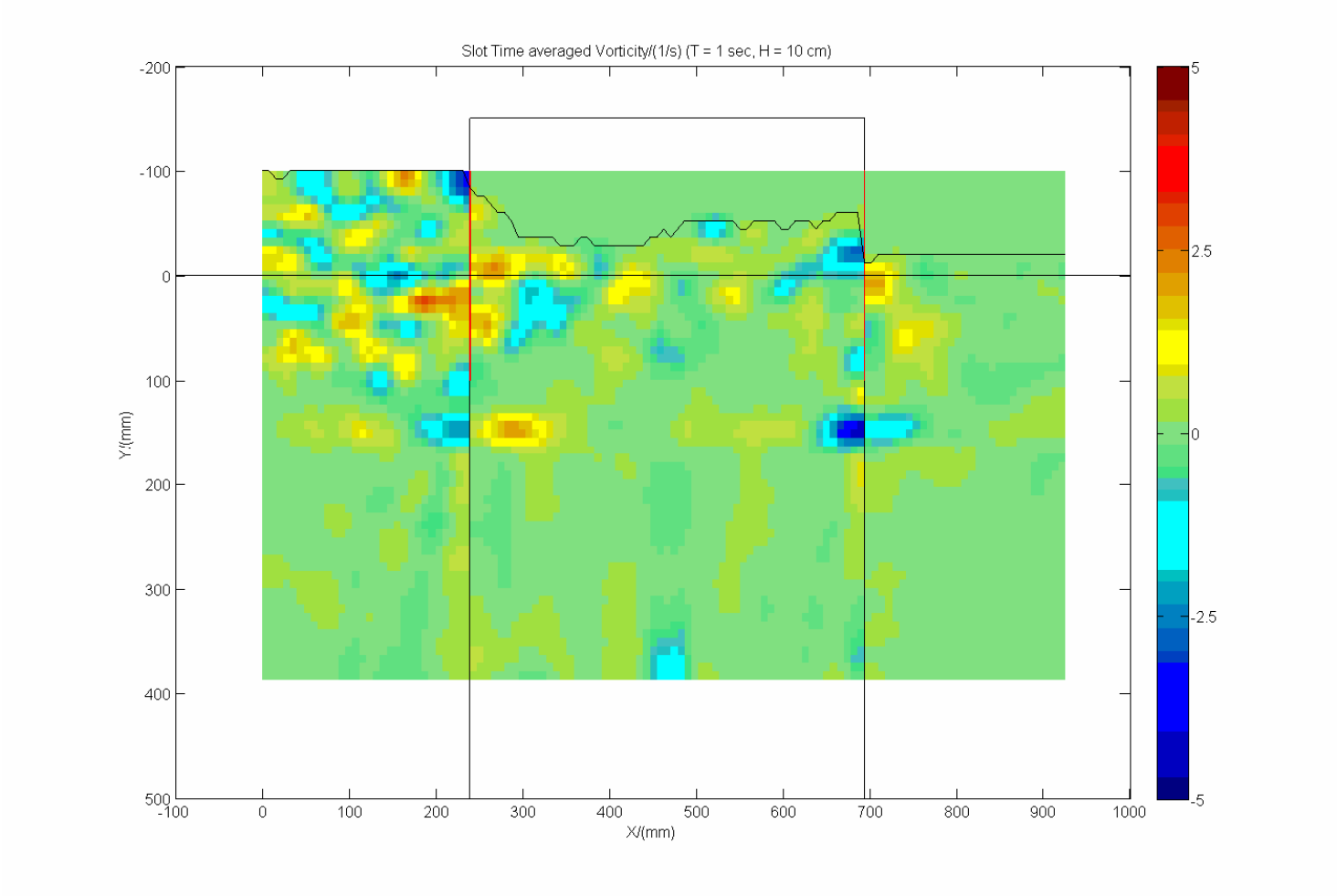

Fig. 5.3. continued.

(e)

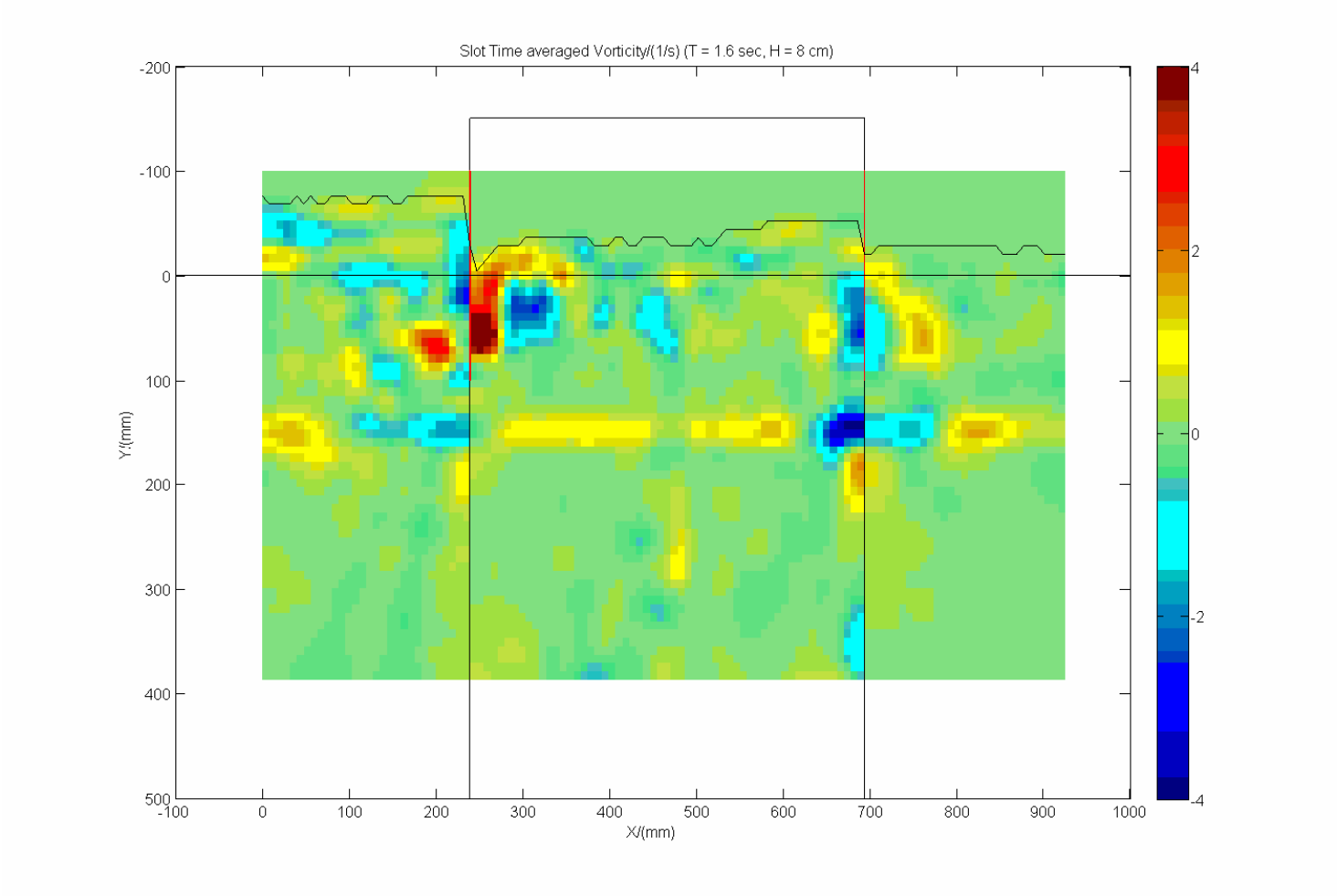

Fig. 5.3. continued.

(f)

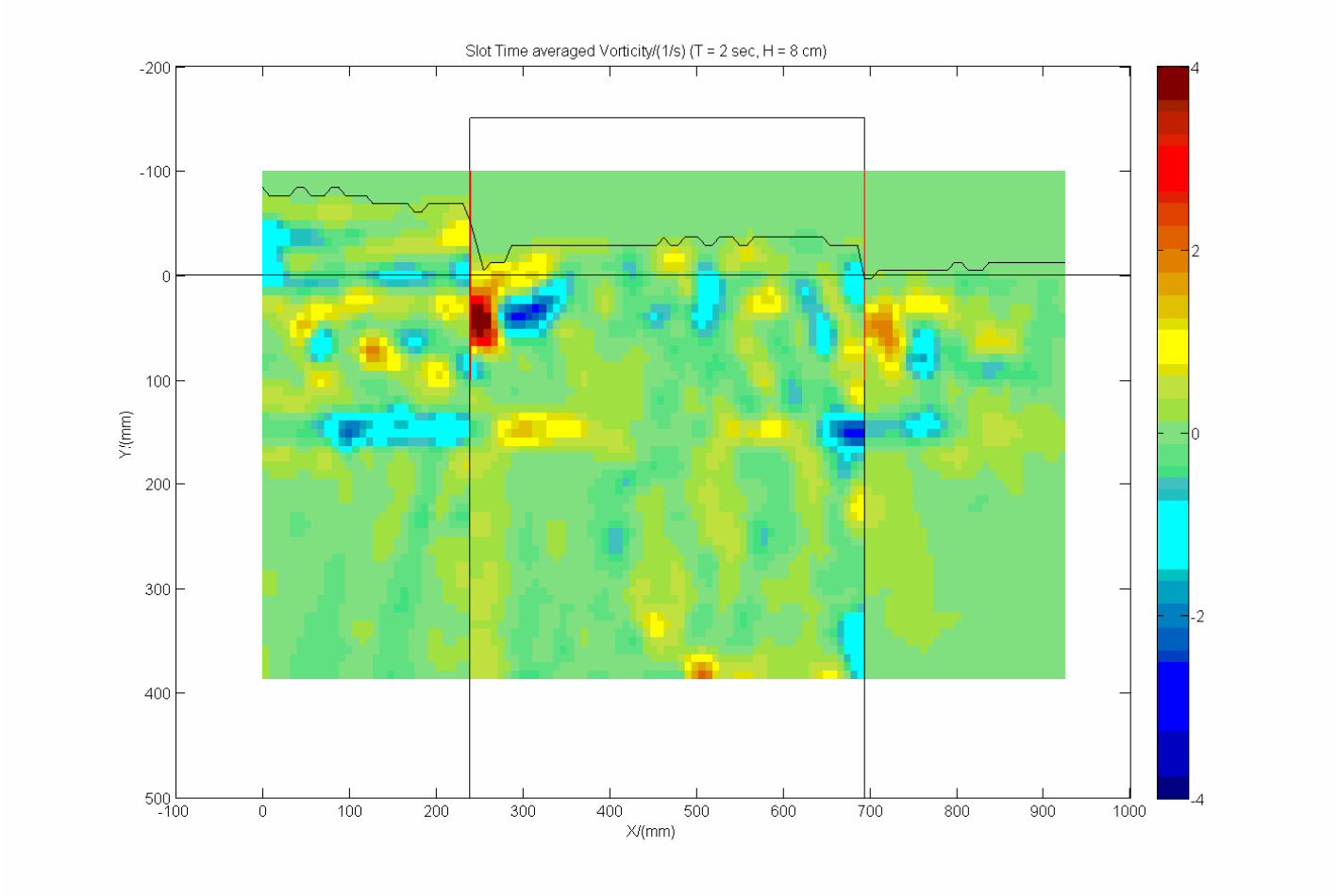

Fig. 5.3. continued.

(g)

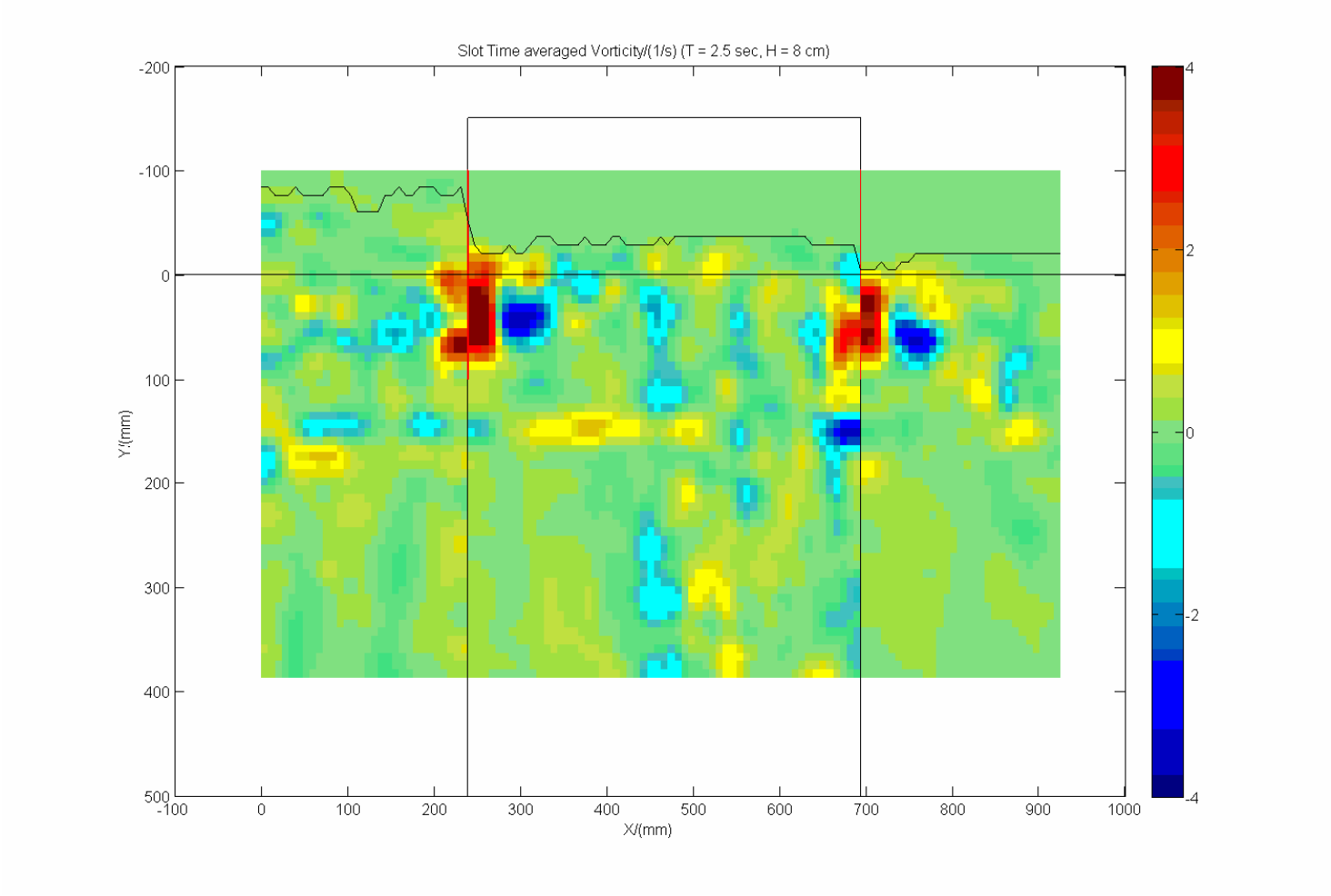

Fig. 5.3. continued.

There is a difference in water level near the front wall for the light sheet through slot, this can be due to the fact that the slot (2 cm wide) height is only one third of the structure height. Since the wall acts as a barrier to the incoming wave the flow slows near the wall, hence there is a phase lag in between the waves infront of front wall and inside the chamber. This can be clearly seen in wave measurement data (see figure 5.4 and 5.6). In the measurement data there is a phase lag in wave elevation measured data for gauges in front of front wall and inside the chamber (gauges 2, 3), see figure 5.5 for gauge locations.

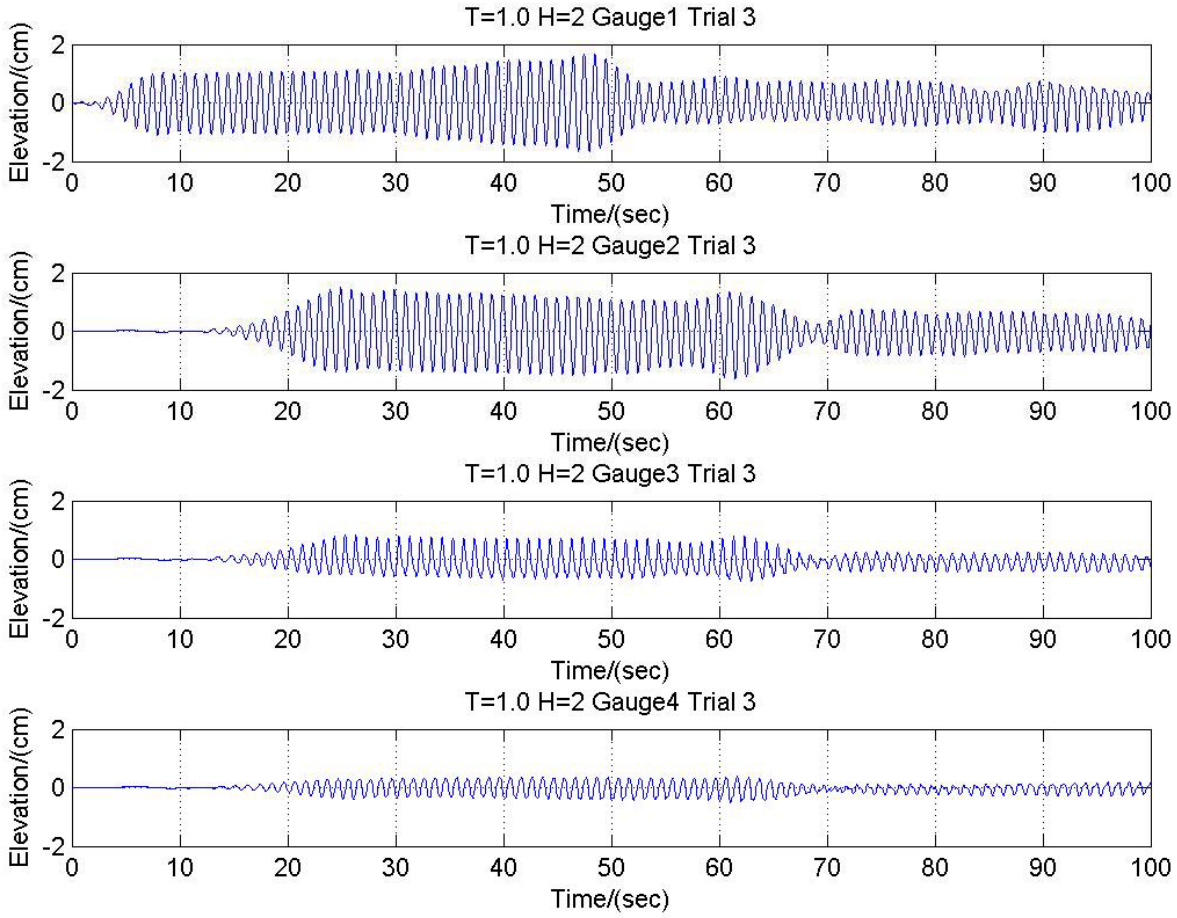

Fig. 5.4. Measured wave elevation data.

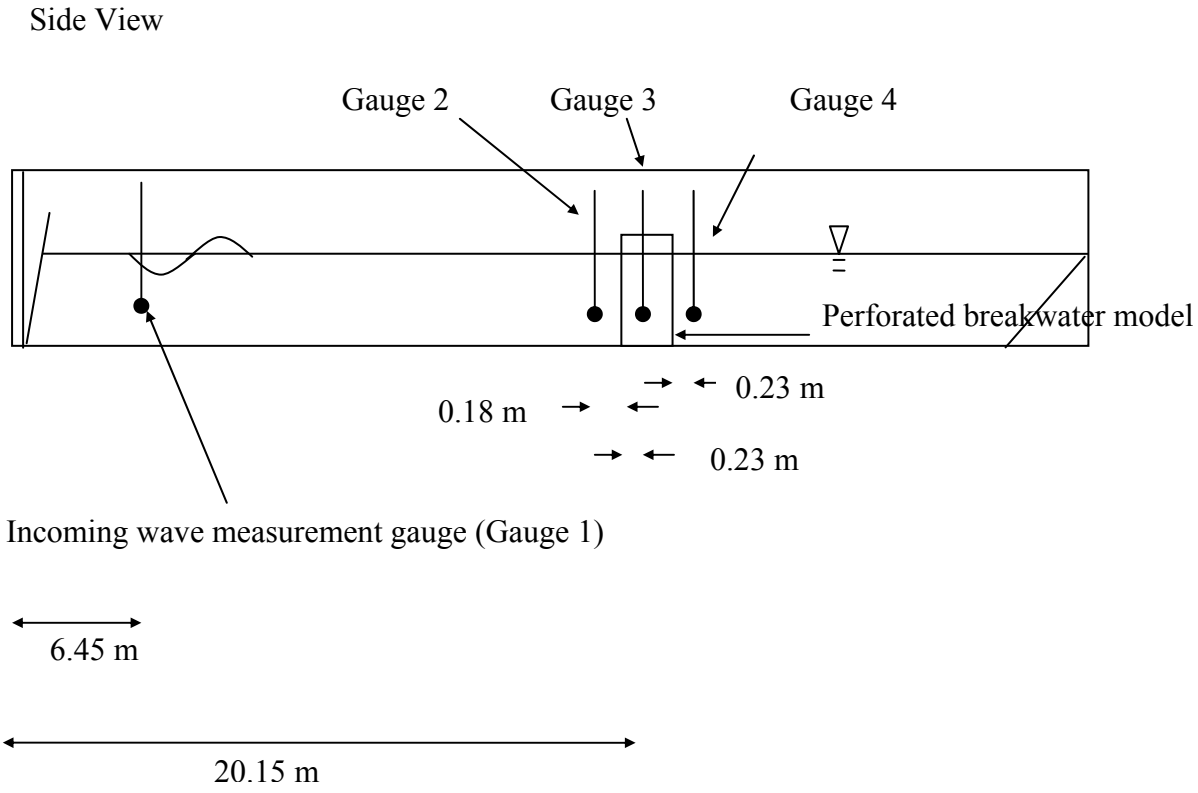

Fig. 5.5. Gauge locations.

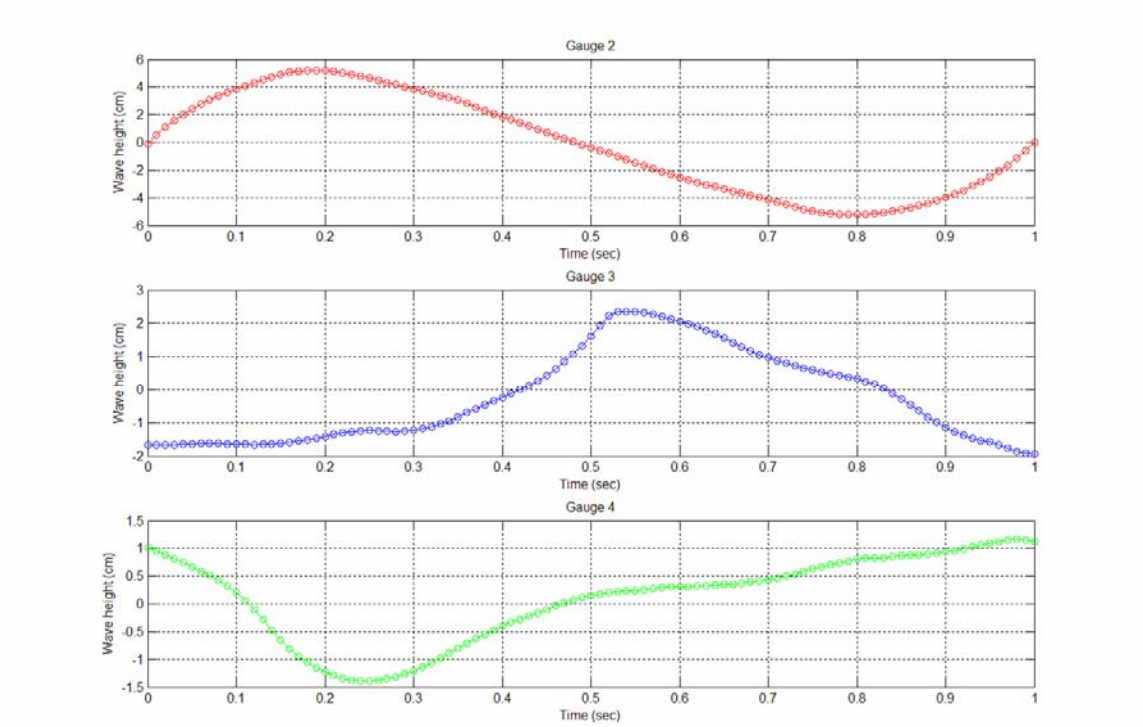

Fig. 5.6. Phase difference in measured data for gauges 2,3 and 4.

CHAPTER VI

TURBULENT INTENSITY AND TURBULENT KINETIC ENERGY FIELDS IN THE VICINITY OF THE STRUCTURE

6.1. Turbulence intensity field

Turbulent intensity for 2 D flow is defined as

$$I = (u'u' + v'v')^{\frac{1}{2}} \qquad (6.1)$$

Where

u' – turbulent velocity in x-direction

$= u_i - u_{mean}$

where

u_i = instantaneous velocity in x direction

v' – turbulent velocity in y-direction

$= v_i - v_{mean}$

where

v_i = instantaneous velocity in y direction

Turbulent intensity was calculated for each phase and each wave condition. The phase average turbulence intensity was calculated taking the average of the ten phases (see fig. 6.1).

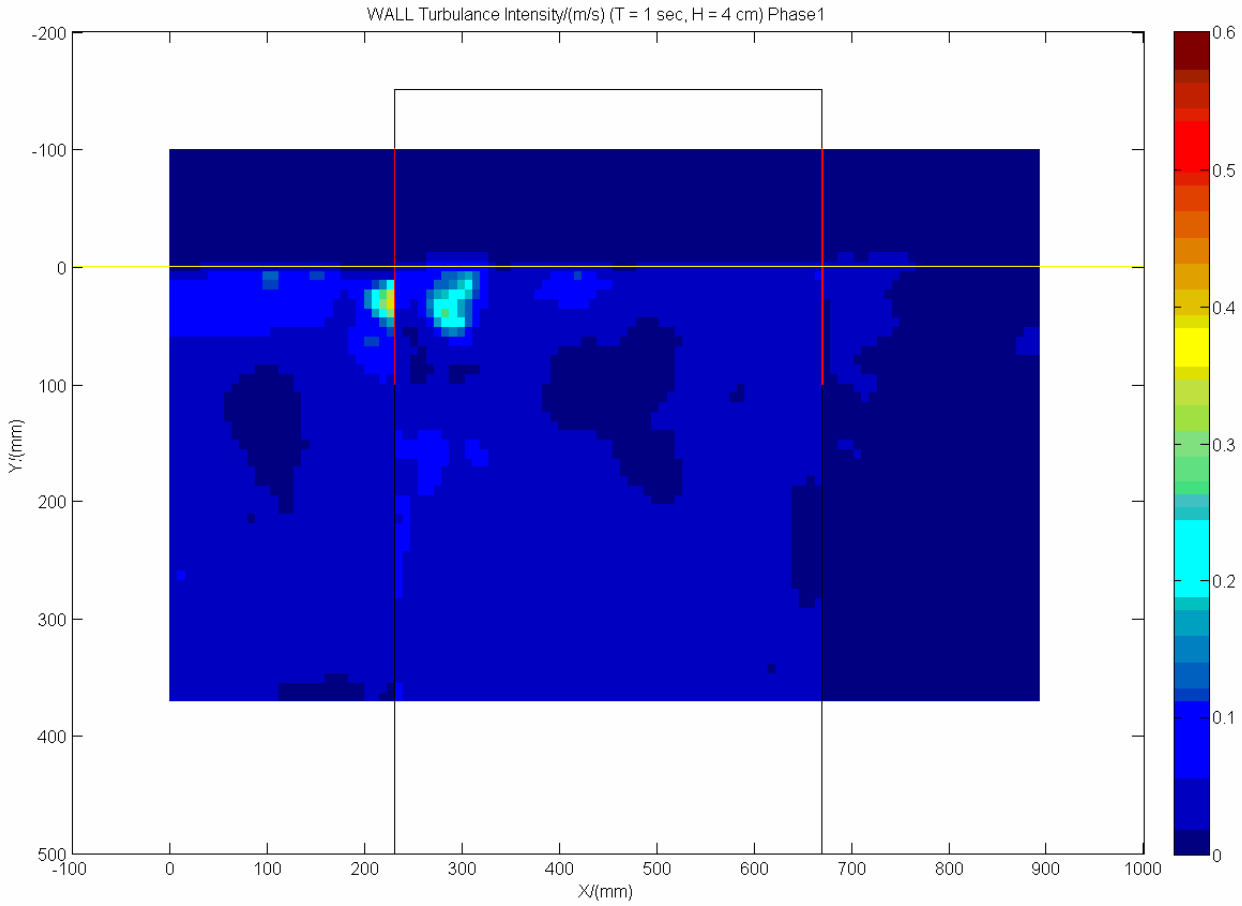

Fig. 6.1. Calculated turbulence intensity field in the vicinity of the structure for wave condition $T = 1$ sec, $H_i = 4$ cm, Phase 1.

6.2. Turbulent kinetic energy field

After calculating turbulence intensity, the turbulent kinetic energy was calculated as,

$$TKE \approx (1.33 / 2)\, I^2 \qquad (6.2)$$

(Svendsen, 1987)

For the light sheet through wall, for all wave conditions, turbulent kinetic energy appears near the front wall and near free surface. First it appears in a smaller area, and with time it spreads in to a wider area and then fades away. For wave condition T = 1 sec, H_i = 4, 6, 8 cm for most of the phases turbulent kinetic energy concentrates near front wall. The magnitude of turbulent kinetic energy is higher for light sheet through slot than that for light sheet through wall. Behind back wall there is no turbulent kinetic energy. For both light sheets phase averaged turbulent kinetic energy concentrates near front wall and the magnitude is higher for the light sheet through slot.

When wave conditions get larger (T = 1 sec, H_i = 10 cm, T = 1.6, 2, 2.5 sec, H_i = 8 cm) turbulent kinetic energy appears not only near the free surface and near the front wall but also under the free surface and inside the chamber. For the first time turbulent kinetic energy appears behind the back wall for T = 1 sec, H_i = 10 cm. It spreads to a wider area and a clear discontinuity can be seen near walls. For all the wave conditions, turbulent kinetic energy behind the back wall is very small.

For the light sheet through slot, the pattern of turbulent kinetic energy is same as that for the light sheet through wall, but turbulent kinetic energy appears in many areas, and when wave conditions get larger (T = 1 sec, H_i = 10 cm, T = 1.6, 2, 2.5 sec, H_i = 8 cm), it forms behind the back wall as well. It shows a continuity near walls.

After calculating the turbulent kinetic energy field for each phase, the time average turbulent kinetic energy field was calculated by taking the average of the ten phases (see figures 6.2 and 6.3). In the figures the free surface is marked with a yellow colour line.

(a)

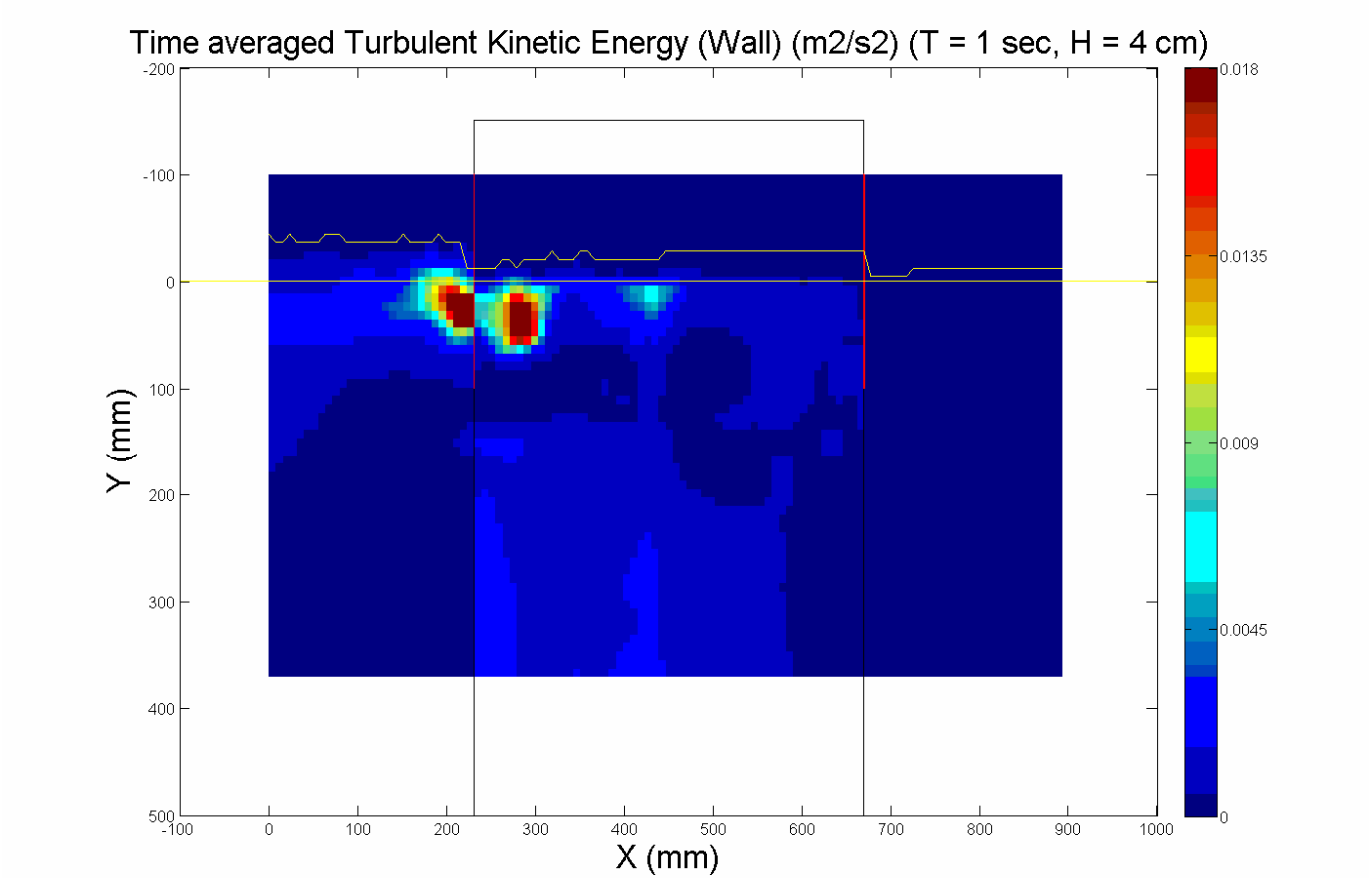

Fig. 6.2. Time averaged turbulent kinetic energy fields through wall. (a) T = 1 sec, H = 4 cm. (b) T = 1 sec, H = 6 cm. (c) T = 1 sec, H = 8 cm. (d) T = 1 sec, H = 10 cm. (e) T = 1.6 sec, H = 8 cm. (f) T = 2 sec, H = 8 cm. (g) T = 2.5 sec, H = 8 cm.

(b)

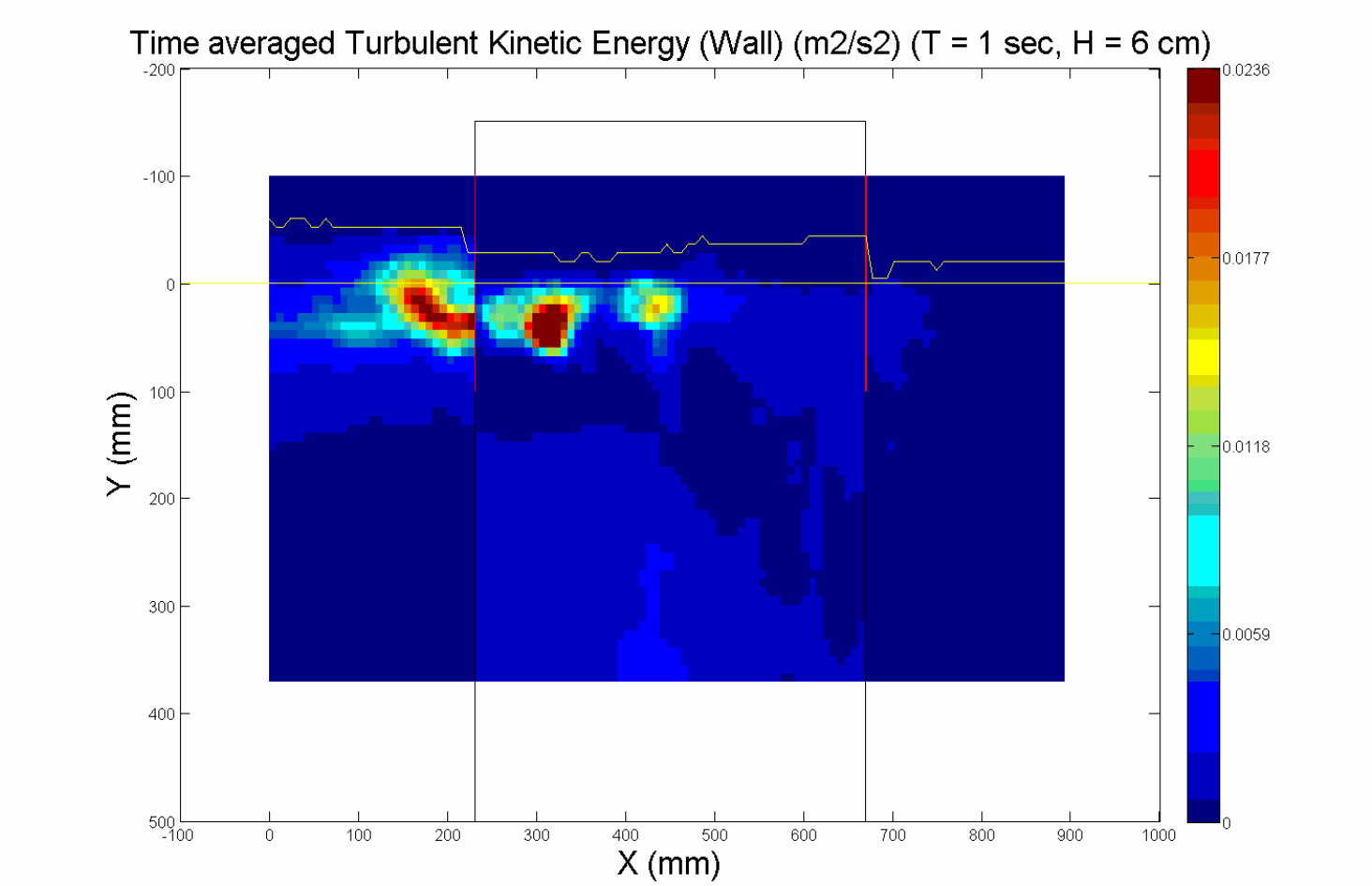

Fig. 6.2. continued.

(c)

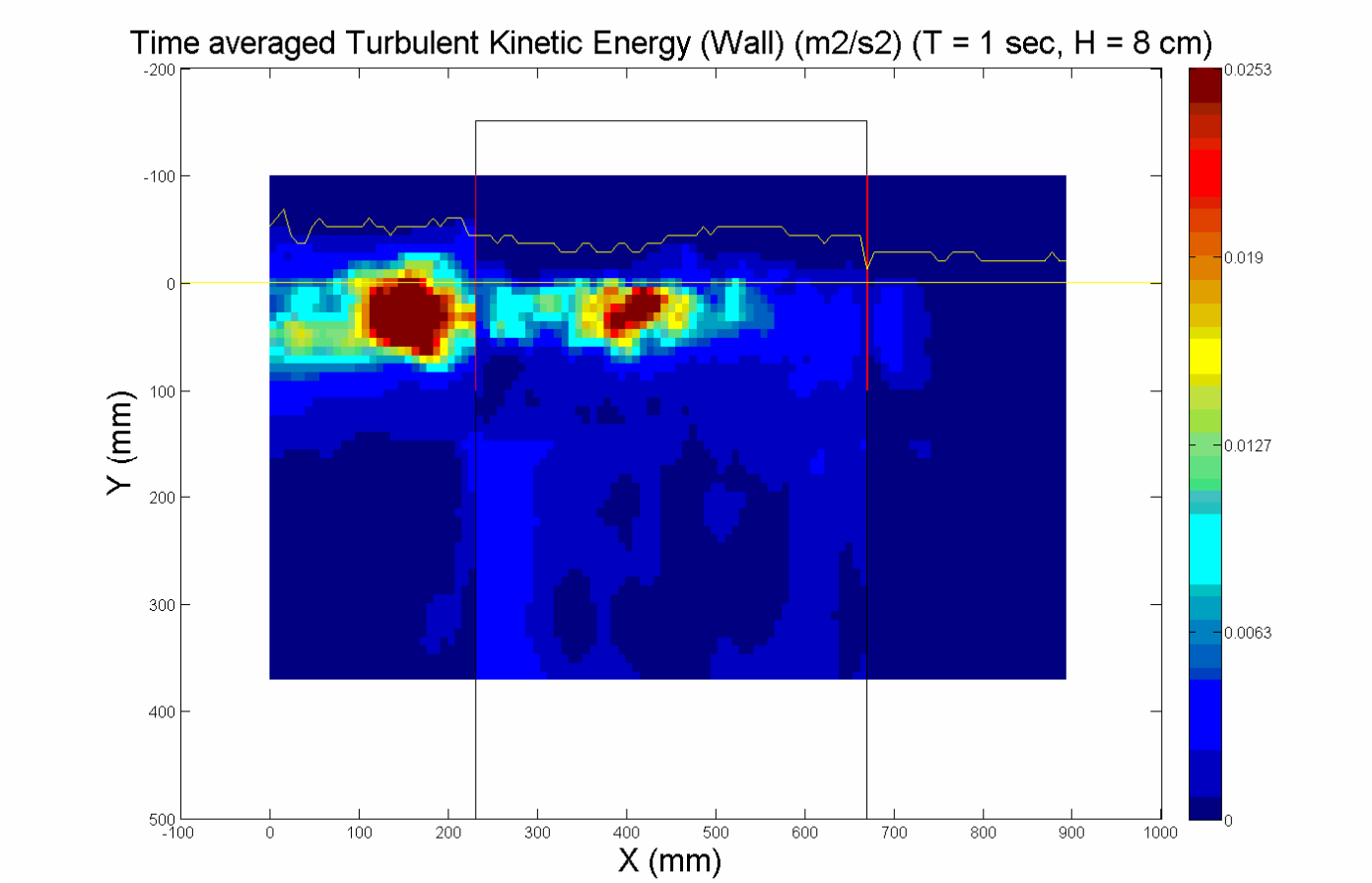

Fig. 6.2. continued.

(d)

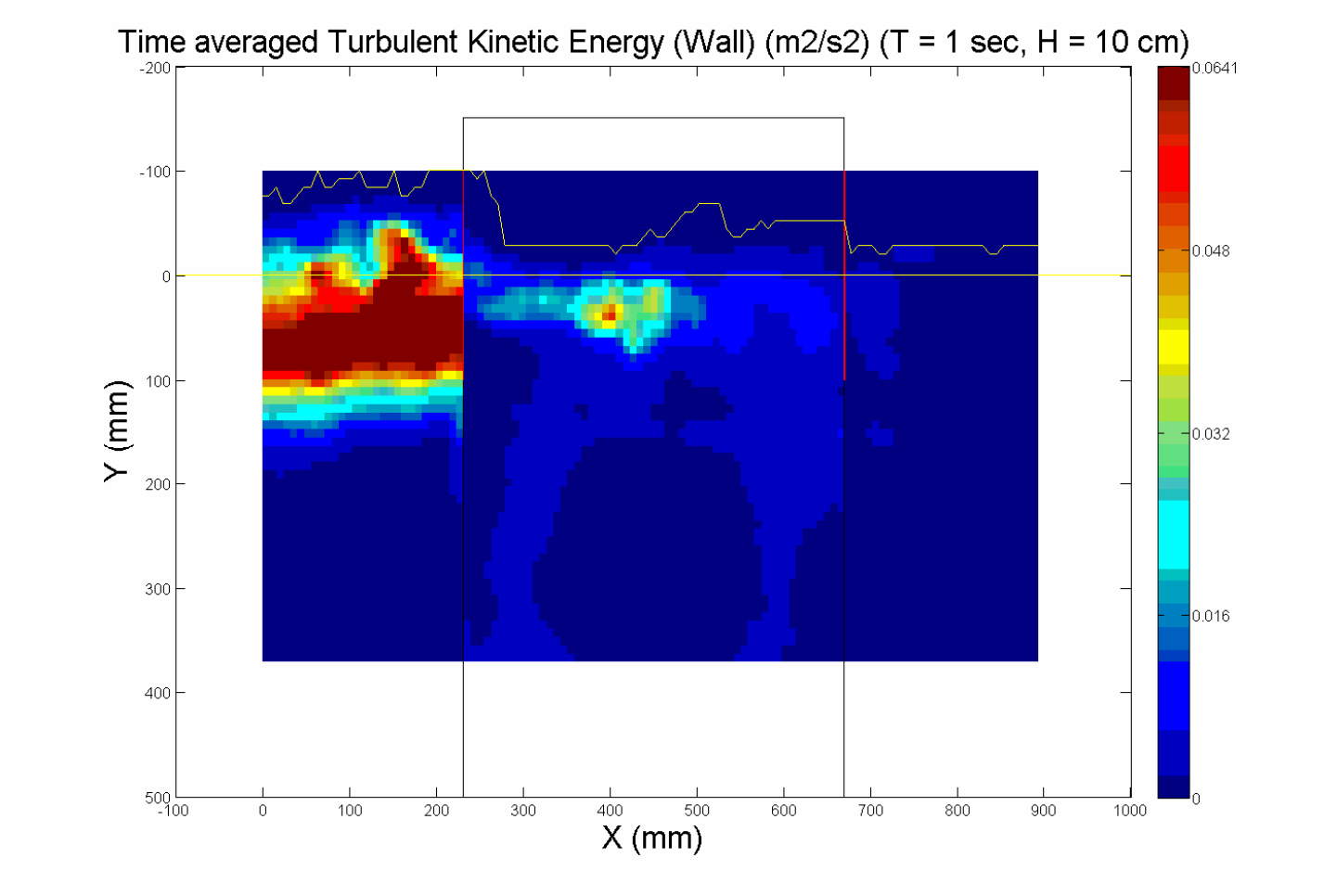

Fig. 6.2. continued.

(e)

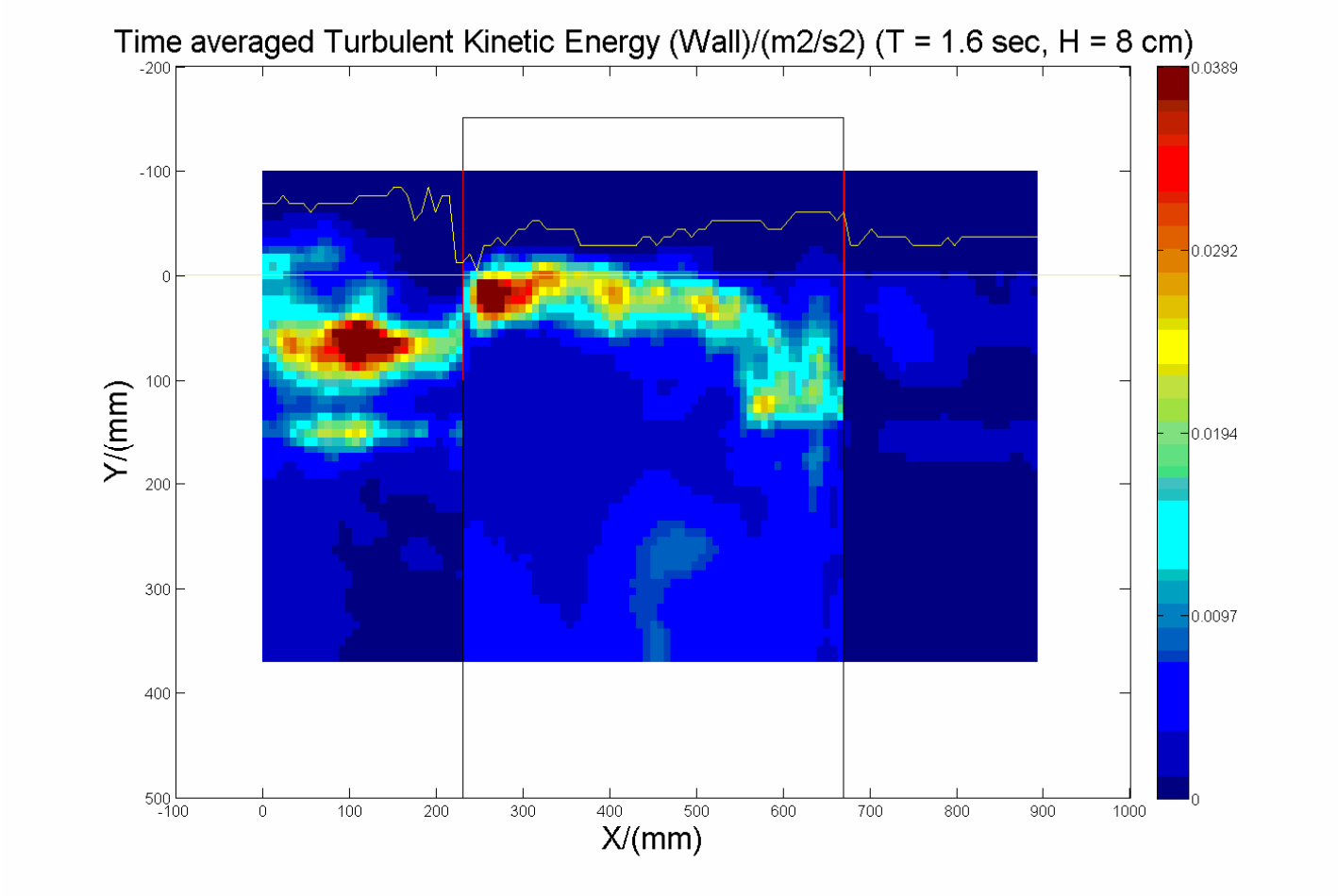

Fig. 6.2. continued.

(f)

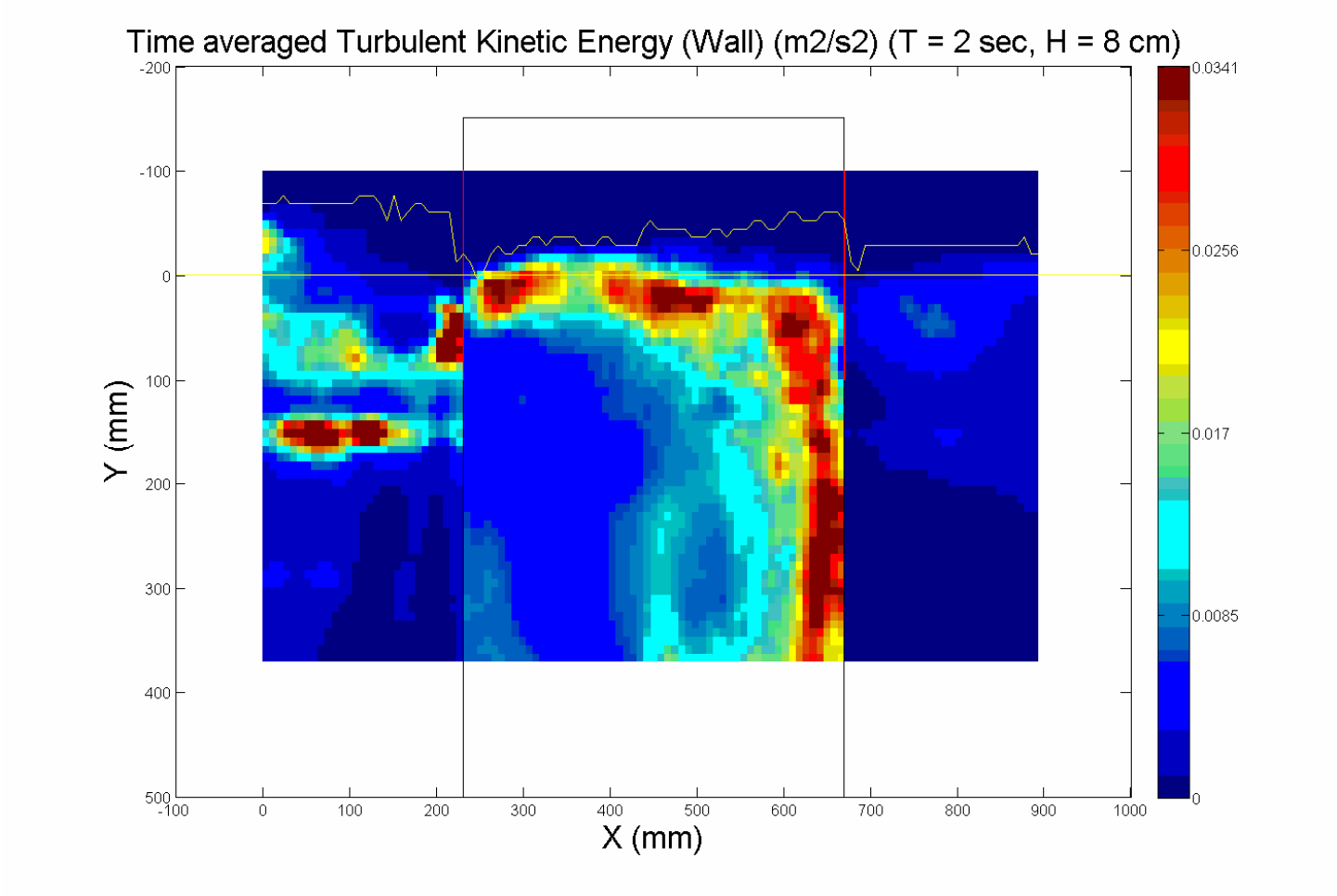

Fig. 6.2. continued.

(g)

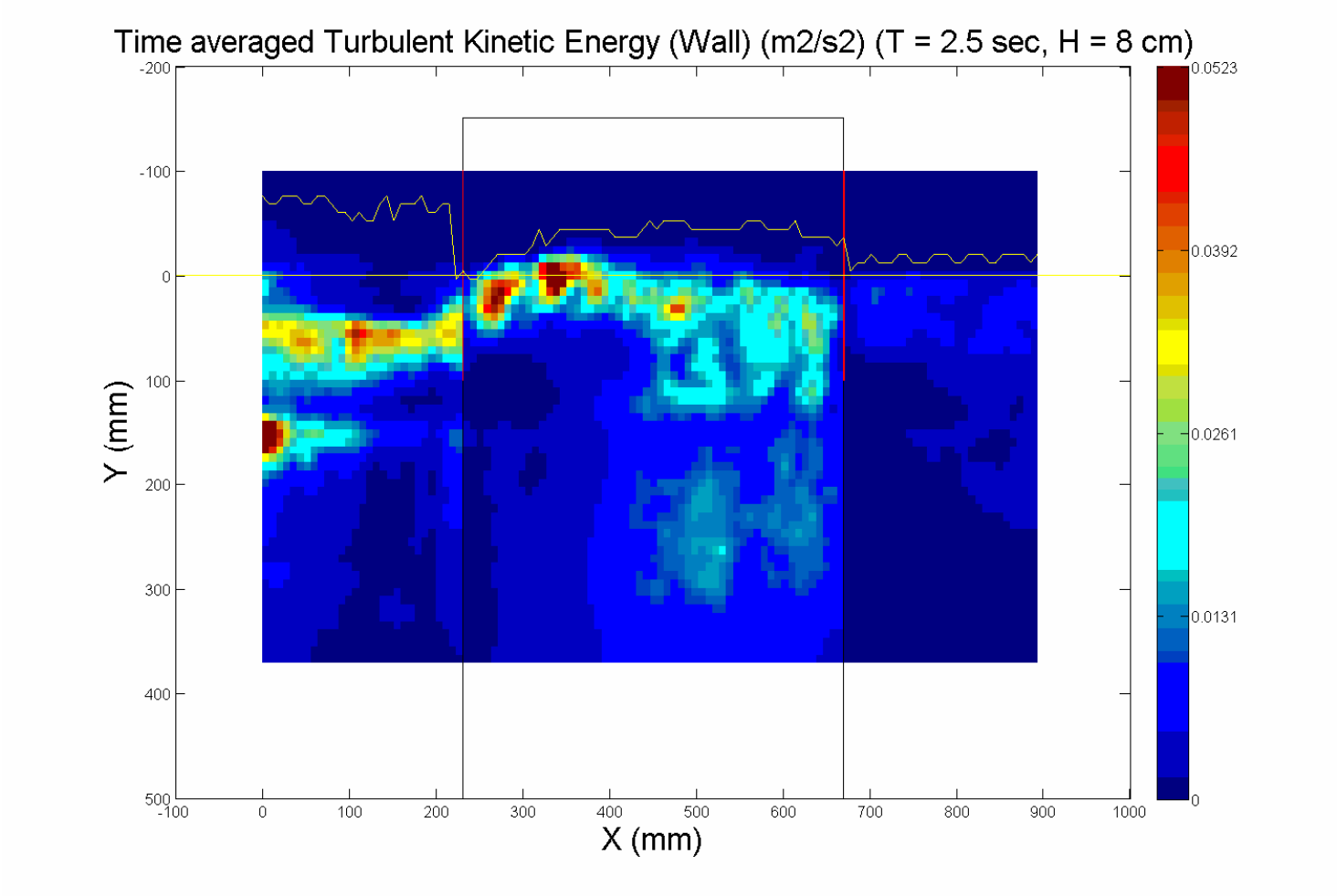

Fig. 6.2. continued.

(a)

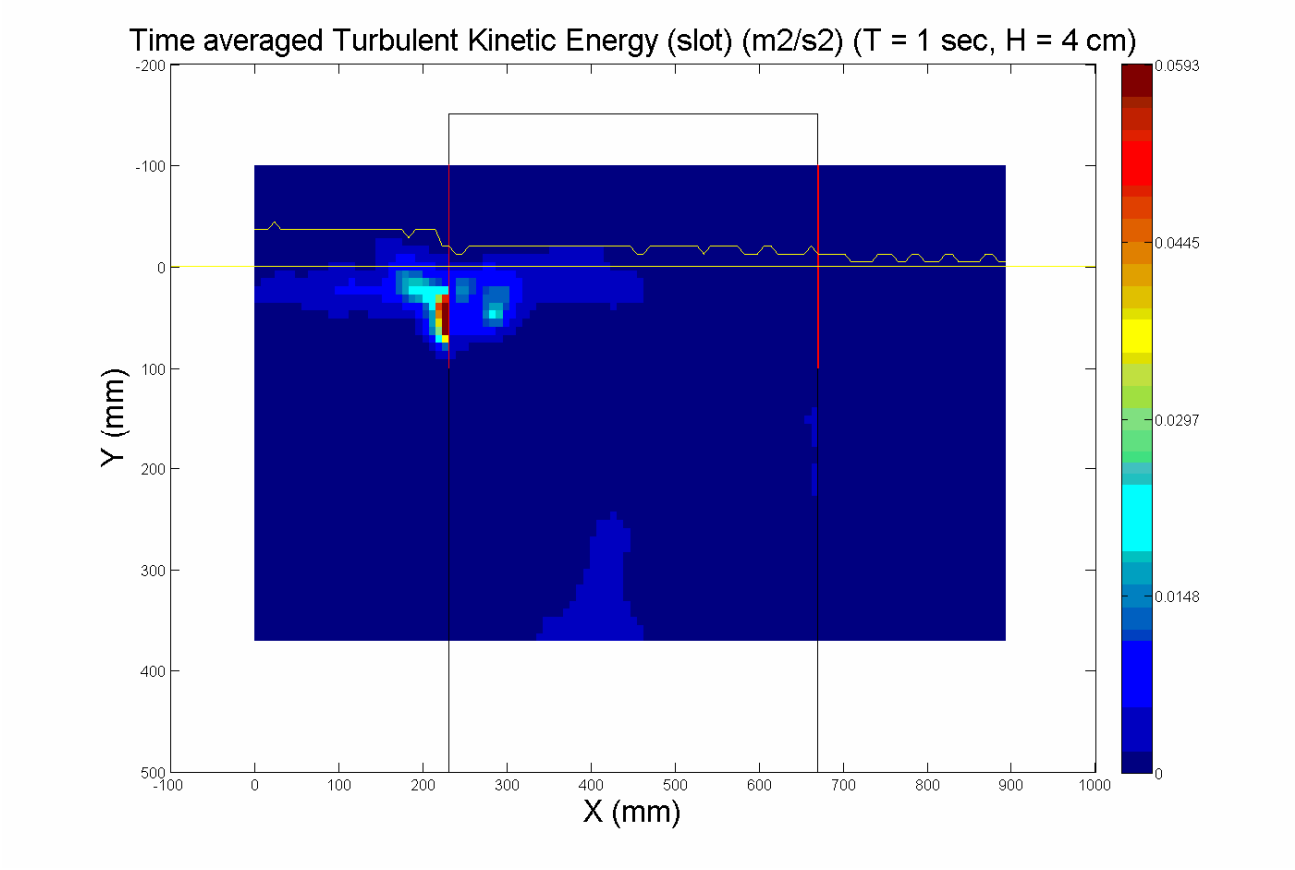

Fig. 6.3. Time averaged turbulent kinetic energy fields through slot. (a) T = 1 sec, H = 4 cm. (b) T = 1 sec, H = 6 cm. (c) T = 1 sec, H = 8 cm. (d) T = 1 sec, H = 10 cm. (e) T = 1.6 sec, H = 8 cm. (f) T = 2 sec, H = 8 cm. (g) T = 2.5 sec, H = 8 cm.

(b)

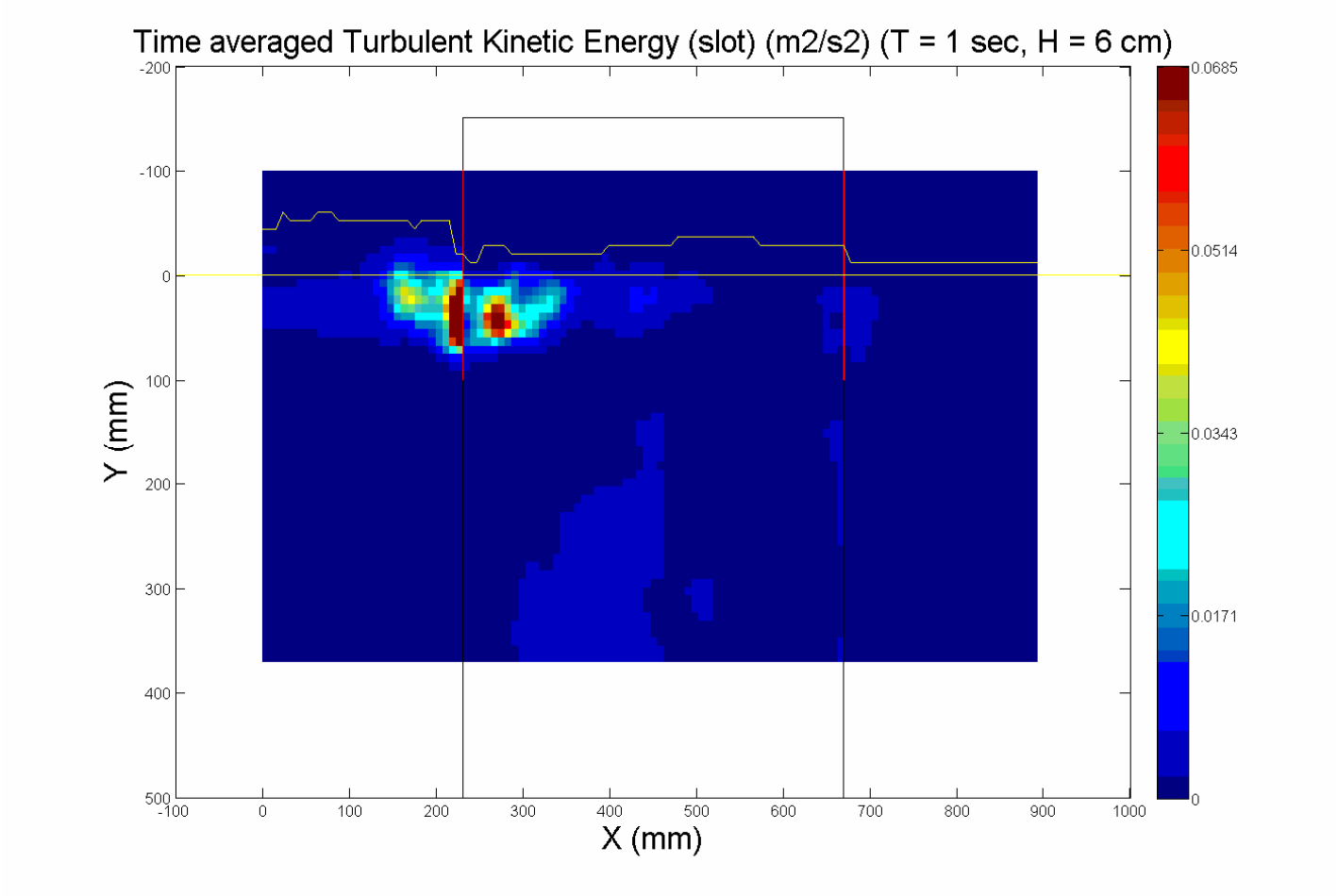

Fig. 6.3. continued.

(c)

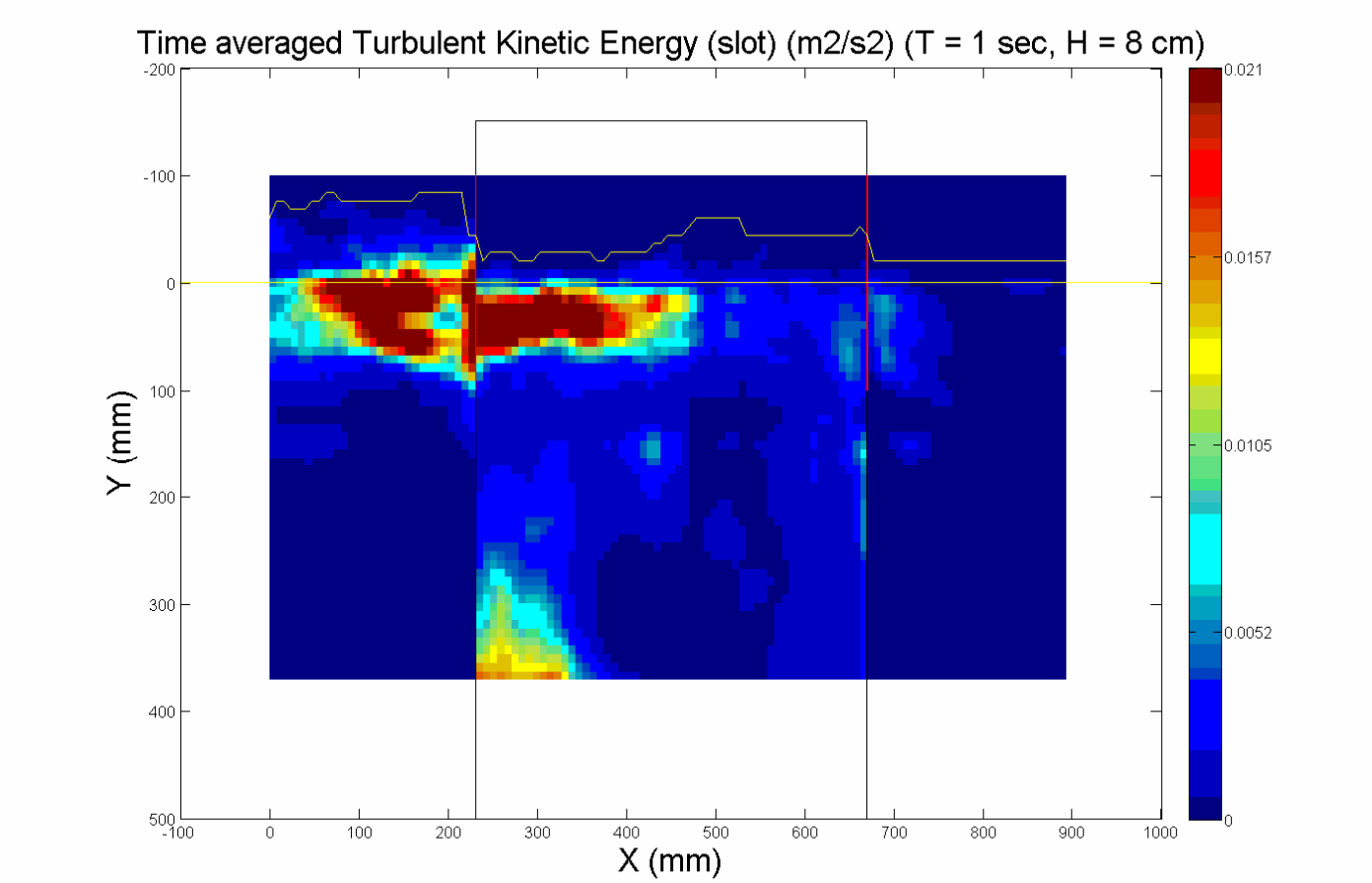

Fig. 6.3. continued.

(d)

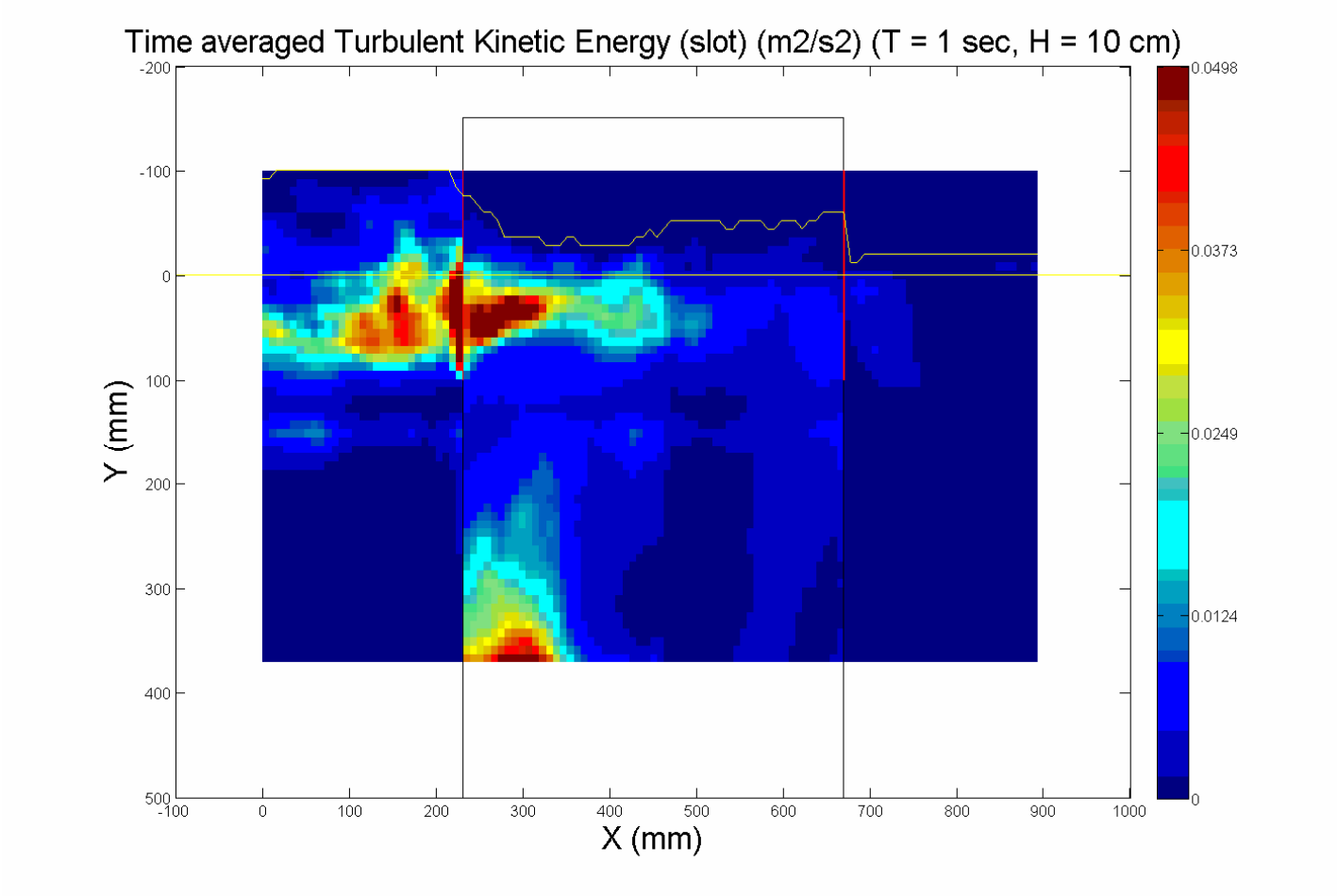

Fig. 6.3. continued.

(e)

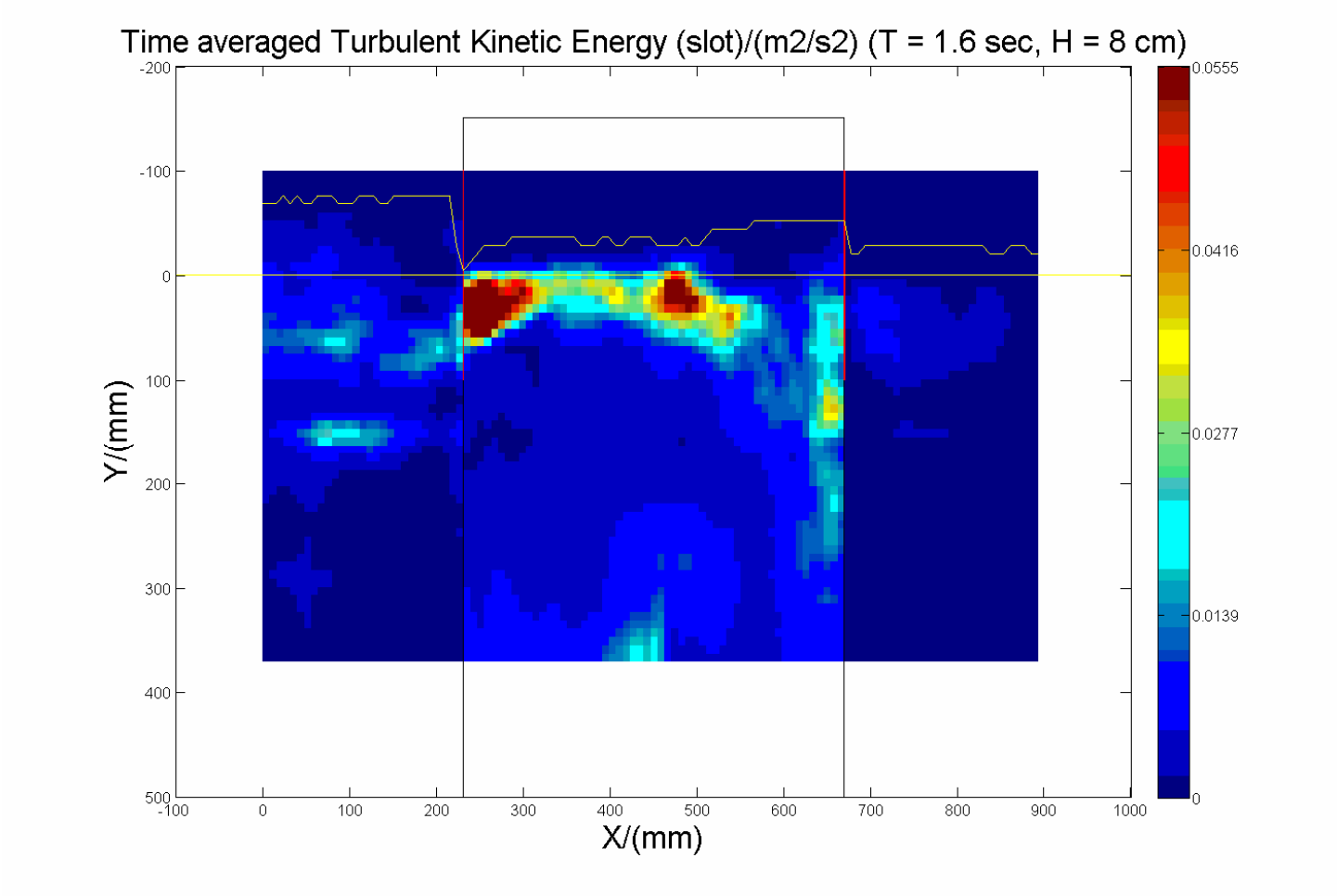

Fig. 6.3. continued.

(f)

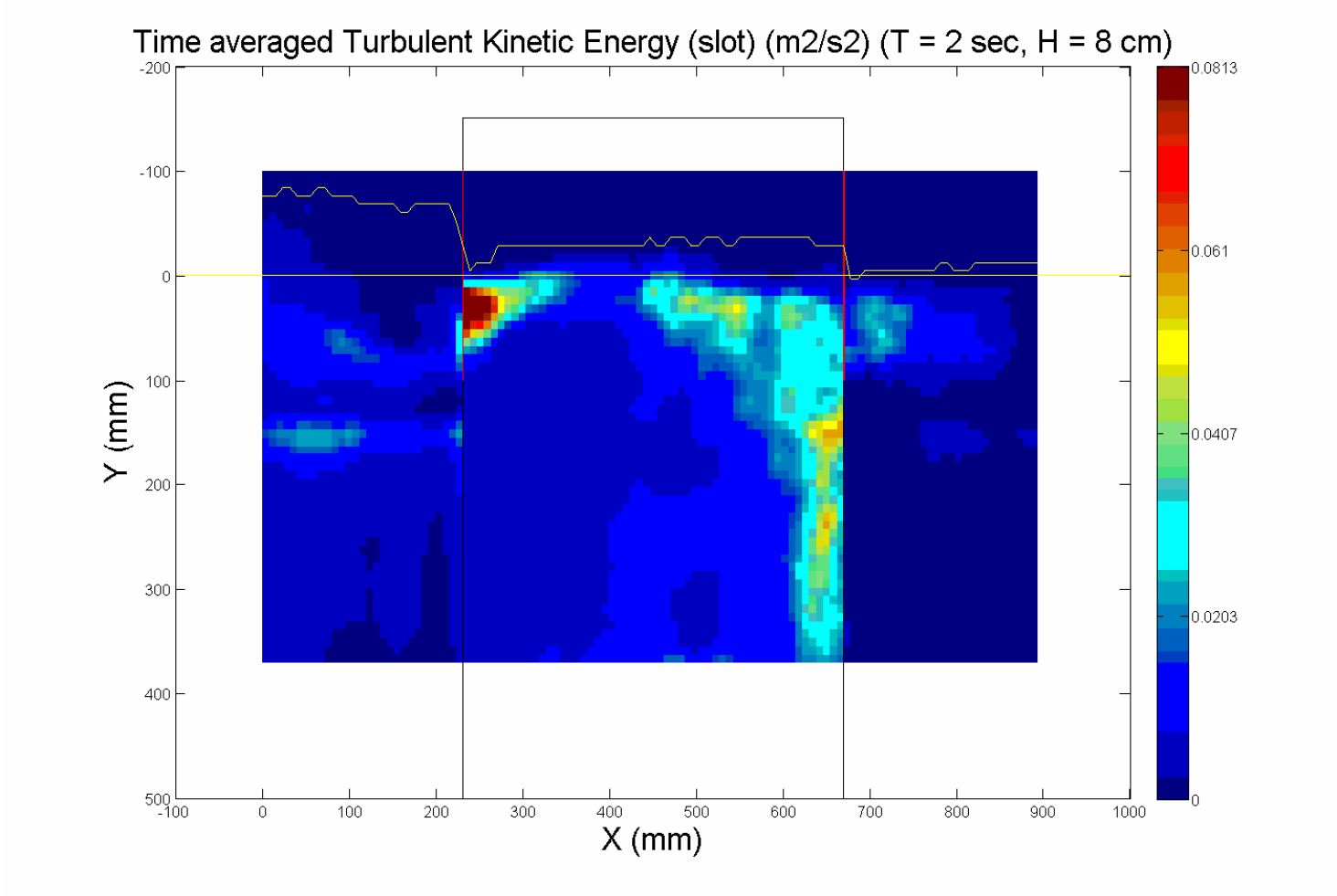

Fig. 6.3. continued.

(g)

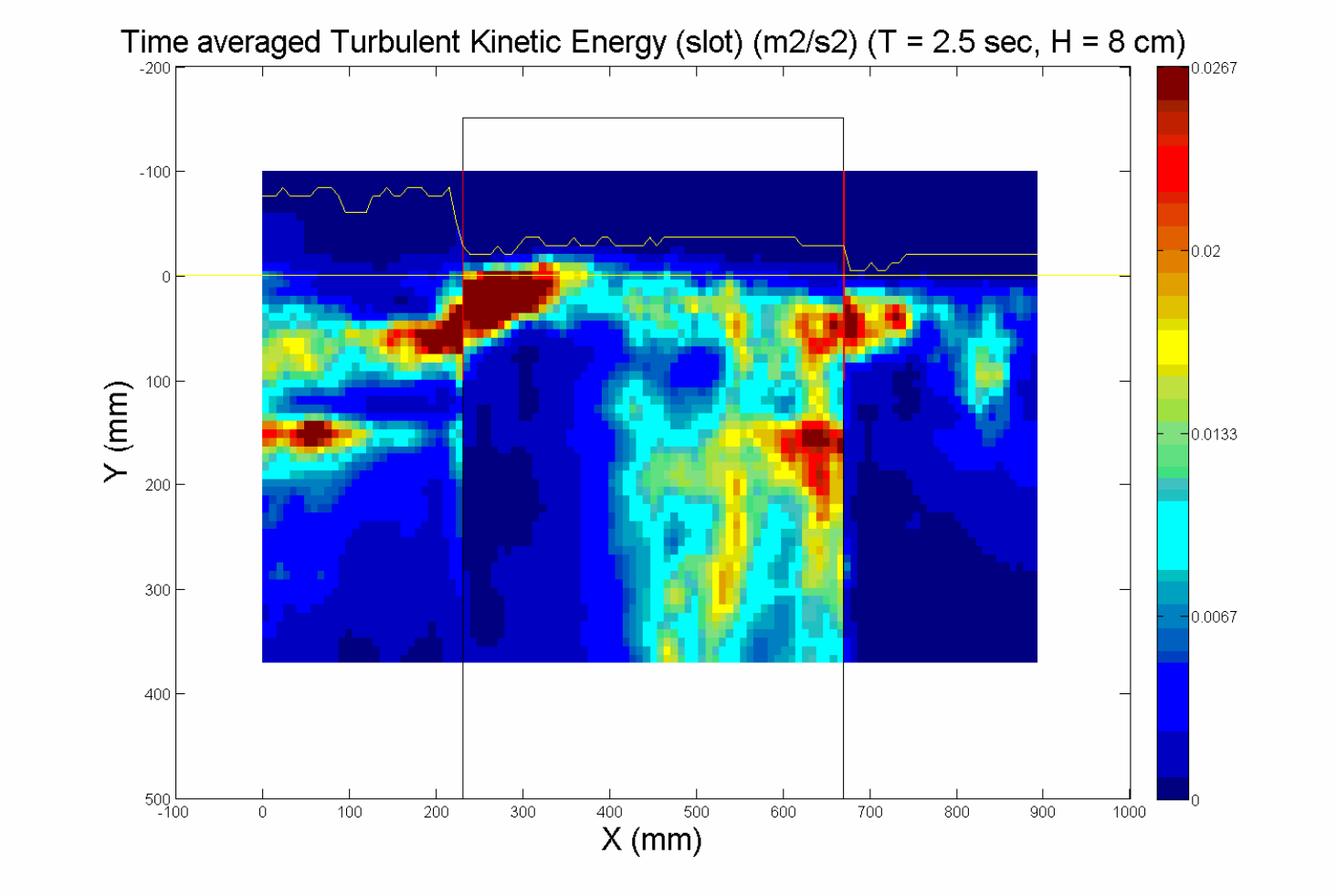

Fig. 6.3. continued.

6.3 Depth averaged turbulent kinetic energy field

To examine the variation of turbulent kinetic energy with wave propagation direction, the depth average turbulent kinetic energy was calculated for each wave condition (see figure 6.4). Considering figure 6.4, for both light sheets there is a clear change in the variation of turbulent kinetic energy near walls. The change is large near the front wall, where as it is small near back wall. It is clear that for small wave heights, the depth average turbulent kinetic energy is higher for the light sheet through slot (ex, for T = 1 sec, H_i = 4 cm and T = 1 sec, H_i = 6 cm). For larger waves (T = 1.6, 2, 2.5 sec, H_i = 8 cm), there is not much difference in turbulent kinetic energy through light sheets. For small waves, most of the turbulent kinetic energy is concentrated near front wall. When the wave conditions get larger, the depth average turbulent kinetic energy gets higher near front wall and inside the chamber. For all wave conditions the turbulent kinetic energy is higher near the front wall and inside the chamber whereas the turbulent kinetic energy behind the back wall is very small, near 0.001 m^2/s^2.

For T = 1 sec, H_i = 4 cm for the light sheet through slot the highest turbulent kinetic energy of 0.009 m^2/s^2 appears just in front of the front wall. Turbulent kinetic energy inside the chamber for all points is below 0.002 m^2/s^2. Behind the back wall turbulent kinetic energy is very small and the value closes to zero. For the light sheet through wall there are three local maxima, two near front wall and one inside the chamber. The maximum turbulent kinetic energy appears behind the front wall and the value is around 0.0035 m^2/s^2. The second peak is around 0.003 m^2/s^2 and appears just in

front of front wall. There is a local maxima inside the chamber around 0.0015 m^2/s^2. Behind the back wall the turbulent kinetic energy is very small and the value is closer to zero.

For T = 1 sec, H_i = 6 cm for light sheet through slot there are two local maxima. The maximum turbulent kinetic energy is around 0.015 m^2/s^2 and occurs just in front of the front wall. The other local maximum is around 0.008 m^2/s^2 and occurs just behind the back wall. For light sheet through wall there are three local maxima. The maximum is at 0.004 m^2/s^2 and appears just behind the front wall. The other maxima are, one in front of the front wall around 0.003 m^2/s^2 and one inside chamber at 0.002 m^2/s^2. For both light sheets the turbulent kinetic energy behind the back wall is very small and the value is around zero.

When the wave height gets larger (T = 1 sec, H_i = 8 cm) the clear peak disappears and the turbulent kinetic energy variation becomes complex. But still most of the turbulent kinetic energy concentrates near the front wall. For T = 1 sec, H_i = 8 cm for the light sheet through slot there are few peaks and the maximum is around 0.0075 m^2/s^2 and appears just in front of the front wall. For the light sheet through wall also there are few peaks and the maximum is around 0.007 m^2/s^2 and occurs in front of front wall. Still the turbulent kinetic energy behind the back wall is small.

For T = 1 sec, H_i = 10 cm the turbulent kinetic energy variation becomes even more complex. There are few peaks for both the light sheets. For the first time the maximum turbulent kinetic energy appears for the light sheet through wall. The peak appears in front of the front wall and the value is around 0.0275 m^2/s^2. For the light sheet

through slot the peak is around 0.02 m^2/s^2 and appears just in front of the front wall. Still the turbulent kinetic energy behind the back wall is small for both light sheets and most of the turbulent kinetic energy concentrates near the front wall and inside the chamber.

For T = 1.6 sec, H_i = 8 cm the variation gets even more complex, many peaks occur in the variation of turbulent kinetic energy for both light sheets. More of the turbulent kinetic energy appears in side chamber. The maximum turbulent kinetic energy appears for the light sheet through slot, for the first time the maximum appears in side the chamber and the value is around 0.013 m^2/s^2. The maximum turbulent kinetic energy for the light sheet through wall is around 0.009 m^2/s^2 and appears in front of front wall. The turbulent kinetic energy behind back wall is small.

For T = 2 sec, H_i = 8 cm the variations of turbulent kinetic energy gets less complex, clear peaks can be seen for both light sheets. For both light sheets the maxima appear at the same location. For light sheet through slot there are two maxima.

The maximum is just above 0.025 m^2/s^2 and appears just in front of the back wall, and the other local maximum is near front wall at a value of 0.015 m^2/s^2. For the light sheet through wall, the maximum is around 0.025 m^2/s^2 and appears just in front of the back wall. Behind the back wall the turbulent energy is small compared to other areas.

The turbulent kinetic energy variation becomes complex for T = 2.5 sec, H_i = 8 cm. There are many peaks for both light sheets. The maximum value appears for the light sheet through wall. The value is around 0.015 m^2/s^2 and appears a bit away from the front wall. For the light sheet through slot the maximum is around 0.0125 m^2/s^2 and appears just in front of the back wall. For the first time the turbulent kinetic energy behind the back wall is comparable to other areas.

Depth average turbulent kinetic energy variations for two light sheets are shown in figure 6.4.

(a)

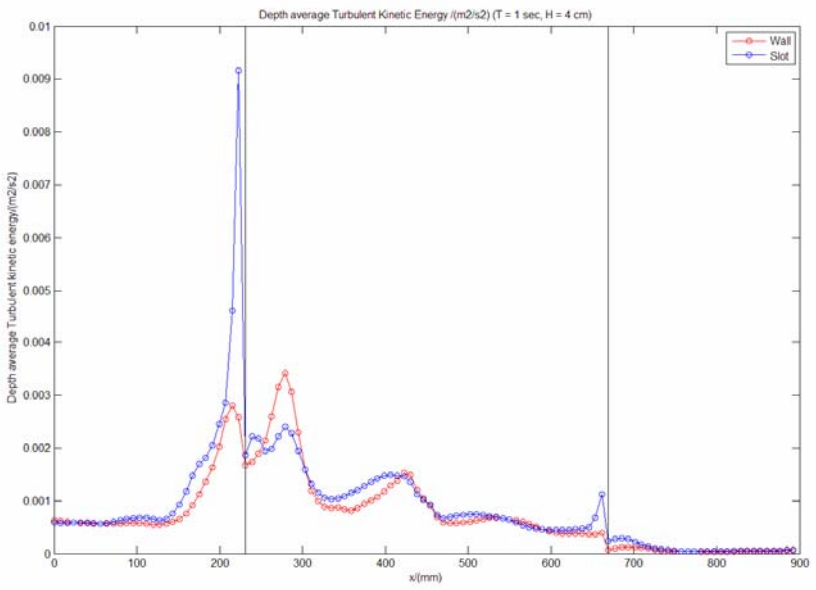

(b)

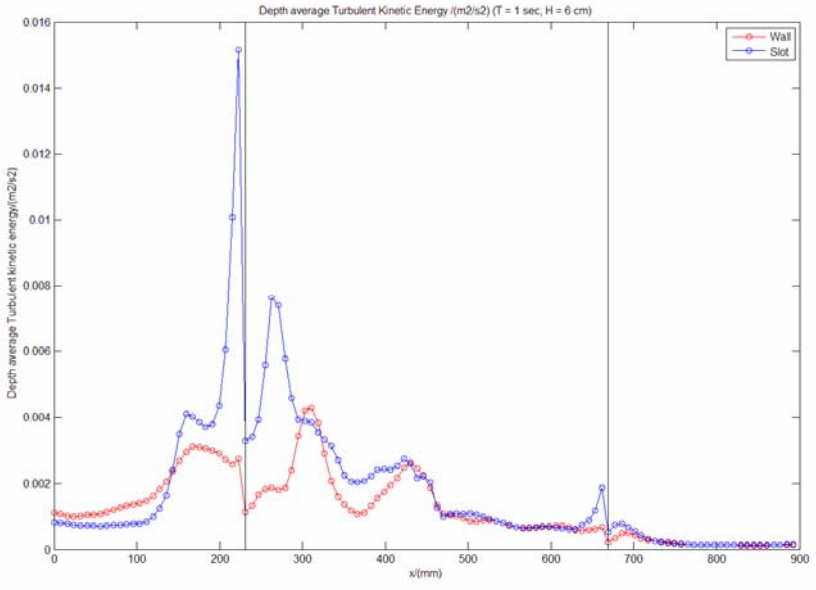

Fig. 6.4. Depth averaged turbulent kinetic energy for different wave conditions. (a) T = 1 sec, H = 4 cm. (b) T = 1 sec, H = 6 cm. (c) T = 1 sec, H = 8 cm. (d) T = 1 sec, H = 10 cm. (e) T = 1.6 sec, H = 8 cm. (f) T = 2 sec, H = 8 cm. (g) T = 2.5 sec, H = 8 cm.

(c)

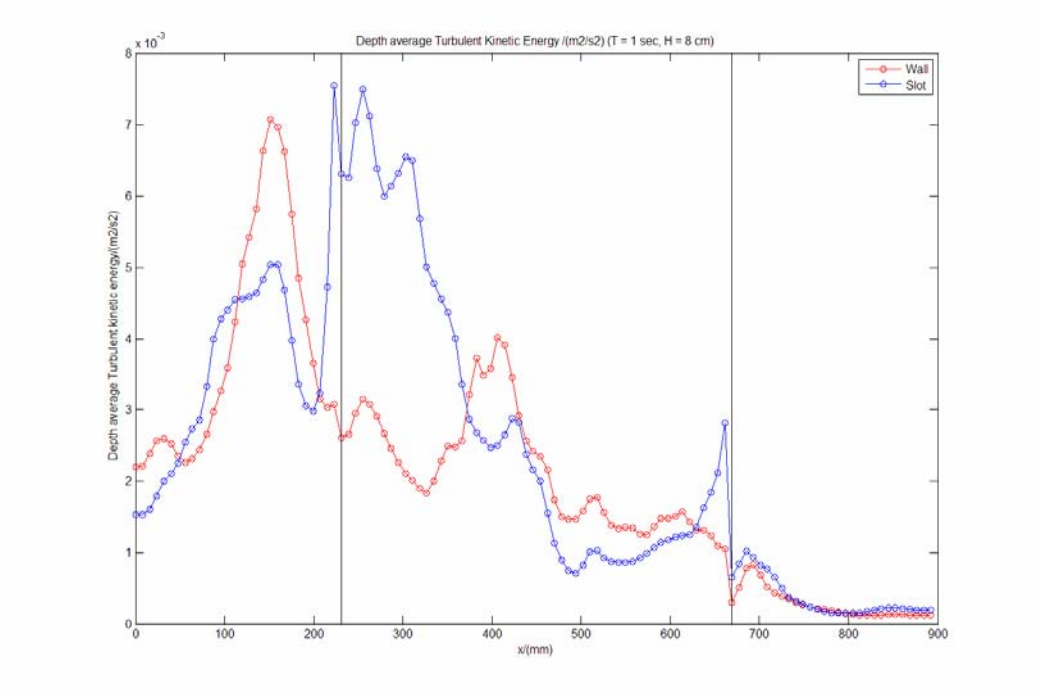

(d)

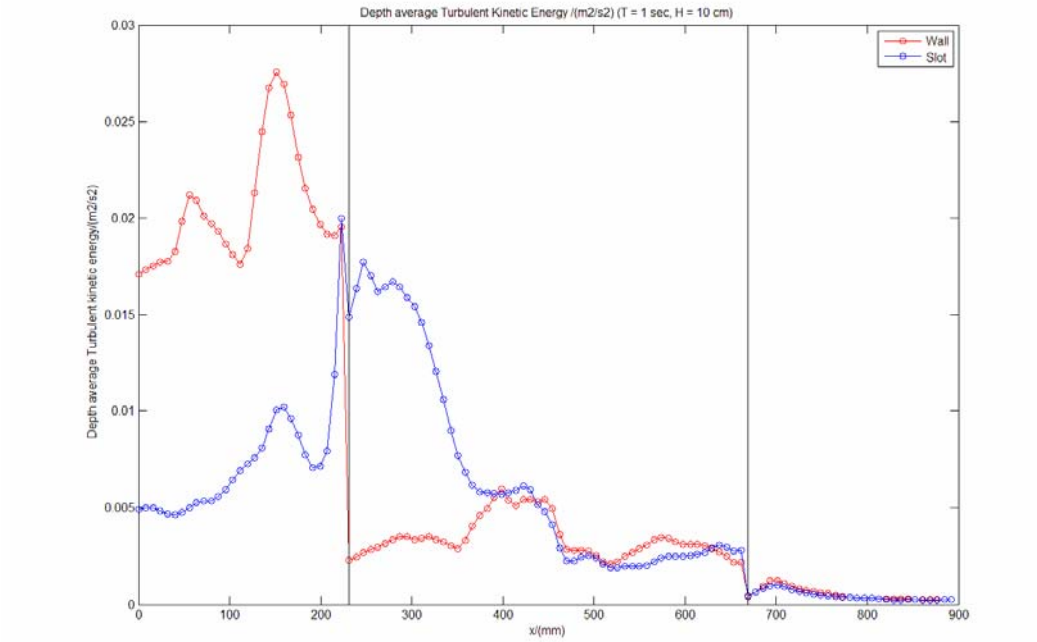

Fig. 6.4. continued.

(e)

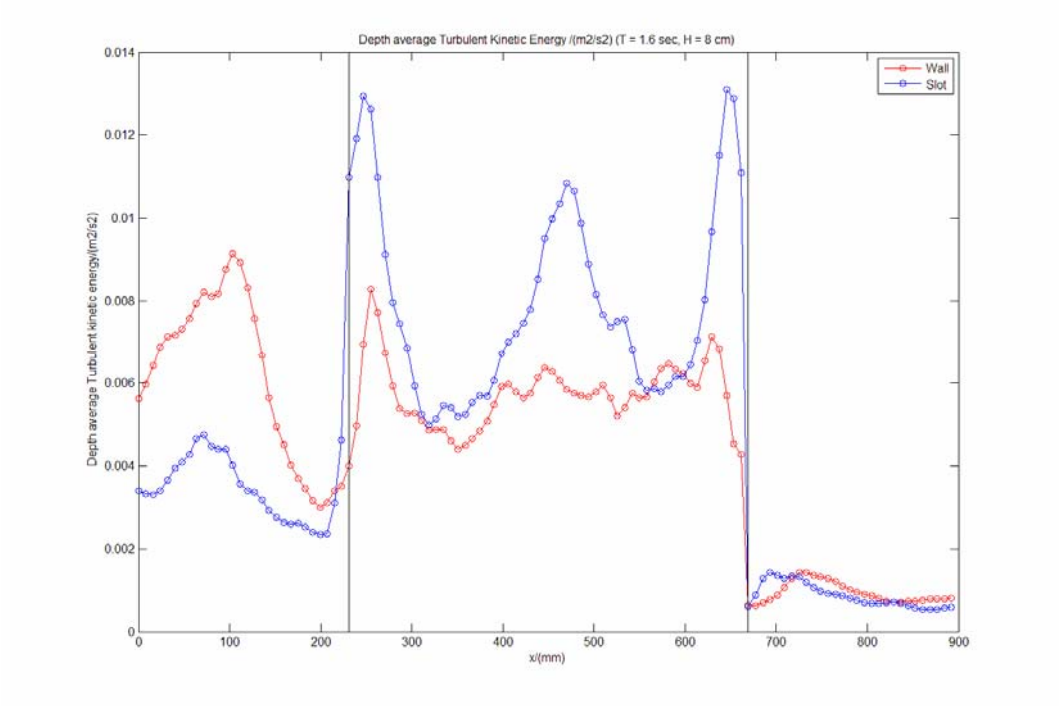

(f)

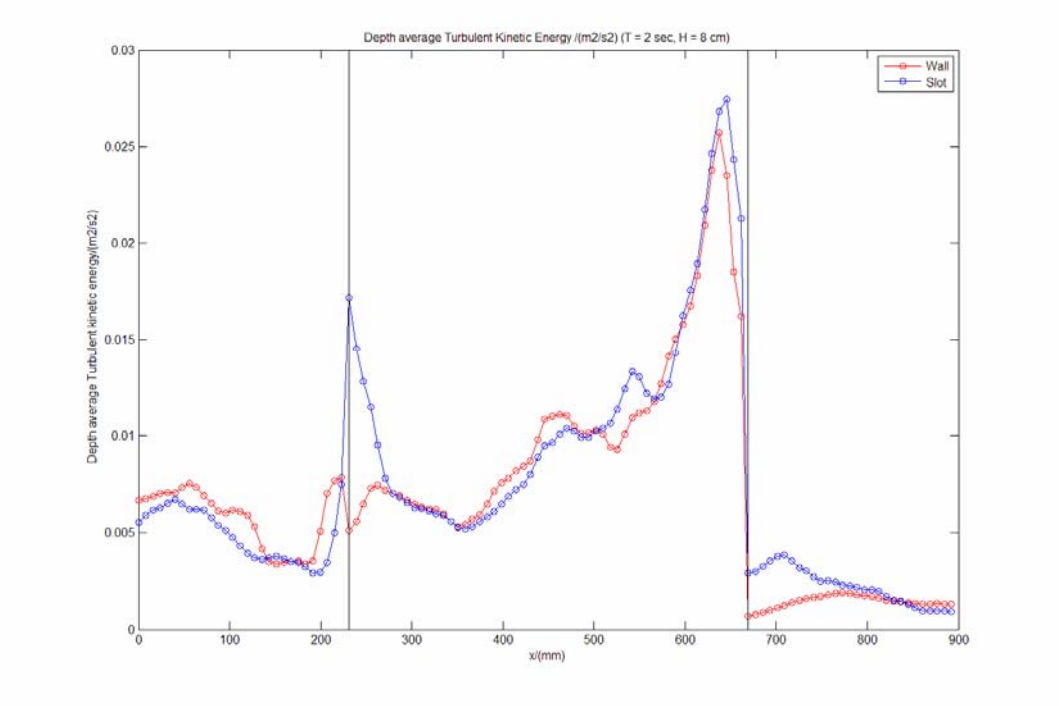

Fig. 6.4. continued.

(g)

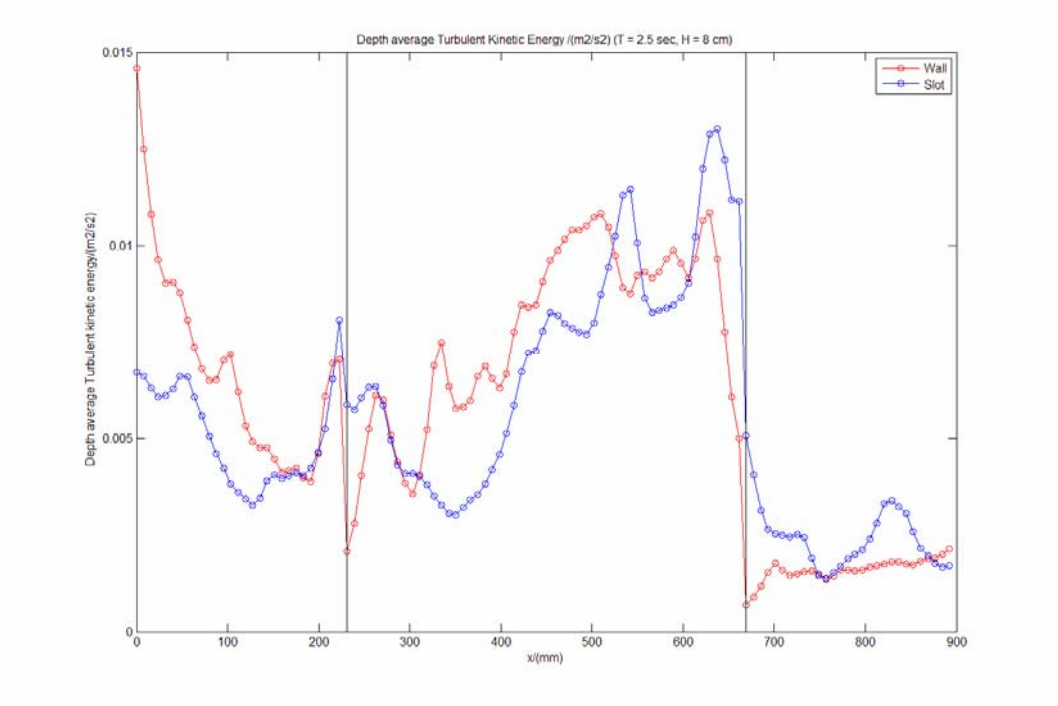

Fig. 6.4. continued.

To examine the depth averaged turbulent kinetic energy variation with wave conditions for each light sheet, plots were made (see figure 6.5). It is clear from the figures that for most of the wave conditions the depth average turbulent kinetic energy is smaller for the light sheet through wall compared to that through slot. For both light sheets the depth average turbulent kinetic energy is higher for wave conditions, T = 1 sec, H_i = 10 cm and T = 2 sec, H_i = 8 cm. For all the wave conditions the depth averaged turbulent kinetic energy concentrates near the front wall where as it is very small behind the back wall. Positions and value of maximum depth average turbulent kinetic energy for tested wave conditions are shown in table 6-1, and Positions of x,y are shown in figure 6.6. Considering figure 6.5 the maximum depth average turbulent kinetic energy for the light sheet through wall is around 0.0275 m^2/s^2, occurs for wave condition T = 1 sec and H_i = 10 cm where as for the light sheet through slot the value is around 0.0275 m^2/s^2, occurs for wave condition T = 2 sec and H_i = 8 cm.

(a)

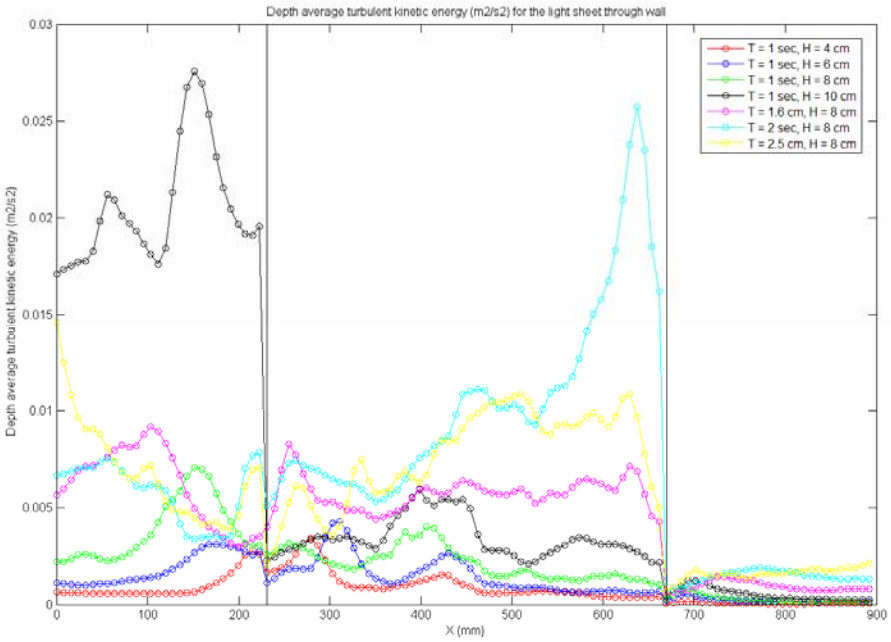

(b)

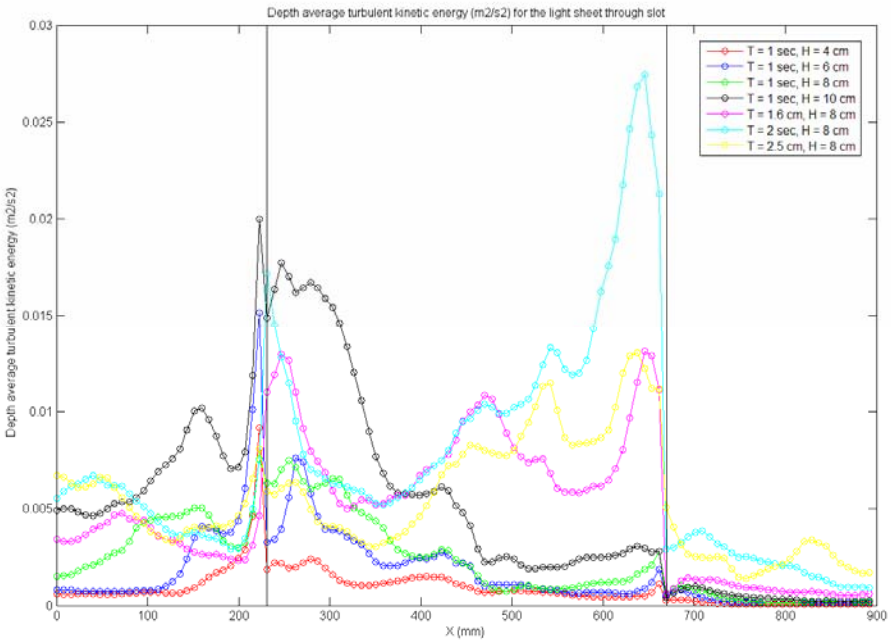

Fig. 6.5. Depth average turbulent kinetic energy variation with wave conditions. (a) Light sheet through wall. (b) Light sheet through slot.

Table 6-1

Positions and value of maximum depth average turbulent kinetic energy for tested wave conditions

Wave condition	Light sheet through Slot		Light sheet through Wall	
	Value (m^2/s^2)	Position x (mm)	Value (m^2/s^2)	Position x (mm)
T = 1 sec, H_i = 4cm	0.009	223.108	0.003	278.884
T = 1 sec, H_i = 6 cm	0.015	223.108	0.004	310.776
T = 1 sec, H_i = 8 cm	0.008	223.112	0.007	151.399
T = 1 sec, H_i = 10 cm	0.020	223.100	0.028	151.358
T = 1.6 sec, H_i = 8 cm	0.013	645.441	0.009	103.593
T = 2 sec, H_i = 8 cm	0.027	645.338	0.026	637.554
T = 2.5 sec, H_i = 8 cm	0.013	637.455	0.015	0.000

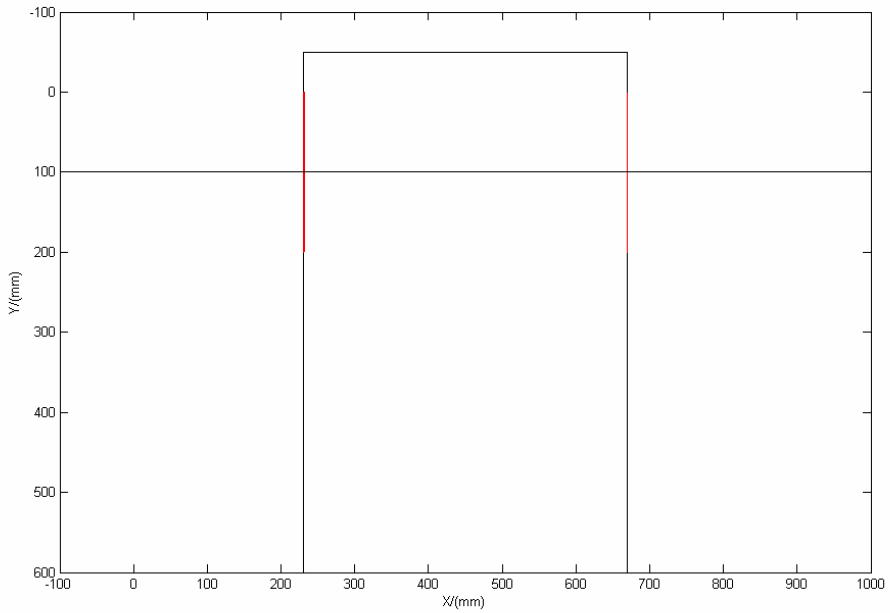

Fig. 6.6. Positions of x,y.

6.4. Horizontally averaged turbulent kinetic energy field

To examine the variation of turbulent kinetic energy with the depth, horizontally average turbulent kinetic energy was calculated for each wave condition (see figure 6.7). Considering figure 6.7, it is clear that for most of the wave conditions the horizontally averaged turbulent kinetic energy for the light sheet through wall is smaller than it for the light sheet through slot. For all the cases, the maximum horizontally averaged turbulent kinetic energy is near the free surface. There is another local maximum around a depth of 250 mm; this can be due to an experimental error. The position of this local maximum coincides with the position where bottom FOV and top FOV were added. The error can be due to missing of few velocity vectors in the process of addition of top and bottom FOV.

(a)

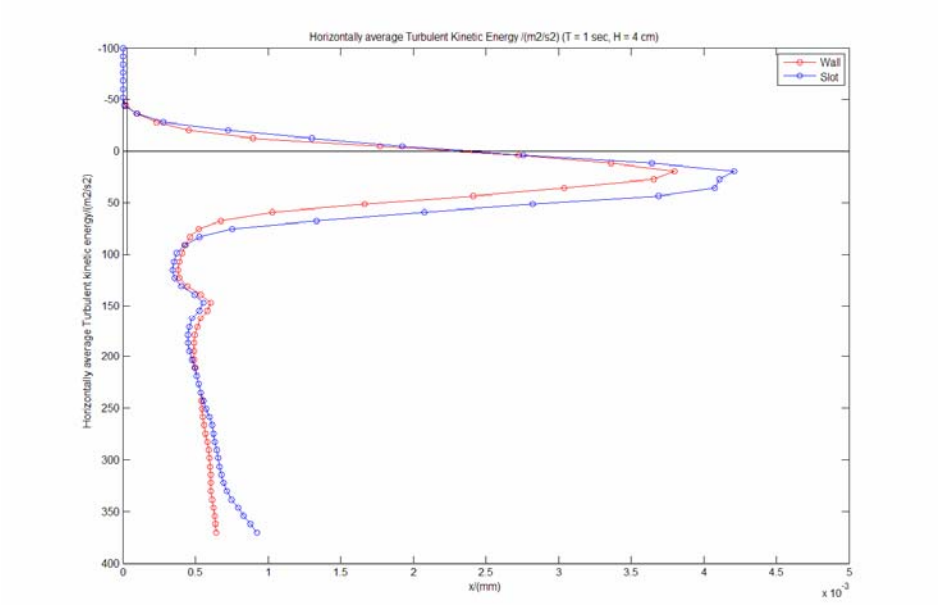

(b)

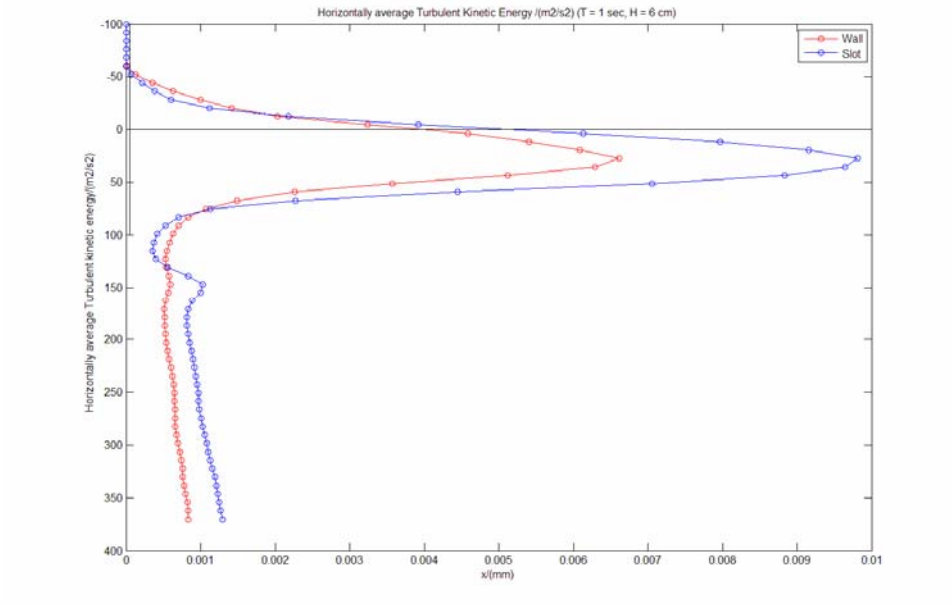

Fig. 6.7. Horizontally averaged turbulent kinetic energy for different wave conditions. (a) T = 1 sec, H = 4 cm. (b) T = 1 sec, H = 6 cm. (c) T = 1 sec, H = 8 cm. (d) T = 1 sec, H = 10 cm. (e) T = 1.6 sec, H = 8 cm. (f) T = 2 sec, H = 8 cm. (g) T = 2.5 sec, H = 8 cm.

(c)

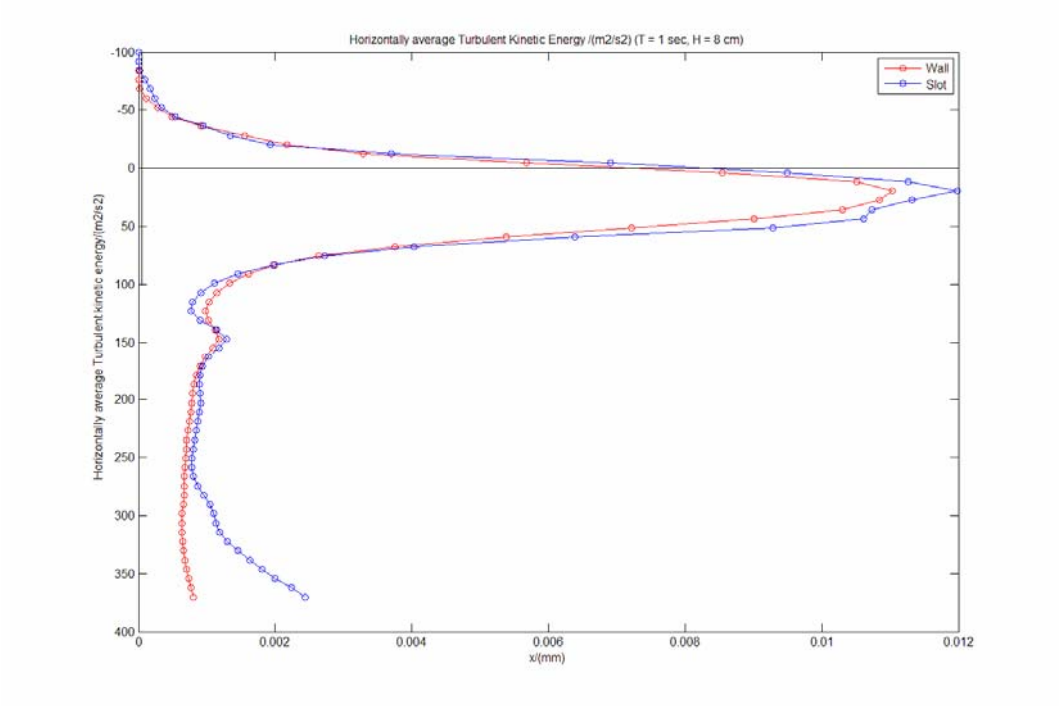

(d)

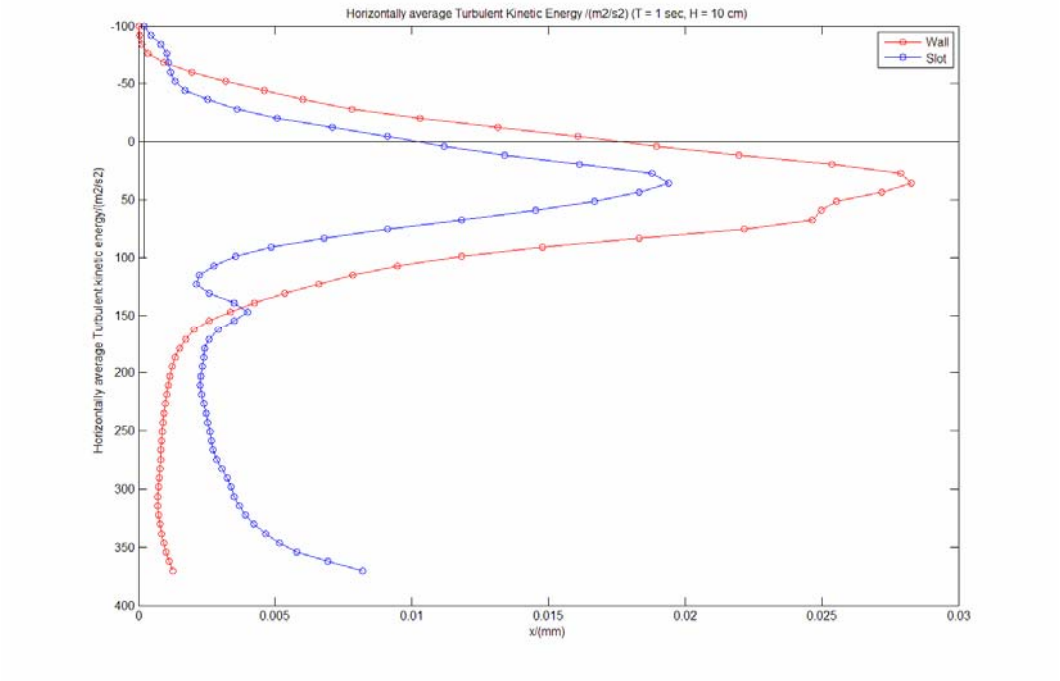

Fig. 6.7. continued.

(e)

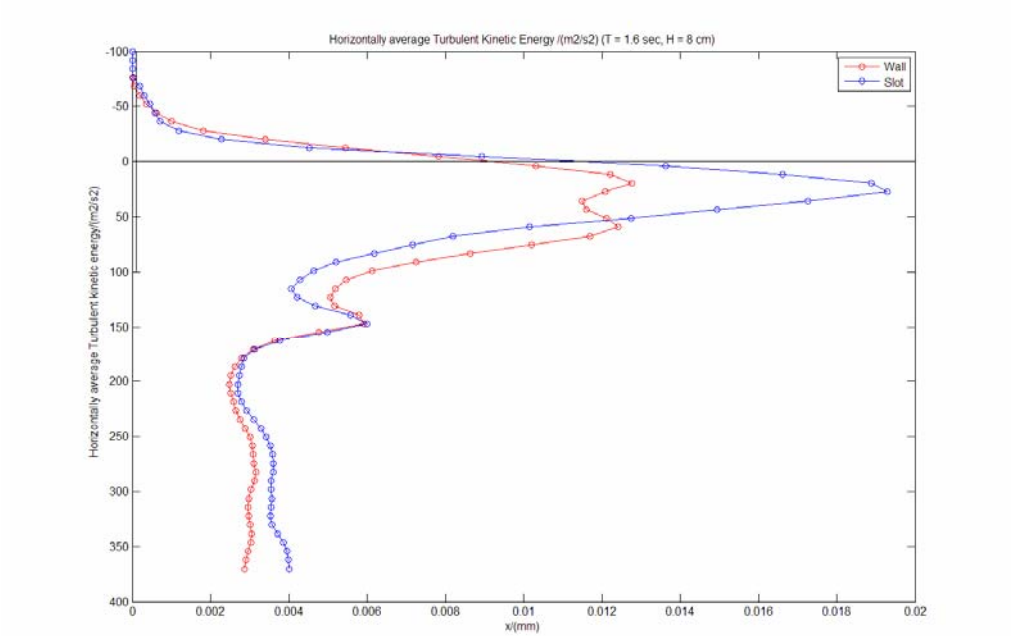

(f)

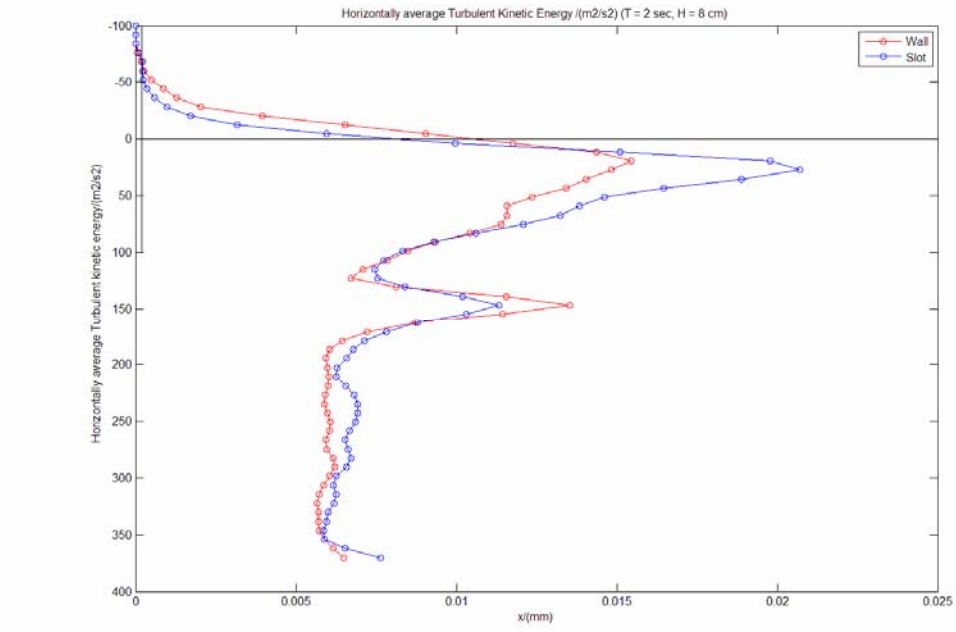

Fig. 6.7. continued.

(g)

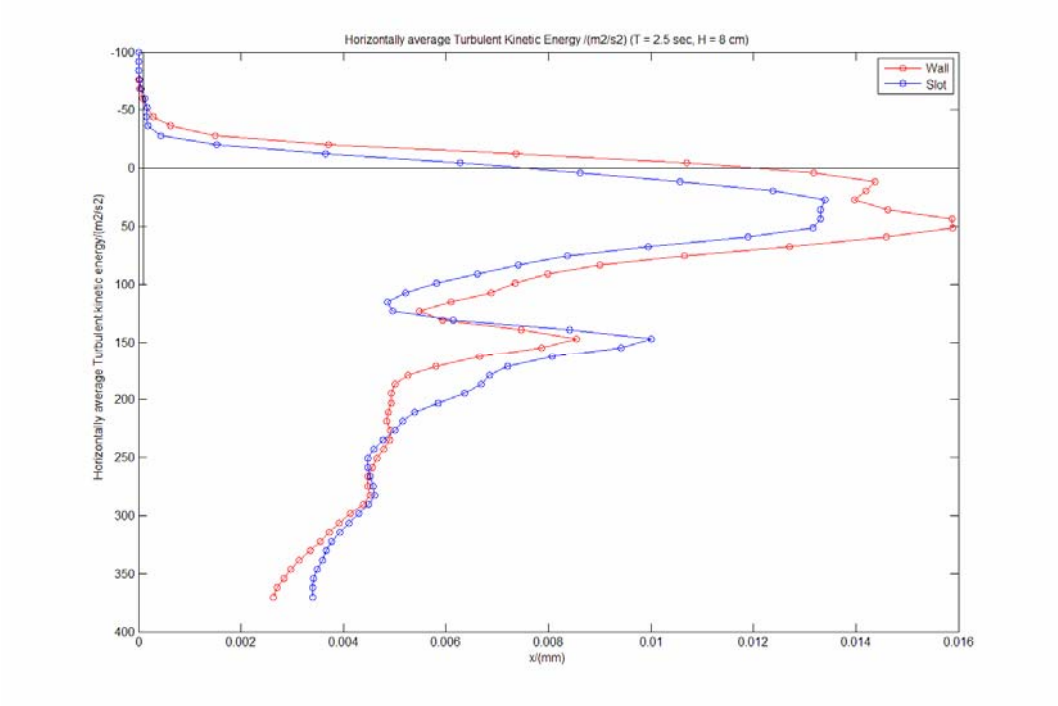

Fig. 6.7. continued.

To examine the horizontally averaged turbulent kinetic energy variation with wave conditions for each light sheet, plots were made (see figure 6.8). Considering figure 6.8, it is clear that for most of the wave conditions, the horizontally average turbulent kinetic energy is higher for the light sheet through slot to that compared to the light sheet through wall. When the wave conditions get larger (T = 1.6, 2, 2.5 sec, H_i = 8 cm), the horizontally averaged turbulent kinetic energy gets larger near free surface. For the light sheet through wall, the maximum horizontally average turbulent kinetic energy is around 0.027 m^2/s^2 and exists for wave condition T = 1 sec, H_i = 10 cm. For the light sheet through slot, the maximum horizontally average turbulent kinetic energy is around 0.02 m^2/s^2 and exists for wave condition T = 2 sec, H_i = 8 cm. Positions and value of maximum horizontally average turbulent kinetic energy for tested wave conditions are given in table 6-2.

(a)

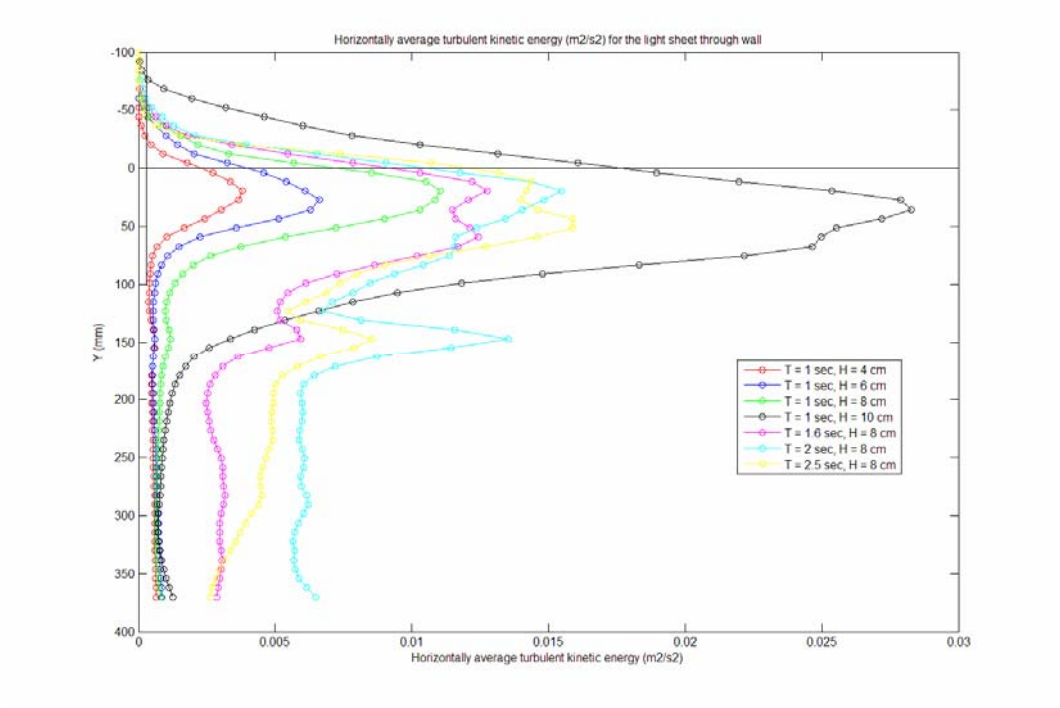

(b)

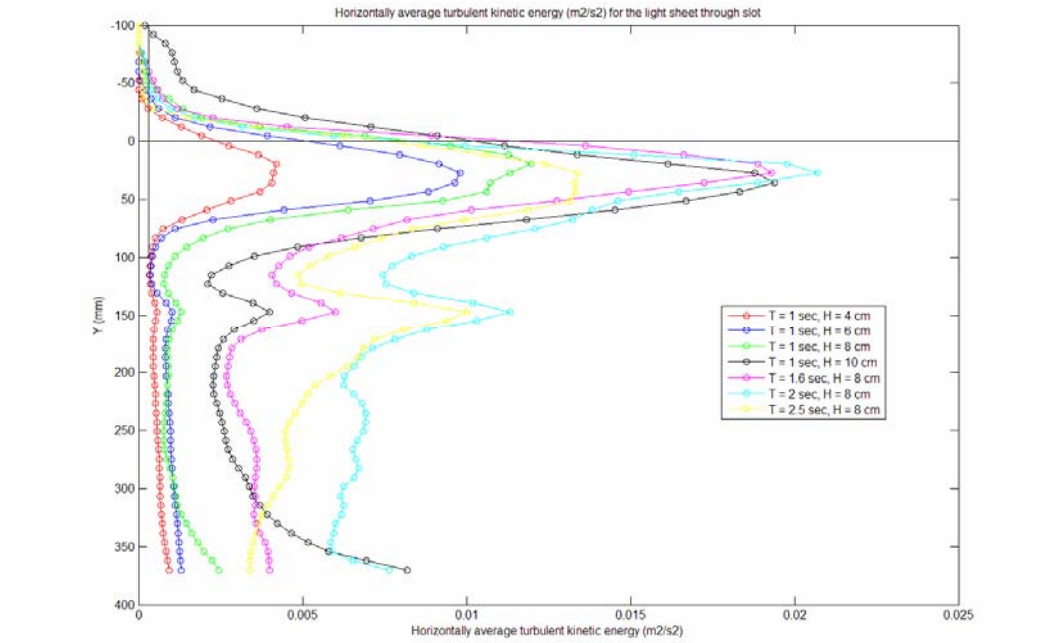

Fig. 6.8. Horizontally averaged turbulent kinetic energy variation with wave conditions.

(a) Light sheet through wall. (b) Light sheet through slot.

Table 6-2

Positions and value of maximum horizontally average turbulent kinetic energy for tested wave conditions

Wave condition	Light sheet through Slot		Light sheet through Wall	
	Value (m^2/s^2)	Position y (mm)	Value (m^2/s^2)	Position y (mm)
T = 1 sec, H_i = 4cm	0.004	119.592	0.004	119.634
T = 1 sec, H_i = 6 cm	0.010	127.534	0.007	127.500
T = 1 sec, H_i = 8 cm	0.012	119.584	0.011	119.572
T = 1 sec, H_i = 10 cm	0.019	135.496	0.028	135.430
T = 1.6 sec, H_i = 8 cm	0.019	127.510	0.013	119.522
T = 2 sec, H_i = 8 cm	0.021	127.512	0.016	119.516
T = 2.5 sec, H_i = 8 cm	0.013	127.460	0.016	151.509

6.5. Spatially averaged turbulent kinetic energy field

In order to examine the average turbulent kinetic energy with time for each wave condition the spatial average turbulent kinetic energy was calculated (see figure 6.9). For smaller wave conditions (ex T = 1 sec and H_i = 4, 6 cm) the spatially averaged turbulent kinetic energy is small for the light sheet through wall to that compared to that for light sheet through slot. When the wave conditions get larger (T = 1.6, 2, 2.5 sec, H_i = 8 cm), the magnitudes of both get comparable. For most of the wave conditions the maximum turbulent kinetic energy occurs at different phases for the two light sheets (see figure 6.10 and table 6-3).

To examine the spatially averaged turbulent kinetic energy variation with wave conditions for each light sheet, plots were made (see figure 6.10). Considering figure 6.10, it is clear that for both light sheets for constant wave period, the spatially averaged turbulent kinetic energy gets higher when the wave height gets larger. For the light sheet through wall, the maximum spatially average turbulent kinetic energy is around 0.025 m^2/s^2 and exists for wave condition T = 1 sec, H_i = 10 cm. For the light sheet through slot, the maximum spatially average turbulent kinetic energy is around 0.02 m^2/s^2 and exists for wave condition T = 1.6 sec, H_i = 8 cm.

(a)

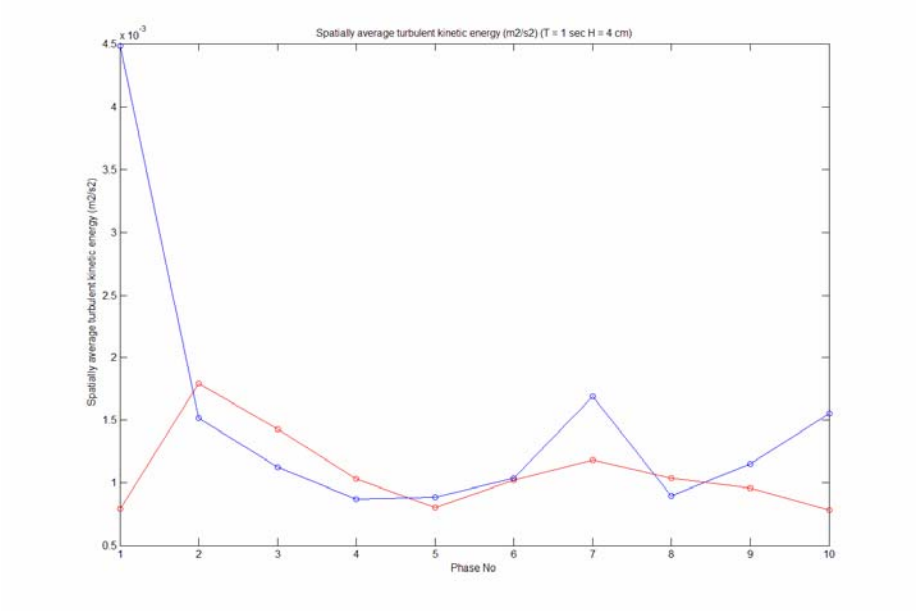

(b)

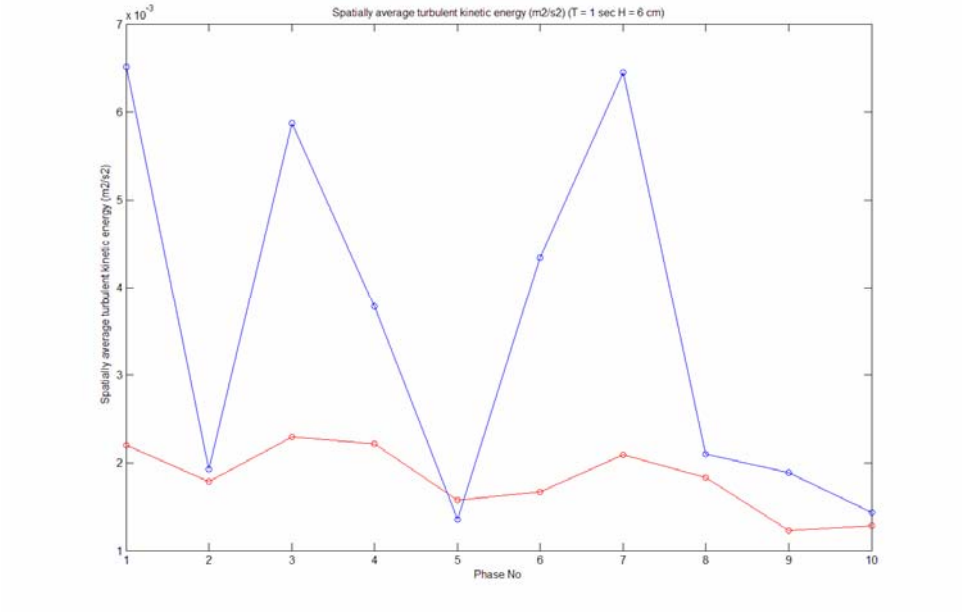

Fig. 6.9. Spatially averaged turbulent kinetic energy for different wave conditions. (a) T = 1 sec, H = 4 cm. (b) T = 1 sec, H = 6 cm. (c) T = 1 sec, H = 8 cm. (d) T = 1 sec, H = 10 cm. (e) T = 1.6 sec, H = 8 cm. (f) T = 2 sec, H = 8 cm. (g) T = 2.5 sec, H = 8 cm.

(c)

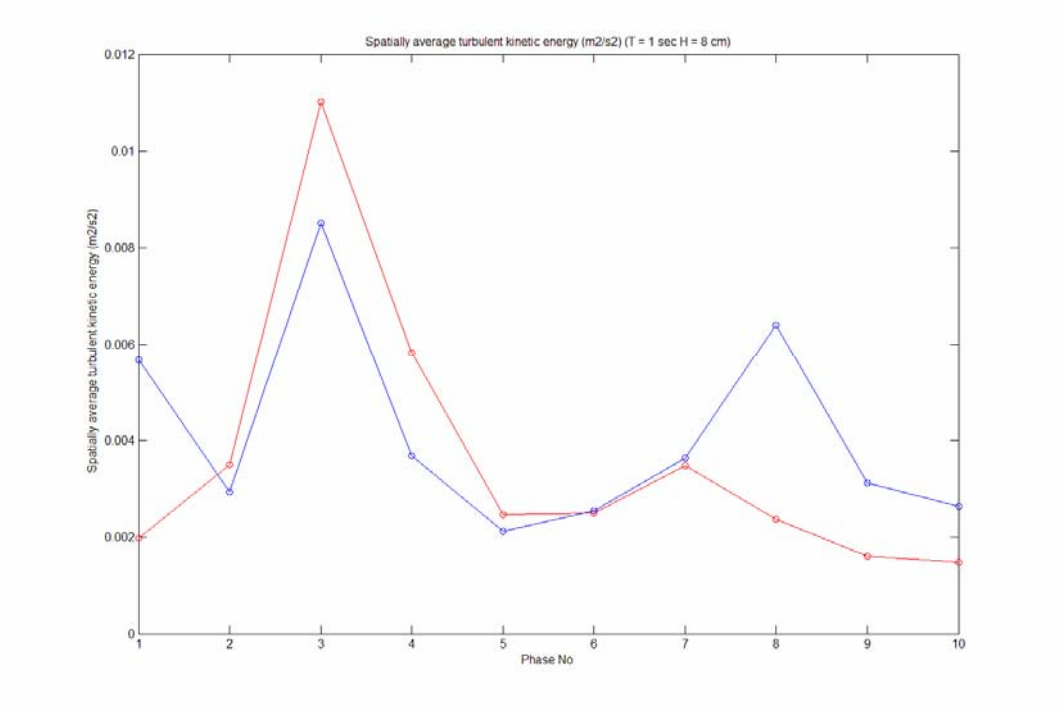

(d)

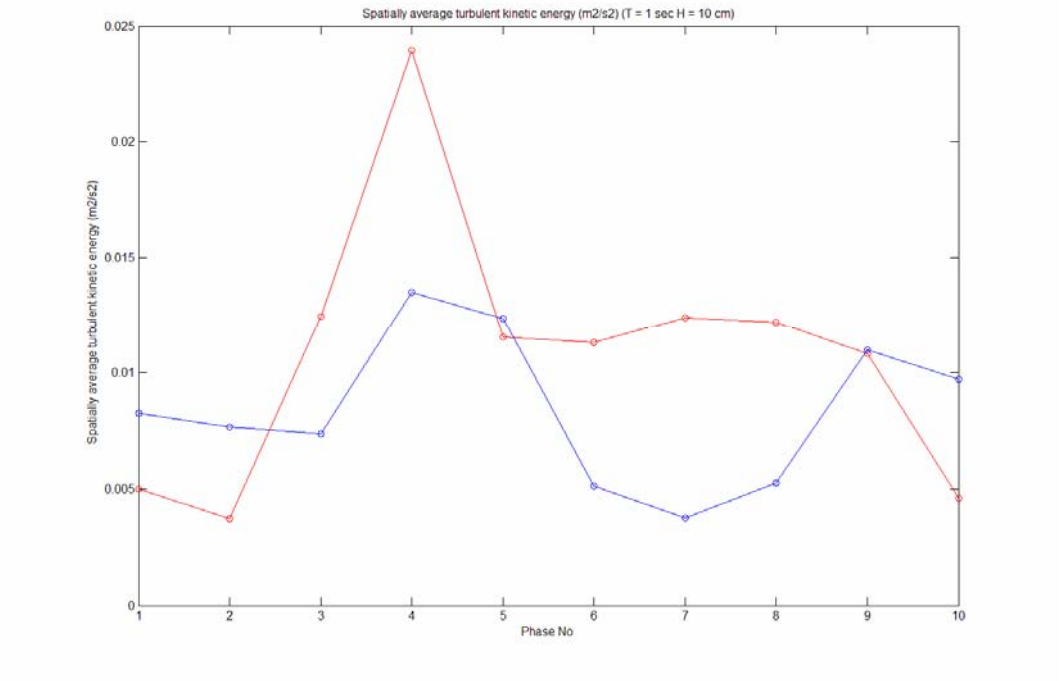

Fig. 6.9. continued.

(e)

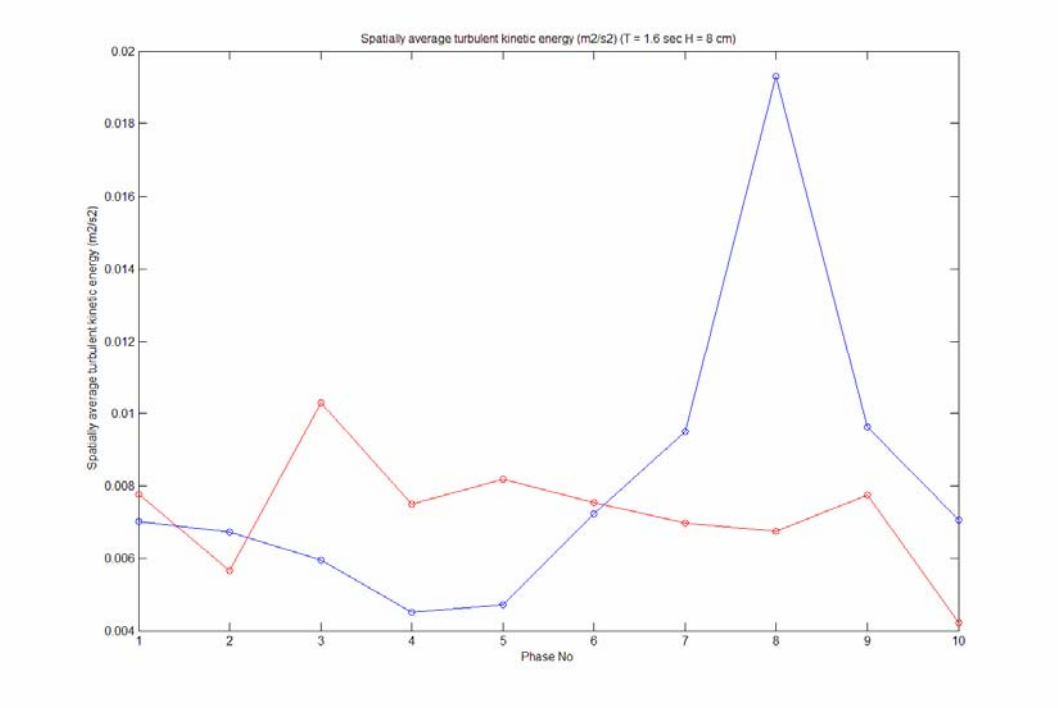

(f)

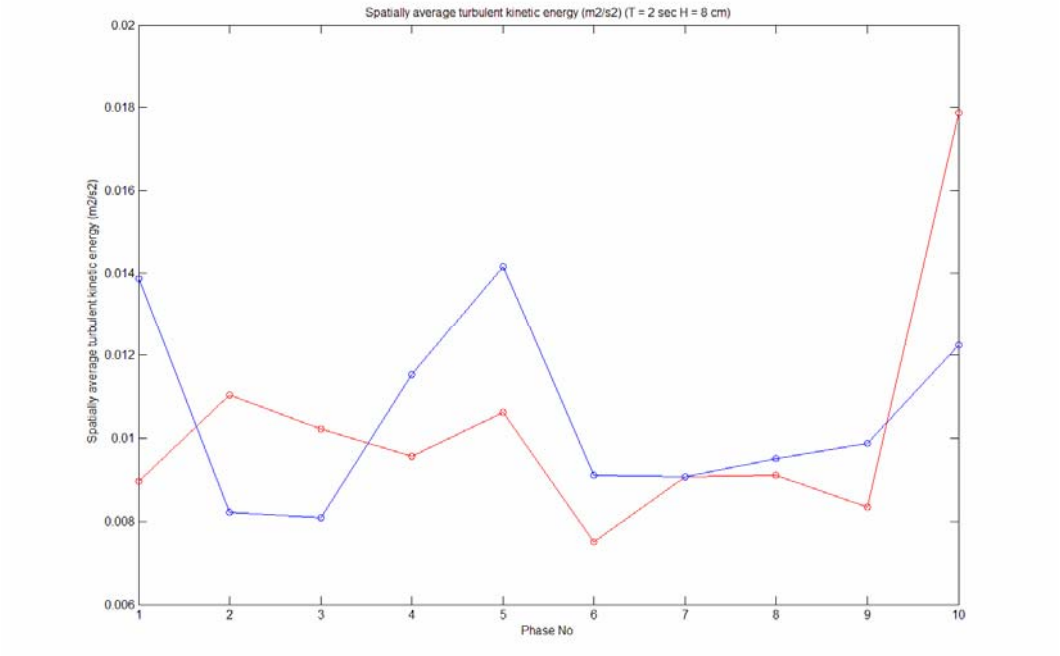

Fig. 6.9. continued.

(g)

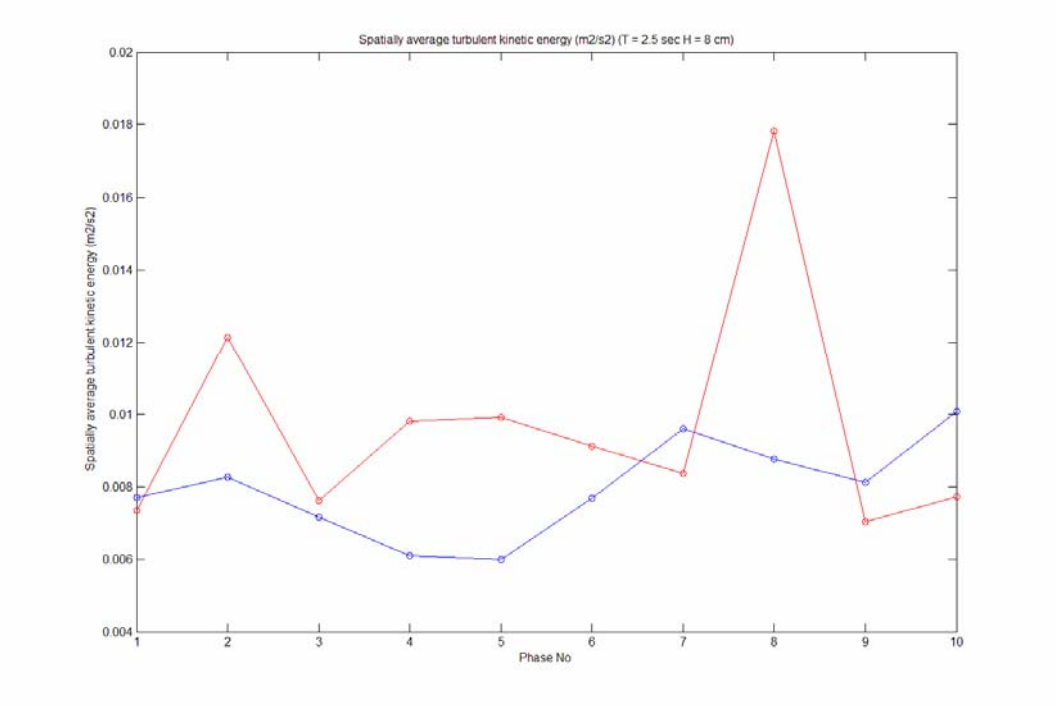

Fig. 6.9. continued.

(a)

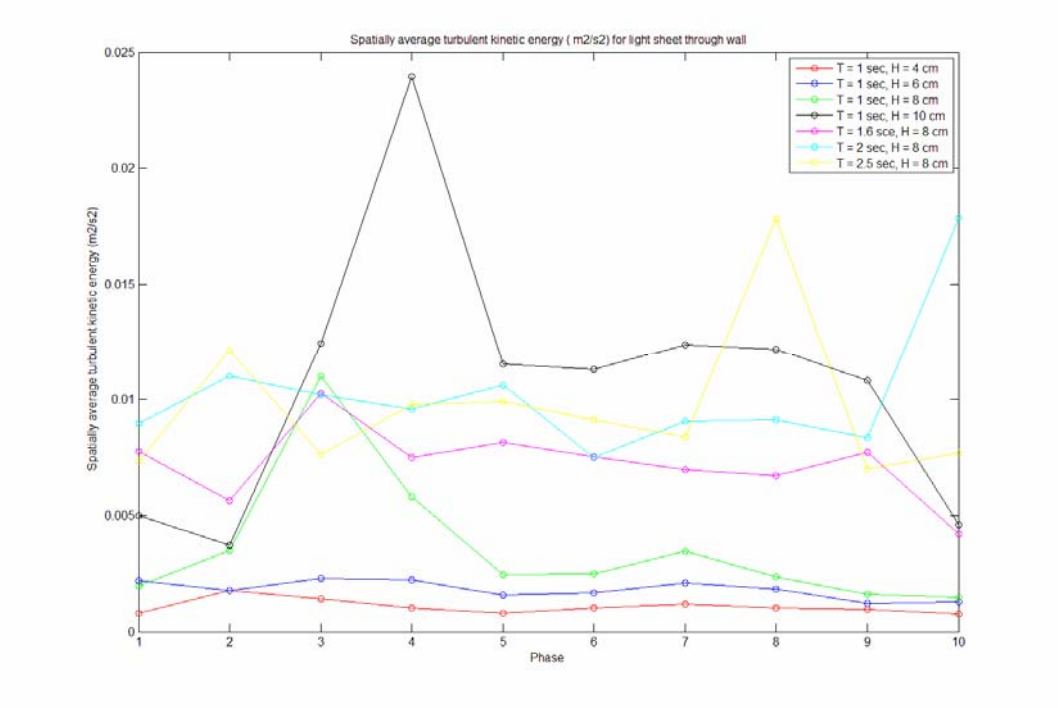

(b)

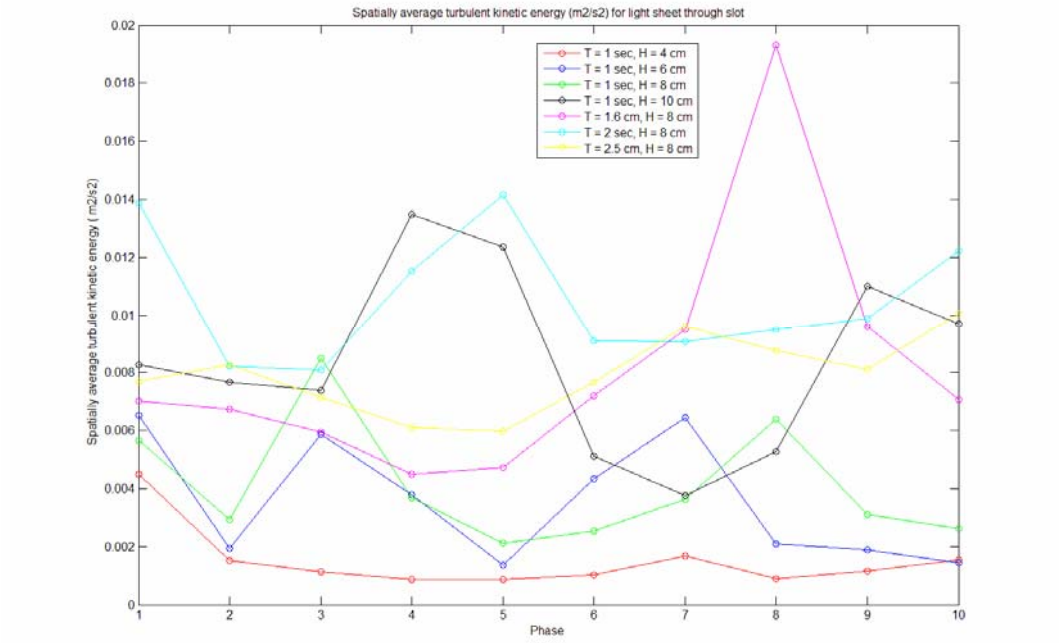

Fig. 6.10. Spatially averaged turbulent kinetic energy variation with wave conditions. (a) Light sheet through wall. (b) Light sheet through slot.

Table 6-3

Phase and value of maximum spatially average turbulent kinetic energy for tested wave conditions

Wave condition	Light sheet through Slot		Light sheet through Wall	
	Value (m^2/s^2)	Phase	Value (m^2/s^2)	Phase
T = 1 sec, H_i = 4cm	0.0044	1	0.0018	2
T = 1 sec, H_i = 6 cm	0.0065	1, 7	0.0023	3
T = 1 sec, H_i = 8 cm	0.0084	3	0.0109	3
T = 1 sec, H_i = 10 cm	0.0134	4	0.0239	4
T = 1.6 sec, H_i = 8 cm	0.0192	8	0.0102	3
T = 2 sec, H_i = 8 cm	0.0141	5	0.0178	10
T = 2.5 sec, H_i = 8 cm	0.0096	7	0.0177	8

6.6 Energy dissipation comparison

The energy dissipation was calculated considering elevation data and the velocity data considering one wavelength and unit width (see figure 6.11).

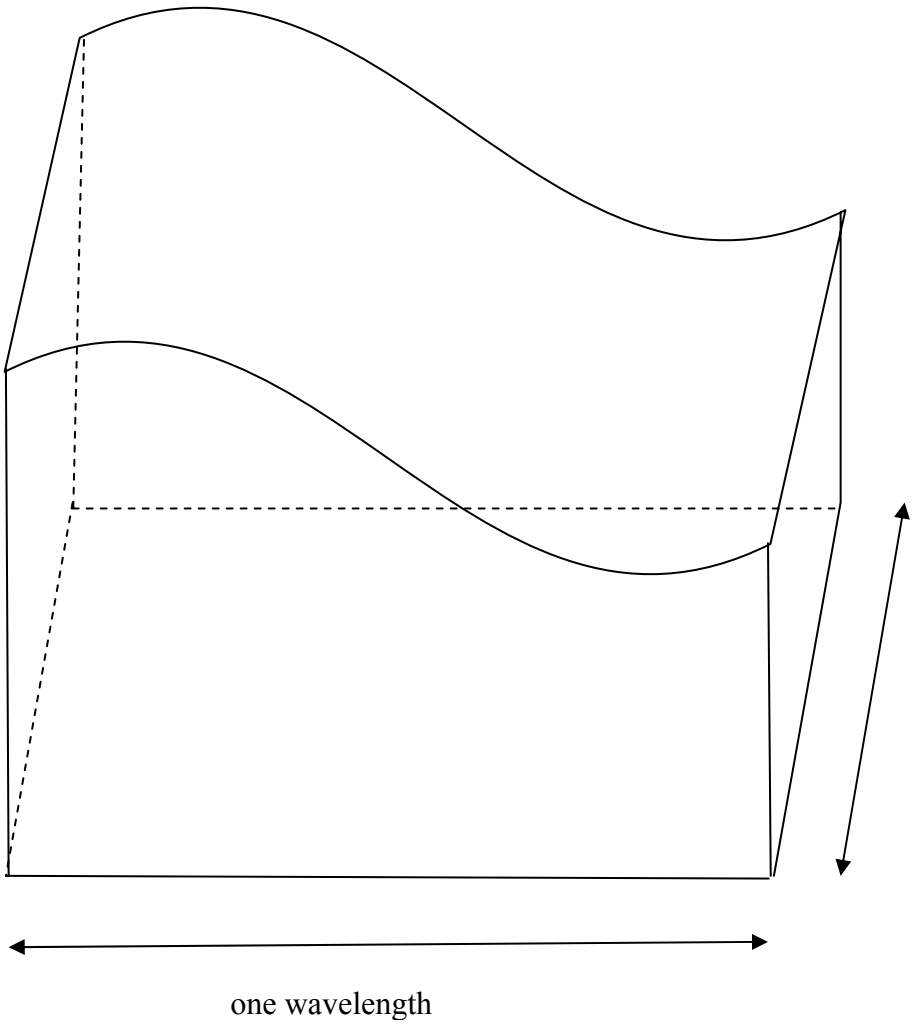

Fig. 6.11. Area considered in energy calculation.

Considering the wave elevation data,

Total energy dissipation per wavelength per unit width,

$$\varepsilon = 1/8\ \rho\ g\ (H_i)^2\ L - 1/8\ \rho\ g\ (H_r)^2\ L - 1/8\ \rho\ g\ (H_t)^2\ L \quad (6.1)$$

Considering the velocity data, turbulent kinetic energy per unit mass

$$TKE = (1.33 / 2) * I^2 \quad (6.2)$$

Total energy dissipation per wavelength per unit width, considering velocity data

$$TKE = (1.33 / 2) * I^2\ m$$

Where

m = mass per wavelength per unit width

In energy calculations, since no measured values were available near bottom, the measured value nearest to the bottom is assumed for missing data points.

Calculated values are shown in table 6-4 and figure 6.12.

After calculating the energy dissipation values, the values were normalized considering incoming wave energy per wavelength per unit width, $1/8\ \rho\ g\ (H_i)^2 L$.

Table 6-4

Energy dissipation

T (Sec)	H_i (cm)	Total Energy dissipation per wave length considering wave elevation data	Energy dissipation per unit mass for the light sheet through wall (m^2/s^2)	Energy dissipation per unit mass for the light sheet through slot (m^2/s^2)	Turbulent kinetic energy dissipation considering velocity data	% of TKE
1.0	4.0	0.722	6.380	7.867	0.253	35.000
1.0	6.0	0.714	10.022	14.622	0.194	27.217
1.0	8.0	0.699	15.682	21.022	0.163	23.286
1.0	10.0	0.701	50.108	50.288	0.285	40.679
1.6	8.0	0.582	36.361	41.052	0.343	59.051
2.0	8.0	0.562	58.680	63.423	0.542	96.450
2.5	8.0	0.637	44.769	43.047	0.390	61.151

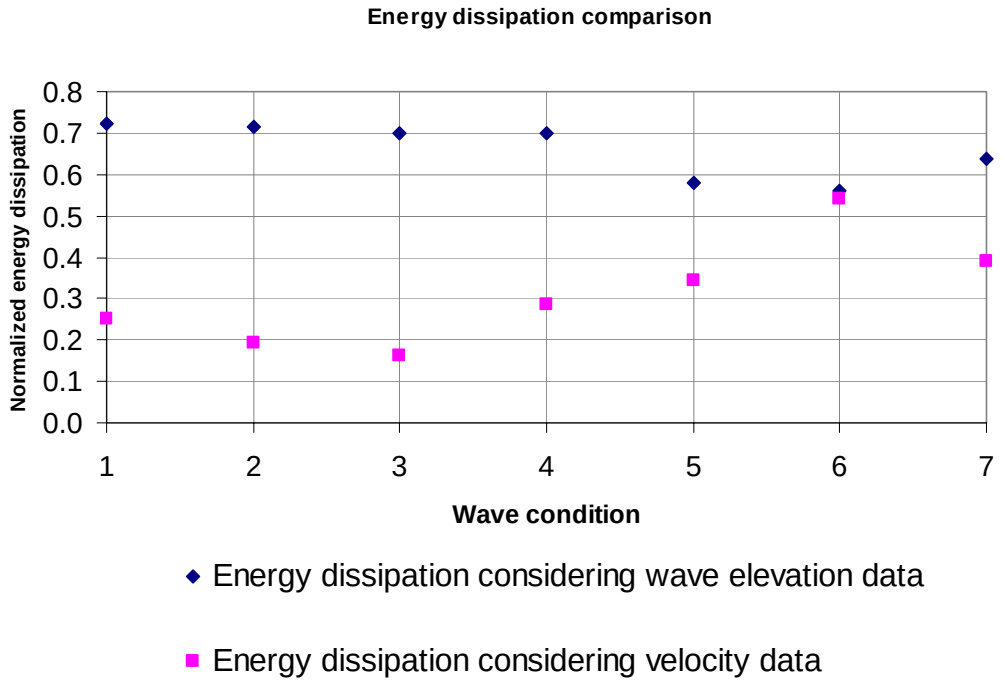

Fig. 6.12. Energy dissipation variations considering wave elevation data and velocity data.

Considering the table 6-4, for small wave conditions (ex T = 1 sec, H_i = 4, 6, 8, 10 cm) the turbulent kinetic energy compared to total energy is smaller, where as for large wave conditions (ex T = 1.6, 2, 2.5 sec H_i = 8 cm) most of the energy dissipation is due to turbulent kinetic energy. There is a difference between the calculated energy dissipation considering wave elevation data and velocity data. The velocity data was measured in the vicinity of the structure, there can be turbulent kinetic energy out of the measured area, hence the calculated value is smaller than the actual value. Also in the present study two dimensional velocity was measured. Hence the calculated turbulent kinetic energy is smaller than the actual value.

CHAPTER VII

SUMMARY AND CONCLUSION

7.1. Wave elevation data

A 2D experimental study was done to study the flow field behaviour in the vicinity of a perforated breakwater and the efficiency of the breakwater under regular waves.

To examine the efficiency of the structure thirteen types of regular wave conditions in an intermediate water depth were tested. The incoming, reflected and transmitted wave heights were measured. The efficiency of the structure was calculated considering the energy balance for the system. The reflection and transmission coefficients variations with various parameters were compared and discussed. The efficiency of the structure for different wave conditions were showed and compared. The followings were observed.

- For the tested wave conditions, the energy dissipation lies between 56% and 78%, and for more than 75% of the tested cases the energy dissipation is above 69%. This means the structure is very effective in energy dissipation
- It was observed that the minimum reflection coefficient occurs at $B/L \approx 0.2 – 0.25$. For small waves the energy dissipation does not change much with B/L, but for larger waves the energy dissipation varies in a wider range with B/L

- Moreover it is observed, for a constant wave period, the reflection coefficient, transmission coefficient and energy dissipation does not change much with wave height
- For a constant wave height, the reflection coefficient, transmission coefficient and energy dissipation varies with wave period
- For kA less than 0.25, reflection coefficient, transmission coefficient and energy dissipation vary in a large range with kA, but for kA larger than 0.25 the above parameters stay constant.

Seven types of regular waves in an intermediate water depth were tested for the flow behaviour study. In order to study the flow field variation with phase, ten phases were considered per one wave. The Particle Image Velocimetry (PIV) technique was employed to measure the two dimensional instantaneous velocity field distribution and MPIV and DaVis were used to calculate the velocity vectors. By repeating the experiments and taking average, the mean velocity field, mean vorticity field, mean turbulent intensity and mean turbulent kinetic energy field were calculated for each phase and for each wave condition. The phase average fields for each wave condition for each of the above mentioned parameters were calculated taking the average of ten phases. The phase averaged velocity, vorticity and turbulent kinetic energy fields are presented and compared. The followings were observed.

7.2. Velocity

- For two light sheets the velocity maps are almost same except near walls
- For most of the phases and for most of the wave conditions more small vortices form near surface
- For light sheet through wall for most of phases and most of wave conditions the magnitude of velocity behind the back wall is smaller compared to that in other areas
- Clear discontinuity of velocity maps near walls in the velocity maps for light sheet through wall
- For all the wave conditions for both light sheets there is a big clockwise vortex inside the chamber
- When wave conditions (wave height and wave period) get bigger the followings were observed
    - the magnitude of the velocity get higher
    - flow inside chamber and near surface get very complex
    - discontinuity of velocity map can be seen clearly near walls for the light sheet through wall
    - many small vortices form not only near free surface but also beneath it
    - magnitude of the velocity behind the back wall gets comparable to other areas

- For light sheet through slot small vortices form even for small wave height and wave periods
- For light sheet through slot for most of the phases and for most of the wave conditions the velocity behind the back wall is comparable to other areas
- For most of the wave conditions the magnitude of velocity is higher for light sheet through slot

7.3. Vorticity

- For small wave heights and wave periods small vortices form near free surface and near front wall
- When wave conditions (wave height and wave period) get bigger many vortices form not only near front wall but also near back wall and beneath free surface
- For most of the phases and for most of the wave conditions a negative vortex form near front wall
- For most of the phases and for most of the wave conditions a positive vortex form near behind back wall
- When the vortices near free surface fade small vortices form beneath free surface and move upward
- For most of the wave conditions the magnitude of vorticity is higher for light sheet through slot

- For the light sheet through wall a clear discontinuity can be seen in vorticity maps even for small wave conditions
- For most of the phases and most of the wave conditions the vorticity pattern is same for two light sheets except in the area near walls
- When wave conditions (wave height and wave period) get bigger the followings are observed
    - the magnitude of the vorticity get higher
    - vortices form beneath free surface
    - vortices form not only near front wall but also near back wall
    - many small vortices form and vortices spreads in a larger area
    - a clear discontinuity near walls for the light sheet through wall

7.4. Turbulent kinetic energy

- For the light sheet through wall for all the wave conditions turbulent kinetic energy appears only near front wall but behind the back wall no turbulent kinetic energy forms
- For most of the phases and for most of the wave conditions turbulent kinetic energy concentrates near free surface
- Magnitude of turbulent kinetic energy is higher for light sheet through slot than that compared to light sheet through wall
- When wave conditions get larger

- the magnitude of the turbulent kinetic energy get higher
- turbulent kinetic energy appears not only near the free surface and near the front wall but also under the free surface and inside the chamber
- shows a clear discontinuity near walls for the light sheet through wall
- turbulent kinetic energy forms behind the back wall for light sheet through slot, but no turbulent kinetic energy behind back wall for the light sheet through wall

7.5. Depth average turbulent kinetic energy

- Clear change in the variation of depth average turbulent kinetic energy near front wall
- For small wave heights, depth average turbulent kinetic energy is higher for the light sheet through slot
- For larger waves (T = 1.6, 2, 2.5 sec, H_i = 8 cm), there is not much difference in turbulent kinetic energy through light sheets
- For small waves, most of the turbulent kinetic energy is concentrated near front wall
- When the wave conditions get larger, the depth average turbulent kinetic energy gets very complex and higher near front wall and inside the chamber

- For all wave conditions the turbulent kinetic energy is higher near the front wall and inside the chamber whereas the turbulent kinetic energy behind the back wall is very small

7.6. Horizontally averaged turbulent kinetic energy

- For most of wave conditions horizontally average turbulent kinetic energy for the light sheet through wall is smaller than that for the light sheet through slot
- For all the cases, the maximum horizontally averaged turbulent kinetic energy is near the free surface
- When the wave conditions get bigger, the magnitude of horizontally averaged turbulent kinetic energy gets bigger near free surface

7.7. Spatially averaged turbulent kinetic energy

- For most of the wave conditions the spatially average turbulent kinetic energy is small for the light sheet through wall compared to that for light sheet through slot
- When the wave conditions get larger, the magnitudes of spatially average turbulent kinetic energy for both light sheets get comparable
- For most of the wave conditions the maximum turbulent kinetic energy occurs at different phases for the two light sheets

- It is clear that for both light sheets for constant wave period, the spatially averaged turbulent kinetic energy gets higher when the wave height gets larger

The energy dissipation was calculated based on wave elevation data and velocity data. For small wave conditions the turbulent kinetic energy compared to total energy is smaller, where as for large wave conditions most of the energy dissipation is due to turbulent kinetic energy.

7.8. Suggestions for energy enhancing and energy extraction

More energy will be dissipated if more perforated walls are used, since more energy will be dissipated near the perforations.

Considering the results, it is clear that most of the energy dissipates near the front wall and near the free surface. This energy may be extracted using floating bodies (energy extraction from heave and pitch motion).

REFERENCES

Aoul, E-H., Lambert, E., 2003. Tentative new formula for maximum horizontal wave forces acting on perforated caisson. Journal of Waterway, Port, Coastal and Ocean Engineering 129 (1), 34-40.

Bennet, G.S., McIver, P., Smallman, J.V., 1992. A mathematical model of a slotted wavescreen breakwater. Coastal Engineering 18, 231-249.

Chang, K-A., 1999. Experimental study of wave breaking and wave-structure interaction. Ph. D. dissertation. Cornell University, Ithaca, NY.

Dean, R.G., Dalrymple, R. A., 1992. Water wave mechanics for engineers and scientists. Second edition. World Scientific Publications. Singapore.

Deutsch, C.V., Journel, A. G., 1998. GSLIB Geostatistical Software Library and User's Guide. Second edition. Oxford University Press, Oxford, United Kingdom.

Hagiwara, K., 1984. Analysis of upright structure for wave dissipation using integral equation. Proc. Coastal Engineering, 2810-2826.

Isaacson, M., Baldwin, J., Allyn, N., Cowdell, S., 1998a. Design of a perforated breakwater. Proc. Ports '98 Conf., 2, 1189-1198.

Isaacson, M., Premasiri, S., Yang, G., 1998b. Wave interactions with vertical slotted barrier. Journal of Waterway, Port, Coastal and Ocean Engineering 124 (3), 118-126.

Isaacson, M., Baldwin, J., Allyn, N., Cowdell, S., 2000. Wave interactions with perforated breakwater. Journal of Waterway, Port, Coastal and Ocean Engineering 126 (5), 229-235.

Jarlan, G.E., 1961. A perforated vertical wall breakwater. The Dock and Harbour Authority 41, 394-398.

Kakuno, S., Oda, K., Liu, P. L-F., 1992. Scattering of water waves by vertical cylinders with a back wall. Proc. Coastal Engineering, 1258-1271.

Kondo, H., 1979. Analysis of breakwaters having two porous walls. Proc. Coastal Structures, 962-977.

Kondo, H., Toma, S., 1972. Reflection and transmission for a porous structure. Proc. of 13th Coastal Engineering Conf., 3, 1847-1866.

La Vision, 2000. PIV Flow Master Manual. La Vision GmbH, Gottingen, Germany.

Li, Y., Dong, G., Liu, H., Sun, D., 2003. The reflection of oblique incident waves by breakwaters with double-layered perforated wall. Coastal Engineering 50, 47-60.

Losada, I.J., Losada, M.A., Baquerizo, A., 1993. An analytical method to evaluate the efficiency of porous screens as wave dampers. Applied Ocean Research 15, 207-215.

Mallayachari, V., Sundar, V., 1994. Reflection characteristics of permeable seawalls. Coastal Engineering 23, 135-150.

Massel, S.R., Mei, C.C., 1977. Transmission of random wind waves through perforated or porous breakwaters. Coastal Engineering 1, 63-78.

Mori, N., Chang, K-A., 2003. Introduction to MPIV. User manual and program available online at http://sauron.civil.eng.osaka-cu.ac.jp/~mori/softwares/mpiv/

Raffel, M., Willert, C., Kompenhans, J., 1998. Particle image velocimetry, A practical guide. Springer – Verlag, Berlin, Heidelberg, Germany.

Requejo, S., Vidal, C., Losada, I.J., 2002. Modelling of wave loads and hydraulic performance of vertical permeable structures. Coastal Engineering 46, 249-276.

Suh, K.D., Park, W.S., 1995. Wave reflection from perforated-wall caisson breakwaters. Coastal Engineering 26, 177-193.

Suh, K.D., Choi, J.C., Kim, B.H., Park, W.S., Lee, K.S., 2001. Reflection of irregular waves from perforated-wall caisson breakwaters. Coastal Engineering 44, 141-151.

Suh, K.D., Son, S.Y., Lee, J.I., Lee, T.H., 2002. Calculation of irregular wave reflection from perforated-wall caisson breakwaters using a regular wave model. Proc. 28th International Conf. on Coastal Engineering, 1709-1721.

Suh, K-D., Park, J.K., Park, W.S., 2006. Wave reflection from partially perforated-wall caisson breakwater. Coastal Engineering 33, 264-280.

Takahashi, S., Shimosako, K., 1994. Wave pressure on a perforated caisson, Proc. of the Hydro-Port ’94, 1, 747-764.

Takahashi, S., Tanimoto, K., Shimosako, K., 1994. A proposal of impulsive pressure coefficient for the design of composite breakwaters, Proc. of the Hydro-Port ’94, 1, 489-504.

Terrett, F.L., Osorio, J.D.C., Lean, G.H., 1968. Model studies of a perforated breakwater. Proc. 11th ASCE Conf. Coastal Engineering, 1104-1109.

Twu, S.W., Lin, D.T., 1991. On a highly effective wave absorber. Coastal Engineering 15, 389-405.

Twu, S.W., Wang, Y.T., 1994. A computational model of the wave absorption by the multilayer porous media. Coastal Engineering 24, 97-109.

Urashima, S., Ishizuka, K., Kondo, H., 1986. Energy dissipation and wave force at slotted wall. Proc. 20th Coastal Engineering Conf., 3, 2344-2352.

Yip, T.L., Chwang, A.T., 2000. Perforated wall breakwater with internal horizontal plate. Journal of Engineering Mechanics 126, 533-538.

Zhu, S., Chwang, A.T., 2001. Investigations on the reflection behaviour of a slotted seawall. Coastal Engineering 43, 93-104.

APPENDIX A

ERROR CALCULATION

Definition of error,

% Error = (obtained value – expected value) / expected value * 100 % (A-1)

In Turbulence intensity calculation,

Turbulence intensity $= f(u'^2)$

Where u' is the turbulent velocity

$u' = u_t' + u_e$

where

u_t' - true turbulent velocity

u_e - error

$u'^2 = (u_t' + u_e)^2$

$= u_t'^2 + u_e^2 + 2\, u_t'\, u_e$

$2\, u_t'\, u_e \approx 0$

Normally $u_e \approx 0.1 – 0.2$ pixels / sec

Say, $u_e = 0.15$ pixels / sec

% Error = (obtained value – expected value) / expected value * 100 %

$= (u' - u_t') / u_t' * 100\ \%$

$= (u' - (u' - u_e)) / (u' - u_e) * 100\ \%$

$= u_e / (u' - u_e) * 100\ \%$

Calculated % errors for different wave conditions and different light sheets are shown in Table A-1.

Table A-1

Calculated % error for wave conditions and for light sheets

Wave condition	Horizontal velocity, U		Vertical velocity, V	
	Light sheet through wall	Light sheet through slot	Light sheet through wall	Light sheet through slot
T = 1 sec, H_i = 4cm	2.215	2.582	3.324	4.252
T = 1 sec, H_i = 6 cm	2.564	1.660	2.709	1.605
T = 1 sec, H_i = 8 cm	1.860	4.118	1.465	1.761
T = 1 sec, H_i = 10 cm	0.826	0.572	1.252	0.504
T = 1.6 sec, H_i = 8 cm	1.339	1.817	0.399	0.590
T = 2 sec, H_i = 8 cm	0.917	0.786	0.376	0.348
T = 2.5 sec, H_i = 8 cm	0.691	0.707	0.345	0.326

Considering the table A-1, the maximum error is 4.252% and for wave condition T = 1 sec H_i = 4 cm for the light sheet through slot.

APPENDIX B

MEASURED WAVE ELEVATION DATA

(a)

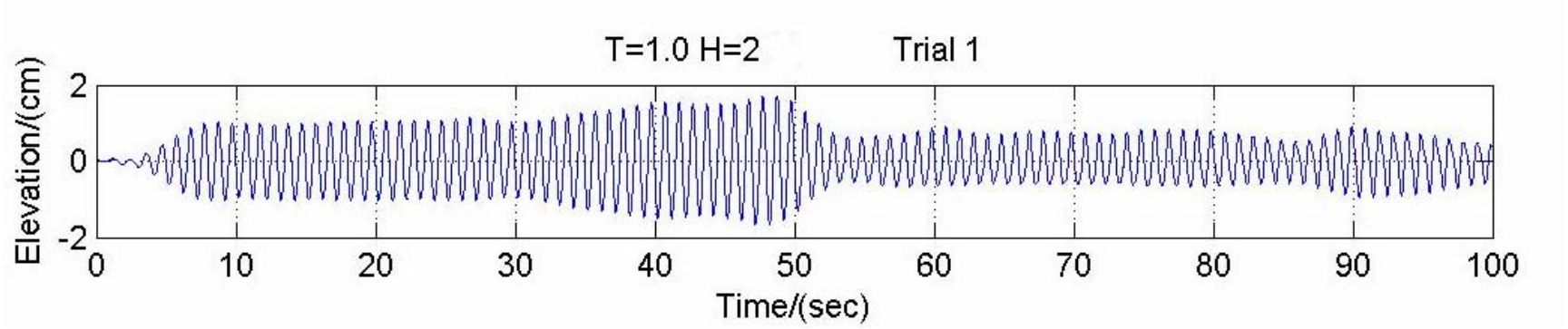

Fig. B.1. Measured incoming wave data for wave condition T = 1 sec, Hi = 2 cm. (a) Trial 1. (b) Trial 2. (c) Trial 3.

(b)

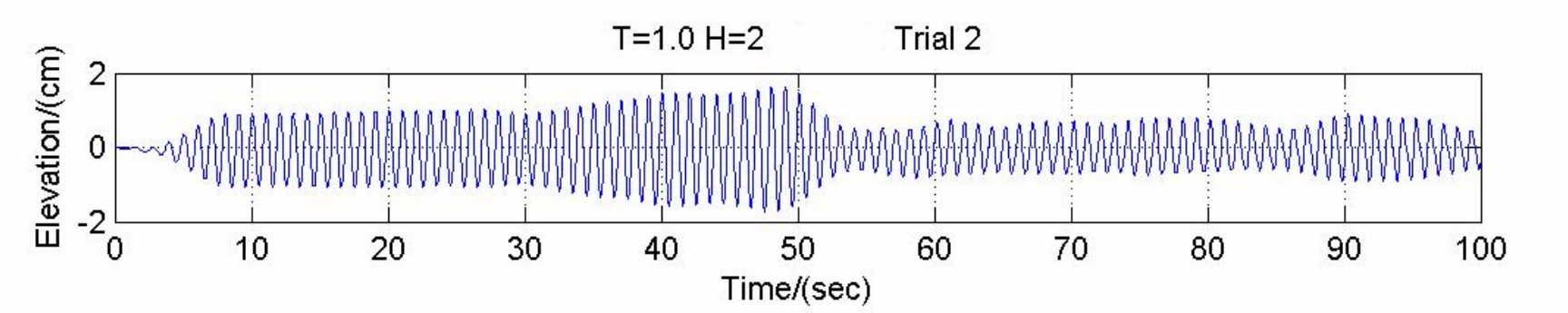

(c)

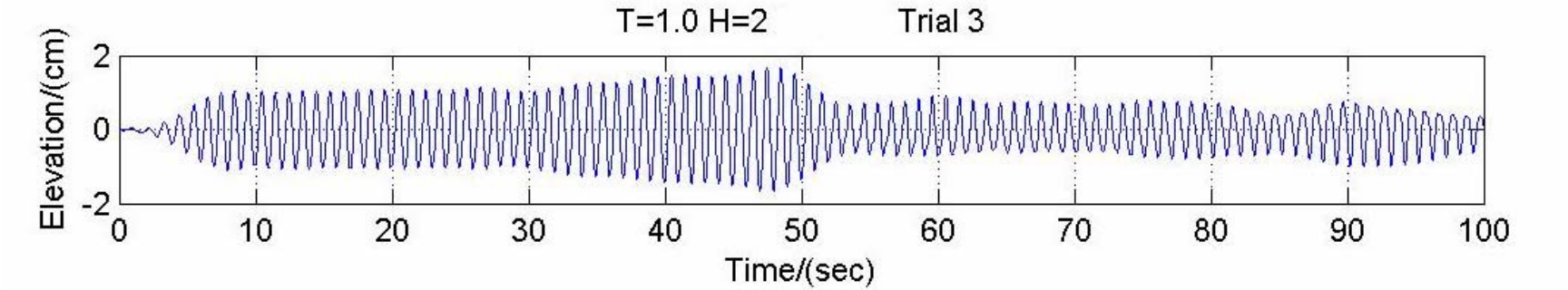

Fig. B.1. continued.

(a)

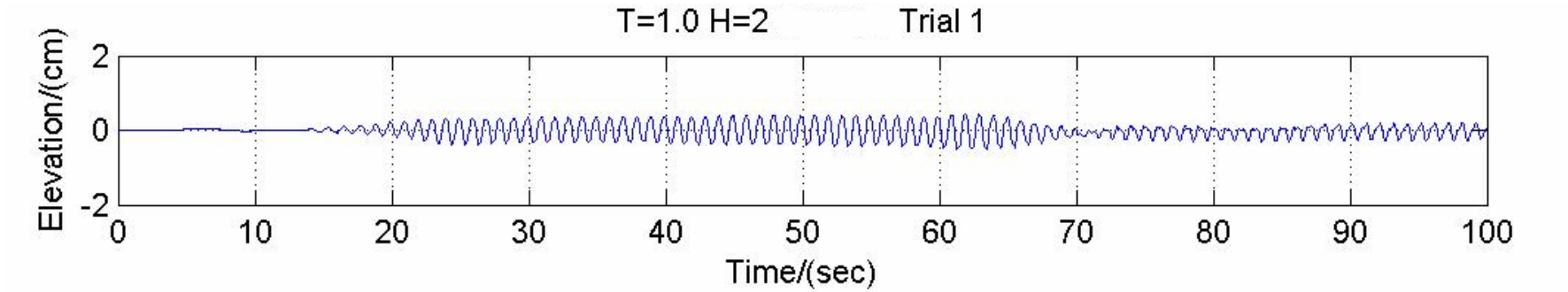

Fig. B.2. Measured transmitted wave data for wave condition T = 1 sec, H_i = 2 cm. (a) Trial 1. (b) Trial 2. (c) Trial 3.

(b)

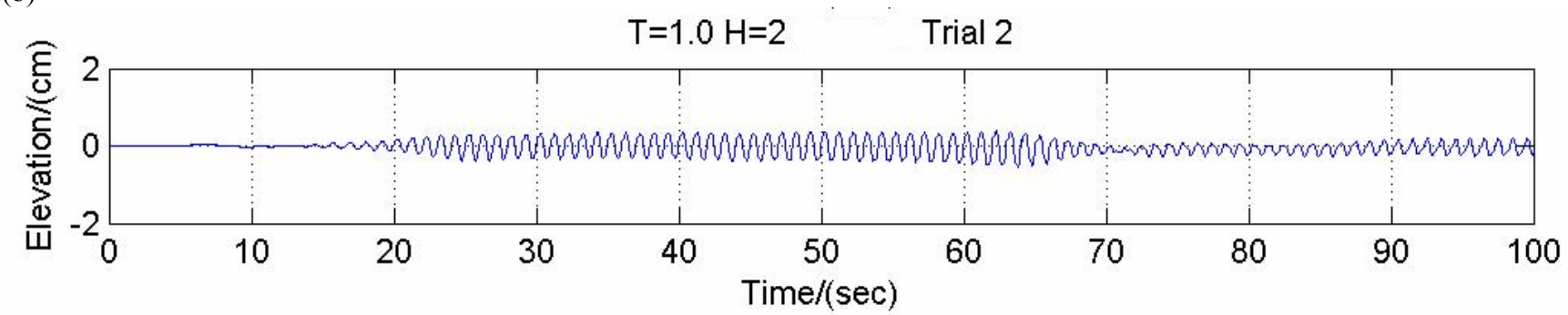

(c)

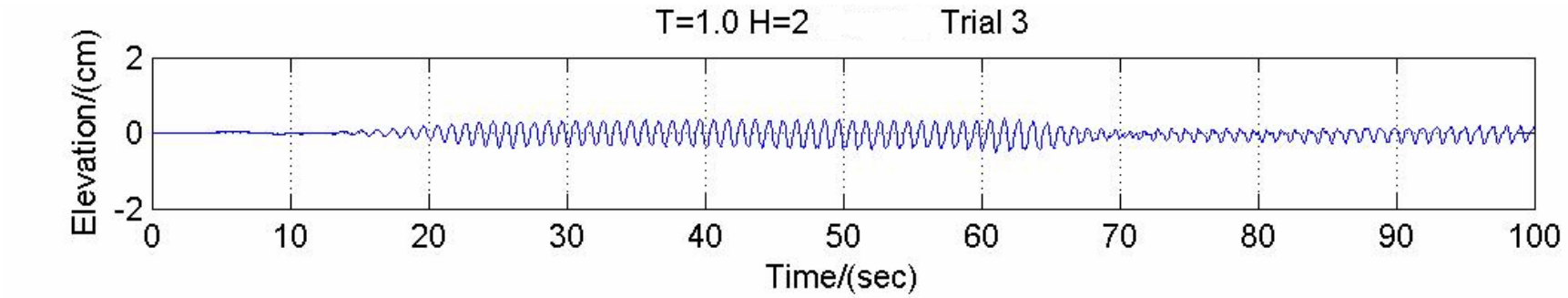

Fig. B.2 Continued.

APPENDIX C

CALCULATED VELOCITY, VORTICITY, AND TURBULENT KINETIC ENERGY DATA

Appendix C contains movie files of velocity, vorticity and turbulent kinetic energy variations with phases for wave conditions *T = 1 sec,* H_i *= 4 cm* and *T = 2 sec,* H_i *= 8 cm*. This appendix accompanies this thesis as a separate file available for downloading.

VITA

Name: H. A. Kusalika Suranjani Ariyarathne

Address: 1/29, Godagandeniya, Peradeniya, Sri Lanka

Email Address: kusalika@yahoo.com

Education: B.S., Civil Engineering, University of Peradeniya, Sri Lanka 2001
M.S., Oceanography, University of Peradeniya, Sri Lanka 2005
M.S., Civil Engineering, Texas A&M University, USA 2007